PAUL SCHERRER INSTITUT

PSI

Annual Report 2019

Laboratory of Radiochemistry

Cover

The Laboratory of Radiochemistry operates two integral neutron irradiation facilities at the Swiss Spallation Source SINQ, namely the NAA and PNA facilities. Both are run by our Neutron Irradiation Service (NIS), which irradiates samples for PSI-based users and outside partners for the purpose of material sciences or isotope production. Furthermore, our laboratory uses the SINQ Gas-Jet system for tracer experiments, such as needed in preparation of studies with transactinide elements (Z>103). The core of this setup is a ^{235}U-target installed inside SINQ itself. Both installation underwent substantial revision and upgrade works during the long SINQ-shutdown 2019/2020

The photographs show Alexander Vögele and Dominik Herrmann, members of the Heavy Elements group (NES), and Christoph Stettler of the Control Systems group (LOG) during their works at the NAA/PNA facilities as well as with the SINQ Gas-Jet system.

PAUL SCHERRER INSTITUT

Annual Report 2019

Laboratory of Radiochemistry

Editors
R. Eichler, A. Blattmann

Paul Scherrer Institut
Labor für Radiochemie
5232 Villigen PSI
Switzerland
Sekretariat +41 56 310 24 01
Fax +41 56 310 44 35

Reports are available from
Angela Blattmann
angela.blattmann@psi.ch
Paul Scherrer Institut
5232 Villigen PSI
Switzerland

See also our web-page
https://www.psi.ch/lrc/

TABLE OF CONTENTS

EDITORIAL

Dear reader,

Traditionally, we summarize our successes and ongoing projects in radiochemical research performed in our laboratory during the year in an annual report. Please find below the one of year 2019.

At the beginning, I want to point out that our Laboratory of Radiochemistry – the LRC – has a great standing internationally as well as here at our home institute - the Paul Scherrer Institute. The responses I get from people, which I meet abroad at conferences and in local meetings are generally exceptionally positive towards our professional work here at LRC and our outstanding scientific achievements. This makes me proud, as I was appointed as head of the Laboratory for Radiochemistry in July 2019. Consequently, we were excited to be able to appoint Patrick Steinegger as new group leader in tenure track for the *Heavy Elements* group. Welcome back Patrick and all the best for your academic future.

At the 11-th NES PhD-Day on May 24, 2019 Mario Veicht presented the winning contribution for the category *Best 1-st Year PhD*. Sincere congratulations go to the winner – Mario - keep on!

In the recent years, the production capabilities for radioisotopes for our research were diminished due to the long PSI-SINQ and accelerator shutdowns. However, we took the chance to access and refurbish our neutron irradiation stations and to update the fission product gas-jet installation. Big thanks go to our Alexander Vögele and Dominik Hermann and the teams from the LOG and GFA departments for their large efforts to secure a smooth restart of operation in summer 2020.

The positive attitude and the generally respectful and tolerant mood at LRC was illustrated by the results of the 2019 *"Mitarbeiterumfrage"* organized by PSI. I consider these as one of the fundamental cornerstones of our successful daily work.

The traditional joint social activities organized by the members of our laboratory contribute strongly to this important aspect. To name the two largest social activities here:

- Dominik Herrmann and Alexander Vögele perfectly organized our yearly laboratory excursion. On August 16, 2019 we were able to receive a great and interesting tour of the company Climeworks in Hinwil (ZH) – a spinoff company form ETHZ dedicated to the CO_2 removal from air to prepare it for geological CO_2 dumping. After a relaxing boat trip from Rapperswil to Zürich and a short hike to the Badi Chatzensee we had a great BBQ and good swim in the lake at very nice and sunny weather. For the first time we could greet Alva the new little member of Dominik's family.
- Our Christmas party at the MotoZ clubroom was well organized jointly by Patrick Steinegger and Dominik Herrmann. In cozy surroundings and with great food we enjoyed the now almost traditional and funny *Wichtel* (secret Santa) presentations and the nicely selected presents. Some of us were heavily into model car racing.

Dear reader, as announced in the previous editorial of our annual report last year we were actively participating in dedicated scientific festivities and publications celebrating the *International Year of the Periodic Table of Chemical Elements.*

We were able to present the progress of our work dedicated to the structure of the periodic table and devoted to the chemical properties of a vast variety of exciting chemical elements and their exotic isotopes using modern and innovative methods of radiochemistry and nuclear chemistry.

Have a nice read!

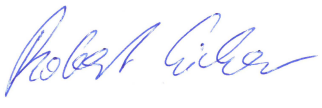

NOVEL METHOD OF SELENIUM COATING SURFACES FOR THE PREPARATION OF GAS CHROMATOGRAPHY COLUMNS

P. Ionescu (Univ. Bern & PSI), R. Eichler (PSI), A. Türler (Univ. Bern)

INTRODUCTION

Selenium is a versatile element with several allotropic forms, crystalline and amorphous, most of which can be found at standard laboratory conditions (SLC) [1]. It has a widespread use, most notably in electronics such as semiconductors [2]. In recent years, selenium has gained considerable interest in the field of transactinide chemistry, where it has been used as a stationary phase in gas chromatography (GC) experiments for determining the adsorption enthalpy of elements Cn (Z = 112) and possibly Fl (Z = 114) [3].

The first step in transactinide research usually is a homolog study, in which the lighter elements of the same group in the periodic table of elemens are investigated in order to prepare for challenging experiments at the one-atom-at-a-time level. In the case of Cn, Hg is the nearest homolog and has been used for these model experiments. It is known that group 12 elements tend to form selenides, however their bonds show a trend of decreasing stability as one moves down the group [4]. First, surprising results were already gathered in 2016 [5]. In order to further investigate, whether the extrapolation of this trend to Cn is indeed valid or not, we require high quality selenium surfaces which can be employed in GC experiments.

Furthermore, the versatile nature of multiple allotropes which can exist at SLC allows experimentalists to tune the surface to their needs and explore different conditions under which a chemical reaction can occur. Most notably, the stable gray trigonal selenium surface (t-Se) is of interest to our work, as it is exceptionally inert and stable under normal atmospheric conditions and therefore can be used up to month-long periods in GC experiments. During this time a stable surface is required, therefore it is of high importance to be able to reliably produce high-quality selenium-coated surfaces. In past experiments an a-Se surface was used, as it is chemically more reactive, however it had spontaneously converted to the gray allotrope under the experimental conditions. Despite this unwanted change and unlike the main fraction of the co-produced $^{182-185}$Hg, two events of Cn were observed on t-Se [5]. This was rather unforeseen due to the expected lower interaction energy of Cn compared to Hg on this Se-surface therefore warranting further investigation.

EXPERIMENTAL

A novel method of coating a quartz tube was devised with the aim of producing a selenium surface of highly consistent thickness and reproducability. The coating method was based on the following reaction:

$$H_2(g) + Se(s) \underset{UV}{\overset{\Delta}{\rightleftharpoons}} H_2Se\,(g)$$

By heating Se in a H_2 gas stream to 400 °C, H_2Se is formed (Fig. 1). Subsequently, the synthesized H_2Se was carried via the gas stream down the column and photolysed using an UV-lamp at 253 nm to trigger the decomposition back to elemental Se, coating the quartz tube in the process. A gas washing trap containing $CuSO_4$ was installed at the end of the column to ensure none of the noxious H_2Se could escape. The coating setup was designed to stop itself when the Se reached a sufficiently thick layer to no longer pass UV light from the lamp.

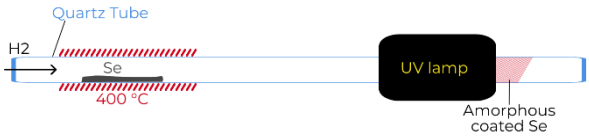

Fig. 1: Schematic of the quartz tube Se coating apparatus.

Produced this way, the resulting selenium coating, deposited in the crimson red amorphous a-Se form, was clean and uniform (Fig. 2). Some regions of the a-Se had been observed to have already changed to the t-Se allotrope due to the heat of the lamp. This however, was seen as unproblematic, as the goal of the procedure was to produce t-Se columns.

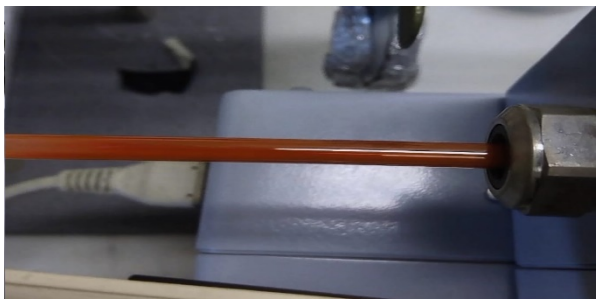

Fig. 2: Newly a-Se coated quartz tube, crimson red.

After the coating was completed, the a-Se column was heated to 200 °C for 72 hours to facilitate the conversion from the red amorphous to the gray trigonal allotrope. The resulting columns were observed to have largely changed to gray, however large portions of the previously uniformly coated column had aggregated, leaving uncoated patches with some red a-Se borders around them (Fig. 3).

Fig. 3: Se coated quartz column after thermal conversion at 200 °C. Both red and grey areas are visible, indicating incomplete conversion.

RESULTS

Initially, the red a-Se coating of columns was largely successful. The limited conversion to gray t-Se during the coating process could be likely avoided with more efficient cooling of the lamp. Further advantages this method brings is that the length of coated columns produced is practically without limits if one were to move the UV lamp along the length of the column as the coating process progessed. Coating did not occur uniformly from the beginning, which was attributed to the UV source not providing the same intensity evenly around the column. This was fixed by rotating and moving the column periodically.

The conversion of red a-Se to gray t-Se caused significant deterioration to the quality of the thin Se film. Mixed surfaces of a-Se and t-Se were observed and large patches where the Se layer had receded were seen also. While the conversion at 200 °C is below the melting temperature of 221 °C, the surface had likely migrated to form thicker regions of t-Se while remaining amorphous in the regions where little Se was found upon inspection. To further improve this method, one could attempt milder temperatures for the conversion process, resulting in a slower crystal growth. Higher intensity UV light could perhaps be employed to ensure a thicker deposit. Currently no quantification of the deposit thickness was made, however the limiting factor of the thickness corresponds to the transmission of UV light through the already deposited Se layer.

In conclusion, the photolysis method of coating quartz tubes shows high potential, particularly for the purpose of creating a thin, uniform a-Se layer of any required length. This technique could also be adapted to be used with other compounds in the same group, such as H_2S, H_2Te, or even similar behaving compounds such as H_3As. Obtaining a t-Se layer through thermal conversion was met with significant problems at the current stage and was deemed not feasible without further in-depth investigations. Other methods currently exist for the preparation of t-Se columns, so that developing this method was deemed too costly to continue pursuing at the present stage.

[1] D. M. Chizikov, V. P. Shchastlivyi, ‘Selenium and Selenides’, *Collet’s Publishers Ltd.*, London, (1968) pp. 1-5.

[2] D. G. Chica et al., Nature **577**, 346 (2020).

[3] N. M. Chiera, ‘Towards the Selenides of the Superheavy Elements Copernicium and Flerovium’, PhD Thesis, University of Bern, (2016).

[4] N. M. Chiera et al., LCH Annual Reports 2013 (2014), pp. 7.

[5] N. M. Chiera, LCH Annual Reports 2015 (2016), pp. 3.

CONTINUED DATA EVALUATION OF DUBNA 2018 EXPERIMENTAL CAMPAIGN AND PREPARATION FOR FUTURE EXPERIMENT

P. Ionescu (Univ. Bern & PSI), R. Eichler (PSI), A. Türler (Univ. Bern), N. V. Aksenov, Yu. V. Albin, G. A. Bozhikov, V. I. Chepigin, I. Chuprakov, S. N. Dmitriev, V. Ya. Lebedev, A. Sh. Madumarov, O. N. Malyshev, O. V. Petrushkin, Yu. A. Popov, A. V. Sabelnikov, A. I. Svirikhin, A. V. Yeremin (FLNR, JINR), R. Dressler, N. M. Chiera, D. Piguet, P. Steinegger, A. Vögele (PSI)

INTRODUCTION

Transactinides, or Superheavy elements (SHE) are the frontier in the discovery and classification of new elements, and thus the expansion of the periodic table. Synthetically prepared in heavy-ion-induced nuclear fusion evaporation reactions at large accelerator facilities such as the U400 cyclotron, SHEs can be chemically characterized to build our understanding of their chemical properties. These properties are of particular interest due to the increasing importance of relativistic effects (scaling with Z^2) affecting the electron shells and thus the physicochemical properties of these elements [1,2]. This work continues the evaluation of the experimental data collected in 2018 focusing on the chemistry of Fl and Cn, and will build on those findigs to prepare for future experimental campaigns. Based on previous observations Cn and Fl are elements of considerable chemical inertness and high volatility [3,4]. To prepare for second generation chemical experiments, the relatively volatile group 12 homologue Hg is used as a surrogate for its heavier homolog Cn. As Hg forms a stable selenide found in nature in the form of Tiemannite, the Hg-Se interaction was chosen as a model for Cn-Se investigations. When moving down group 12 in the periodic table, the M-Se bond (M = Zn, Cd, Hg) decreases in stability, to the point that Cn may not form a stable bond at all [4, 5]. Experiments involve gas chromatography (GC) with Se as stationary phase in a column or channel and Hg tracer isotopes in the mobile gas phase. Previous work established values for the enthalpy of adsorption of Hg on various allotropes of Se with adsorption enthalpy limits $\Delta H_{ads}^{\mathrm{Hg}}(\text{a-Se}) < -85\ \mathrm{kJ/mol}$ and $\Delta H_{ads}^{\mathrm{Hg}}(\text{t-Se}) > -60\ \mathrm{kJ/mol}$ [5]. For the details of the experiment refer to [6].

RESULTS & CONCLUSION

The data evaluation from the previous year's experimental campaign was continued and refined, revealing more information about the experiment and resulting in a deeper understanding of multiple species' behaviour. The COLD experiment is a highly complex one with multiple parameters interacting which all must be carefully considered. It was found that there is a strong indication of a link between operating the Ta-getter oven at a mild 400 °C compared to the normal operation at 950 °C, and the amount of reaction products transported (Fig. 1). Of particular interest were Hg and At, as both exhibit a similar deposition pattern in the COLD. The Ta-getter's function is to remove O_2 from the gas loop, however reducing the O_2 content also elevates H_2 and H_2O levels (see Fig. 1). It stands to reason that there is a likely influence of these residual gases on the transport efficiency of the nuclear reaction products of interest which warrants further close investigation.

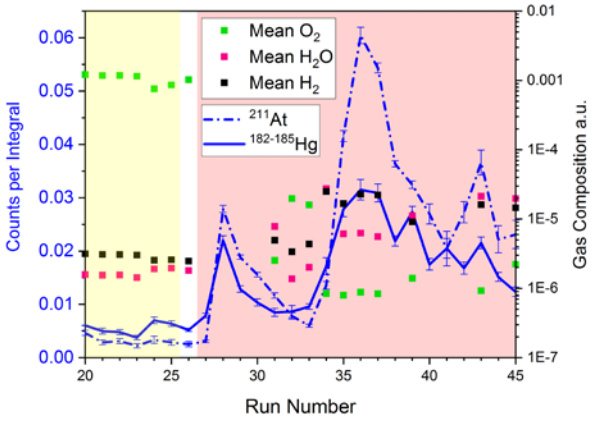

Fig. 1: The total counts per integral in the entire COLD array for ^{211}At and $^{182-185}$Hg for a selected series of experiments (blue lines, left-hand scale); also shown is the mean O_2, H_2O and H_2 content for the given run (scatter plots, right-hand log scale). The yellow shaded part on the left side of the graph indicates a Ta-getter temperature of 400 °C, whereas the red shaded part represents a getter temperature of 950 °C.

A further issue encountered during data analysis indicated a significant portion of the nuclear reaction product $^{182-185}$Hg escaped the COLD channel into the gas loop. As the elements of interest Cn and Fl are expected to be more volatile than Hg, this poses a serious risk in missing SHE, thus resulting in false conclusions drawn due to incomplete data. The cause of this loss can be attributed to two leading factors: the contamination of detector surfaces (i.e., the stationary surface) during extended runs, likely due to organic contaminants, and an insufficiently cooled final portion of the COLD channel (Fig. 2). A thorough analysis of past experiments in this series revealed that all investigations using COLD have experienced significant problems with a suspected non-identified organic substance contamination requiring frequent change and cleaning of detectors. It became apparent that the total amount of $^{182-185}$Hg detected in the COLD generally decreased significantly in successive runs. This was also attributed to the build-up of unknown contaminants on the surface and the deposited amounts could be reproducibly increased when exchanging and cleaning the detector surfaces. For the

efficent adsorption of the relatively volatile elements Hg and Cn, clean Au-surfaces are required in combination with a temperature endpoint of close to -160 °C. However multiple experiments were run with lowest temperatures as high as -140 °C, resulting in the possible escape of Hg, and thus the possibility of Cn or Fl loss is unacceptable.

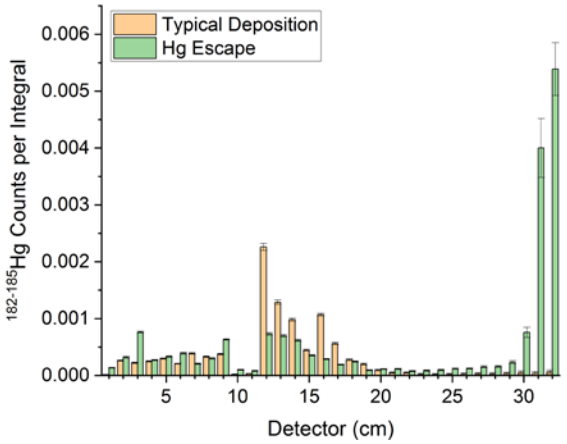

Fig. 2: Typical deposition pattern of $^{182-185}$Hg in COLD compared to a contaminated run with indication of Hg escaping in the rear.

For future experiments, it is aimed to improve the contact to the cooling jacket. Installation of a specialized SAES microtorr gas cleaning filter designed to scrub contaminants and residual gases, as well as a gas collecting tube for analysis of contaminants are suggested. The up-coming experiments 2020/2021 will be conducted behind the Dubna Gas-Filled Recoil Separator II (DGFRS-II) of the new Superheavy Element Factory of the Flerov lab, an important distinction compared to working directly behind the target. To prepare for this change, simulations were run in order to optimize the target window thickness, and the recoil chamber size. A variation to the past gas composition of 7:3 He:Ar has also been suggested, in order to maximize transport efficiency and avoid the potential poisoning of the gas-filled separator. Tables containing projected values are still in compilation, however a list of proposed gas compositions and their expected advantages and disadvantages can be seen in Table 1.

Tab. 1: Proposed gas mixtures for Dubna 2020.

Gas	Advantages	Disadvantages
7:3 He:Ar	Inert, tried and tested	Poisoning of separator gas filling
H_2	Higher carrier gas flows, no poisoning of separator, lower T in COLD	H-embrittlement in heated areas; H_2O formation Less stopping
x:y H_2:Ar	Low risk of separator gas poisoning;	Danger of H-embrittlement in heated areas; H_2O fomation

While the gas mixture used in previous years was effective in stopping/cooling and delivering nuclear reaction products quickly, the new hydrogen-filled separator poses an additional hurdle, should He from the gas loop leak into the low pressure separator volume. A possible workaround would be replacing the He with H_2, as Ar would be less likely to leak through the Mylar separating window. Alteratively, choosing solely H_2 as a carrier gas would be feasible, as it would allow for more intense cooling in the COLD and transport speeds over 3 times faster without the loss of chromatographic resolution (see Fig. 3), however the potential danger of H_2 flammability must be considered carefully.

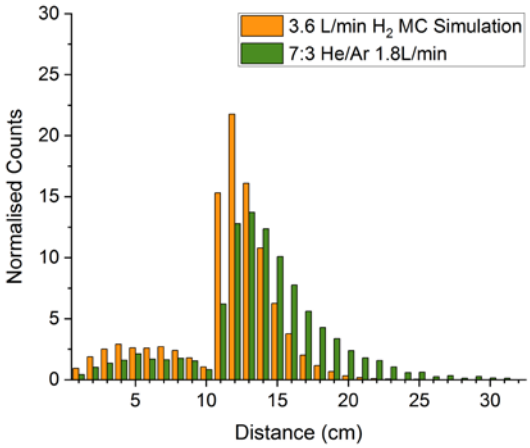

Fig. 3: Deposition pattern of $^{182-185}$Hg in COLD from previous experiments (green) compared to a simulation of three times faster flow rates using a pure H_2 carrier gas.

[1] M. Schädel & D. Shaugnessy (Eds.), The Chemistry of Superheavy Elements, 2nd Ed. Springer (2014).
[2] L. J. Norrby, Journal of Chemical Education, **68** (1991).
[3] R. Eichler et al., Nature **47** (2008).
[4] R. Eichler et al., Radiochimica Acta **98**, 133 (2010).
[5] N. Chiera, 'Towards the Selenides of the Superheavy Elements Copernicium and Flerovium', PhD Thesis, University of Bern, (2016).
[6] P. Ione.scu et al., LRC Annual Report 2018 (2019), pp. 3-4.

BEHAVIOR OF DIAMOND AND SILICON CARBIDE SENSORS AT HIGH TEMPERATURES

B. Kraus (PSI & Univ. Bern), R. Eichler (PSI), M. Camarda (STMicroelectronics, ETHZ), M. Carulla, R. Dressler, D. Herrmann, P. Steinegger (PSI), E. Griesmayer, C. Weiss (CIVIDEC), A. Türler (Univ. Bern)

In need of superior materials for high-temperature α-spectroscopy in gas-adsorption chromatography experiments with Superheavy Elements (SHEs), the Laboratory of Radiochemistry (LRC) evaluated two promising alternatives for the commonly applied Si-based detectors, i.e., electronic grade, single crystal CVD (escCVD) diamond and semiconductor-grade silicon carbide (4H-SiC polytype). Both materials exhibit at room temperature a wide band gap of 5.5 eV and 3.3 eV, respectively [1]. This feature in combination with favorable charge carrier transport properties in both materials enables their application in high temperature environments as sensor for highly ionizing radiation. The theoretical limit for diamond and silicon carbide amounts to 1000 °C and to 600 °C, respectively [2]. However, the current, experimental upper limit for diamond was found to be about 200°C to 300 °C [3-4] and about 375°C for silicon carbide [5]. These lowered values can be explained by the impurity content in both materials, which introduces so-called deep levels in the forbidden band gap. As the production for silicon carbide is more matured, the purity of the semiconductor grade material available today surpasses the one of electronic-grade diamond.
Both materials, i.e., escCVD diamond and 4H-SiC, were investigated from room temperature up to 500 °C in a comparative study with the setup introduced in [6,7]. The two sensors were set-up in the following way (both in parallel-plate geometry):

- escCVD diamond sensor: $4.5 \times 4.5 \times 0.5\ mm^3$, electrodes ($3.5 \times 3.5\ mm^2$) consisting of Cr (20 nm), and Au (80 nm).
- 4H-SiC sensor: $4.5 \times 4.5 \times 0.5\ mm^3$, PIN-structure with 0.5 µm p^+-layer, 100 µm intrinsic layer, 370 µm n^--layer, electrodes consisted of a super-alloy formed by flash-alloying Ti (20 nm), Al (40 nm), and Ni (60 nm) with the Si from the SiC material.

A comparison of the full width at half-maximum (FWHM) in the recorded spectra obtained at room temperature using a triple-line α-source (i.e., ^{239}Pu, ^{241}Am, and ^{244}Cm) revealed very similar energy resolutions for both sensors. The corresponding α-spectra are shown in Fig. 1 and Fig. 2. In fact, both sensors fulfill the minimum requirements for SHE identification (FWHM < 150 keV). The slightly worse resolution in case of the 4H-SiC-based detector in comparison to the escCVD diamond-based one can be explained by a thicker dead-layer in front of the active sensor volume, such as, e.g., a thicker metallization of the electrode facing the α-source. This can be seen clearly in the shape of the alpha peeks forming a larger low-energy tailing in the 4H-SiC spectrum (see Fig. 2).

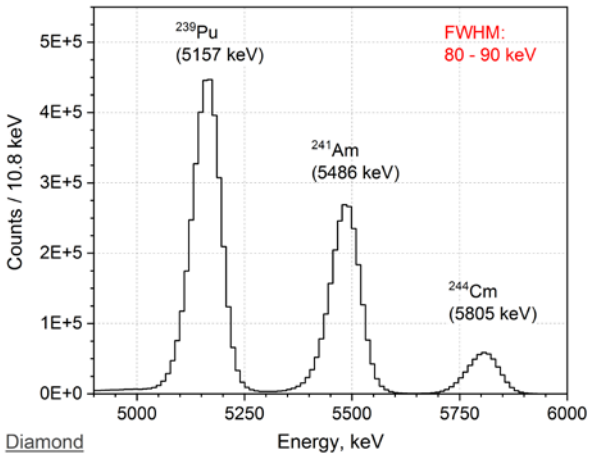

Fig. 1: Recorded spectrum of a triple-line α-source of ^{239}Pu, ^{241}Am, and ^{244}Cm with an esc-CVD diamond sensor at room temperature.

In a second step, the high temperature limits were investigated. Here, the signal traces, induced by individual α-particles of a pure ^{241}Am-source, were recorded with a WaveRunner 640Zi Oscilloscope (*LeCroy*). The ceramic PCB structure, containing the sensors and providing the necessary electrical contacting, were supplied by CIVIDEC Instrumentation GmbH along with the amplifiers (Cx spectroscopic amplifier with a Gaussian shaping time of 1 µs FWHM). The detector structure was stepwise heated up to 500 °C. For each temperature step between 100 °C and 500°C, 100 signal traces were recorded and subsequently averaged (cf. Fig. 3 and 4).

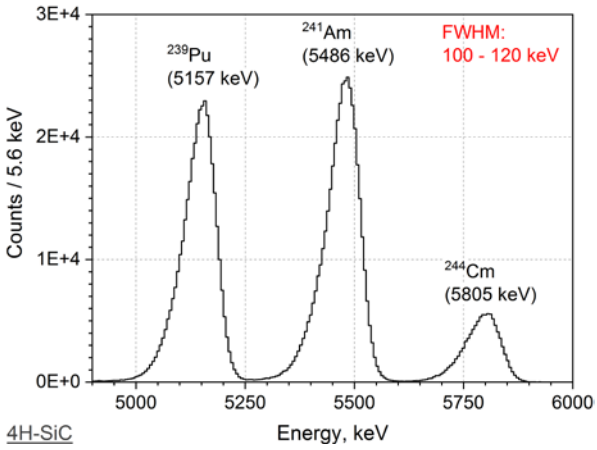

Fig. 2: Recorded spectrum of a triple-line α-source of ^{239}Pu, ^{241}Am, and ^{244}Cm with a semiconductor grade 4H-SiC sensor at room temperature.

In Fig. 3, the signal traces, induced by the impinging α-particle in a diamond sensor, are shown. Up to 200 °C,

the signal traces remain unchanged. However, above that temperature, the performance rapidly degrades. This might be explained by the increasing release of trapped charge carriers, causing a broadening of the traces at 250 °C and 300 °C. Pushing the temperature beyond 300 °C, leads to an additional decrease of the amplitude down to about 100 mV.

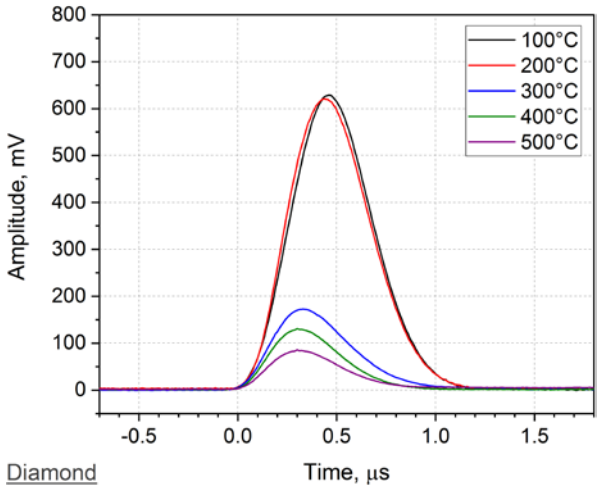

Fig. 3: Signal traces of an escCVD diamond sensor induced by α-particles of ^{241}Am at temperatures between 100 °C and 500 °C.

For silicon carbide (shown in Fig. 4) the signal traces show a different behavior. Up to a temperature of 350 °C, the signal amplitude does not change and thus the spectroscopic behavior is not impaired. At 400 °C, the signal amplitude is slightly reduced, before it drops in a comparable way as in case of the escCVD diamond sensor at temperatures ≥ 450 °C.

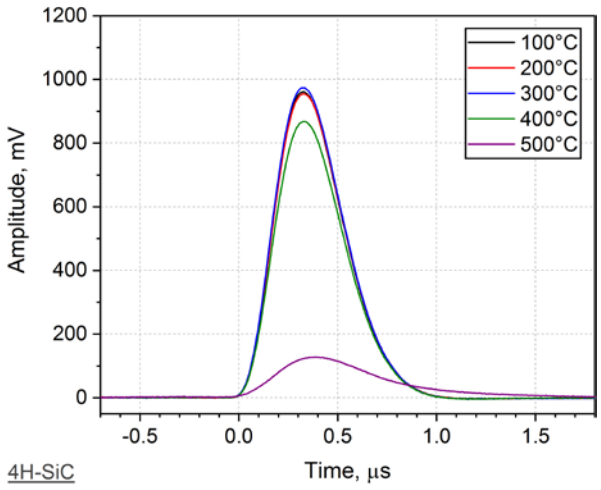

Fig. 4: Signal traces of a 4H-SiC sensor induced by α-particles of ^{241}Am at temperatures between 100°C and 500°C.

However, it is worth mentioning here, that at the current stage these temperature effects cannot be clearly attributed to the sensor bulk material, as electrical contacting at high temperature has to be further improved and could have likely caused the observed effects.

Based on the herein presented experiments, silicon carbide is currently the material of choice for our high-temperature α-spectroscopic activities. An additional point in favor of 4H-SiC-based detectors are the much lower costs per sensor plate, i.e., presently about EUR 20 for a sensor with the same size as the currently largest available escCVD diamond. The latter costs approx. EUR 2000. It is worth mentioning here, that the SiC-based detectors are currently produced in-house at LMN/PSI, which is why the price of a commercially available product might end up to be more costly.
In the future, the behavior of larger area silicon carbide detectors (e.g., 20 × 20 mm^2) will be investigated with the prospect of building a "cubebox"-detector (see Fig. 5), consisting of several large-area 4H-SiC-sensors.

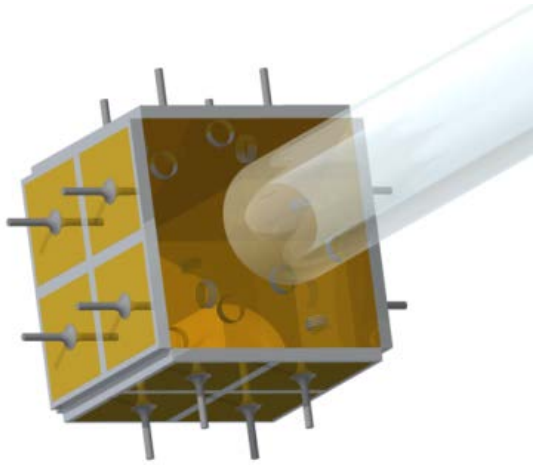

Fig. 5: Cube-box detector as a possible layout using 4.5 × 4.5 mm^2-sized diamond sensors.

Additionally, the spectroscopic performance during long-term exposure to high temperatures shall be investigated.

This work was funded by the Swiss National Science Foundation (Grant no.:200021_162769).

[1] F. Nava et al., Meas. Sci. Technol. **19**, 1 (2008).
[2] M. Gabrysch, Dissertation, Faculty of Science and Technology, Uppsala Universitet (2010).
[3] P. Steinegger et al., Nucl. Instrum. Meth. A **850**, 61 (2017).
[4] A. Kumar et al., Nucl. Instrum. Meth. A **858**, 12 (2017).
[5] E.V. Kalinina et al., Technical Physics Letters **34**, 210 (2008).
[6] B. Kraus et al., LRC Annual Rep. 2017, (2018), pp. 8.
[7] B. Kraus et al., Nuclear Instruments and Methods A (submitted 2019).

ON THE ADSORPTION OF LEAD ON A PLATINUM SURFACE

G. Tiebel (TU Bergakademie Freiberg), B. Kraus (Univ. Bern & PSI), R. Eichler, P. Steinegger (PSI)

The adsorption behavior of Pb on Pt is an important quantity for the description of isothermal vacuum chromatography (IVAC) [1] experiments with an intermetallic ^{227}Ac/platinum source (providing ^{211}Pb over intermediate decay products). Knowledge of this adsorption behavior is important for a complete description of the IVAC experiment with ^{211}Pb on quartz by a Monte Carlo simulation [2]. These experiments are done in preparation of less studied elements, such as, e.g., superheavy elements (SHEs). Thus, predictive conclusions about flerovium (Fl, $Z = 114$) can be obtained from the properties of Pb and its homologs. In a more general context, the development of the IVAC technique will allow to study less volatile and more short-lived chemical species.

Literature data concerning the adsorption of the herein studied model system of Pb on Pt is compiled in Tab. 1. Oxidic species of lead might form even on the Pt-surface during experiments performed in air. This change of the chemical state would significantly influence the observed adsorption interactions. The rather large spread of adsorption data (Tab. 1) indicates a variety of processes involved.

Tab. 1: Compilation of literature date concerning enthalpies of adsorption for Pb species on a Pt-surface.

Atmosphere	T_{dep}, °C	ΔH_{ads}, kJ/mol	Ref.
vacuum	675	-297.30	[5]
vacuum	800	-329.16	[5]
vacuum	795	-333.02	[6]
vacuum	980	-382.81	[6]
air	700	-305.92	[7]
air	800	-336.61	[8]

Another possibility to obtain basic thermodynamic information such as the adsorption enthalpy is to estimate these values using theoretical models. The MIEDEMA model [9] used and advanced by B. Eichler [10] is a semi-empirical adsorption model that enables initial evaluations of the enthalpy of adsorption in a binary system. The MIEDEMA model was used to calculate an enthalpy of adsorption of Pb on Pt amounting to -329 kJ/mol [10]. This value compares fairly well with the above-listed experimental results. However, even by excluding the results measured in air, the variation of the reported results, depending of course on the used experimental setups, are still striking, i.e., featuring differences up to roughly 100 kJ/mol. Despite using vacuum conditions, residual gases can still influence the process of adsorption/desorption as well as the chemical state of the transported species due to adverse side reactions (e.g., O_2, leading to an undesired oxidation of the elemental species and surface).

We report here on another experimental attempt using isothermal vacuum chromatography experiment with ^{211}Pb from an intermetallic ^{227}Ac/Pt-source (see [2] for details). During these experiments, the desorption of Pb from a Pt surface strongly contributes to the overall retention of Pb in the chromatography column and thus influences the determined quantity, the adsorption enthalpy with the applied stationary surface. The herein presented studies were carried out with a constant temperature in the isothermal section during the entire experiment: The isothermal temperature of the quartz column (i.e., the stationary surface) was set to $T_{iso} = 925°C$ while the end oven was operated at $T_{end} = 900°C$. This ensured a lowest possible surface retention of the ^{211}Pb species on quartz. Thus, only the adsorption/desorption phenomena at the source were of significance as the temperature of the start oven was varied between $T_{start} = 825$ °C and 925 °C in steps of $\Delta T_{start} = 25°C$.

The yield of ^{211}Pb measured at the outlet of the chromatography column was determined by measuring the decay daughter ^{211}Bi using a diamond-based α-spectroscopic solid state detector developed in-house at LRC [11]. The obtained results are shown in Fig. 1.

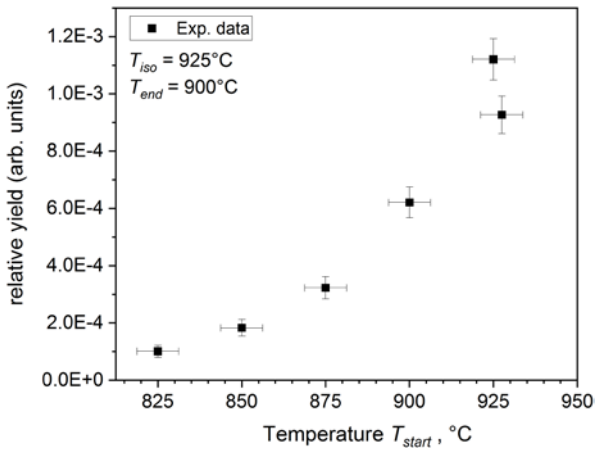

Fig. 1: Relative yield (arb. units) of the transported Pb (black squares) as a function of the source temperature T_{start}; the error bars are based on the statistical counting uncertainty (*y*-error) and the temperature spread (*x*-error), such as obtained during measurements along the Pt source.

The maximum saturation value of the external chromatogram for the Pb transport from the Pt source could not be observed, as the temperature maximum at the source was limited to 925 °C by construction. Therefore, a series of calculations was performed in

order to minimize the difference of relative simulated yields compared to the experimentally determined ones as function of the adsorption enthalpy of lead on platinum. This was done using a Monte Carlo simulation approach for vacuum chromatography coupled to a χ^2-test routine.

The used experimental parameters (fixed) for the simulation were: the length of the column $l = 350$ mm, the diameter of the column $\emptyset_{col} = 3\,mm$, the diameter of the source $\emptyset_{src} = 1.5$ mm, and an enthalpy of adsorption for ^{211}Pb or ^{211}PbO on SiO_2 of $\Delta H_{ads}^{\mathrm{SiO2}}(\mathrm{Pb/PbO}) = -200\ \mathrm{kJ{\cdot}mol^{-1}}$ [2]. The only variable parameter was the enthalpy of adsorption of Pb on Pt, i.e., $\Delta H_{ads}^{\mathrm{Pt}}(\mathrm{Pb})$.

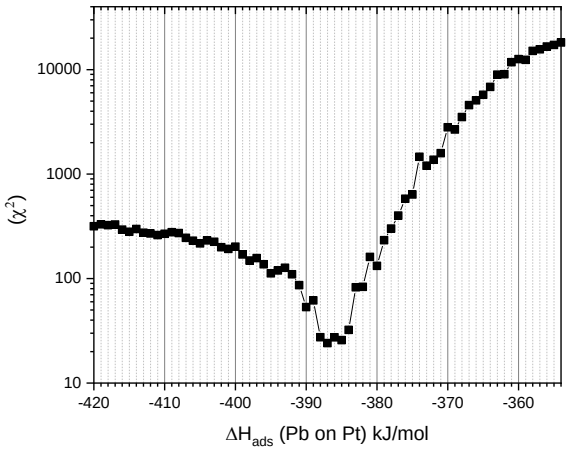

Fig. 2: Result of a χ^2-minimization deviation of the relative yields measured for Pb on Pt from simulated yields based on Monte-Carlo approach of vacuum chromatography; the minimum marks the most probable value. Analysis is ongoing

The preliminary deduced most probable enthalpy of adsorption was found to be $\Delta H_{ads}^{\mathrm{Pt}}(\mathrm{Pb/PbO}) = -386 \pm 5\ \mathrm{kJ{\cdot}mol^{-1}}$ (see χ^2-test results shown in Fig. 1). To further improve these results another parameter shall be varied in the Monte-Carlo simulation, i.e., $\Delta H_{ads}^{\mathrm{SiO2}}(\mathrm{Pb/PbO})$. However, this two dimensional calculation takes a considerable amount of time with the currently used code and thus has not yet been accomplished.

In summary, the enthalpy of adsorption of a Pb species on Pt was successfully determined using vacuum adsorption chromatography. The minor deviations from the above mentioned adsorption model [10] might result from the kinetics of the thermal release of Pb from the bulk of Pt; this is not considered in the applied model and possibly leads to an additional retention. Furthermore, Pt forms a very temperature-stable oxide (stable up to 950°C [13]), that was likely present during our experiments on the surface of the source. The oxidic Pt-compound could be reduced by Pb, which in turn would support the existence of an oxidic species of Pb [2]. In the case of PbO, its bond dissociation energy is tabulated as $D^0(900°\mathrm{C}) = 392.9 \pm 23.5\ \mathrm{kJ{\cdot}mol^{-1}}$ [14]. The possible silicate formation on the surface of the column must be considered too, which is reversible though at temperatures above 660°C [15]. Such reactions generally have a significant influence on the chromatographic retention of ^{211}Pb in the quartz column kept at 925°C. Nevertheless, the dominant retention effect is assumed to be the release (incl. desorption) of Pb from Pt. The influence of chemical compound formation could be further assessed by repeating the measurements with a controlled residual gas composition or using different surfaces. In a first approach, one could reduce all surfaces (i.e., the Pt and quartz column) with a reducing gas such as hydrogen in order to create a preferred oxide-free environment. Also, the vacuum inside the setup shall be improved from 10^{-5} to 10^{-7} mbar to avoid unknown contaminations.

Therefore, further experiments are required to confirm the obtained experimental data and to find an explanation for the relative high adsorption enthalpy for Pb on Pt. The present report intended to provide some inside into this complex chemical system of Pb, Pt, O_2, H_2O, and SiO_2. This system is of further interest for the preparation of intermetallic targets for transactinide research, usually operated at elevated temperatures [16].

---

[1] H. W. Gäggeler et al., Radiochimica Acta, **40**, 3 (1986).

[2] B. Kraus et al., LRC Annual Report 2017 (2018), pp. 13.

[3] D. R. Lide (Ed.), CRC Handbook of Chemistry and Physics, **84** (2003-2004).

[4] D. Kobertz, CALPHAD: Comput. Coupling Phase Diagrams Thermochem. **65** (2019).

[5] H. Schrader, Philos. Mag., **6**, 24 (1912).

[6] M. Hoffer, Sitzungsber. Akad. Wiss. Wien, **144** (1935).

[7] A. B. Wood, Proc. R. Soc. London, Ser. A, **91**, 633 (1915).

[8] S. Loria, Anz. Akad. Wiss. Krakau A (1916), pp. 549.

[9] A. R. Miedema et al., Surf. Sci. **95**, 2 (1980).

[10] B. Eichler, Rep. ZfK-527, Rossendorf bei Dresden, Zentralinstitut für Kernforschung (1984), pp. 16.

[11] P. Steinegger et al. Nucl. Instr. and Meth. in Phys. Res.A **850**, 61 (2017).

[12] I. Zvara, The Inorganic Radiochemistry of Heavy Elements, 1st ed., Springer, 2008.

[13] F. A. Holleman, N. Wiberg, E. Wiberg (Ed.) Anorganische Chemie, Vol. 2, De Gruyter, **103** (2016).

[14] J. B. Pedley et al., J. Phys. Chem. Ref. Data **12**, 4 (1983).

[15] B. Kraus et al., LRC Annual Report 2018, (2019), pp. 5.

[16] I. Usoltsev et al. Nucl. Instr. and Meth. in Phys. Res. B **318**, 297 (2014).

IN SITU PRODUCTION OF BiH_3 IN COLD PLASMAS

G. Tiebel (TU Bergakademie Freiberg), R. Eichler, P. Steinegger (PSI)

During a beam time experiment using the COLD array at FLNR, Dubna, Russia, a thermochromatographic deposition of a ^{213}Bi-containing species was observed at a temperature of approx. -17°C. Due to the observed weak interaction with Teflon and gold surfaces, and a thereof deduced high volatility, the substance is tentatively attributed to bismuthane (BiH_3), a volatile bismuth(III)-hydride ($T_{mp} = -67$ °C, $T_{bp} = 17$ °C [1,2]). Its formation was correlated to the trace amounts of hydrogen in the carrier gas, emerging from the drying process of the gas using tantalum at approx. 900 °C. The carrier gas (incl. hydrogen), flushing the recoil chamber, is excited by the intense heavy ion beam and thus transferred into a plasma state. The recoiling, highly ionized Bi ions, produced in the form of nuclear reaction byproducts, are then thermalized in this very same plasma.

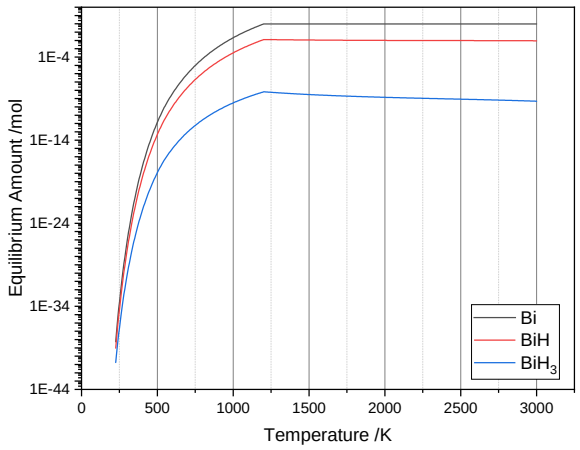

Fig. 1: Equilibrium behavior of the reaction of elemental bismuth with atomic and molecular (excess) hydrogen species at different temperatures.

According to K. C. Sabat [3] there are molecular, molecular-excited, atomic as well as several ionic hydrogen species in a hydrogen(-containing) plasma, all of them with different characteristics and thus different chemical reactivity. Molecular-excited and atomic species are of interest for the hydrogenation since they provide, in contrast to cationic ions, electrons enabling hydride formation. It remains open whether the formation of BiH_3 occurs in the recoil chamber or somewhere else. Futhermore unclear is how the thermally very unstable hydride ($\Delta H_{decomp} = -278$ kJ·mol^{-1} [4]) passes a subsequent quartz filter furnace held at 950 °C, which is used as an aerosol filter. Therefore, there is the possibility, that the BiH_3 is indeed not formed *in-situ* inside the recoil chamber, but forms during transport to COLD by means of recoiling Bi ions following the radioactive decay from parent nucleii.

Modeling thermodynamic equilibrium states using the method of minimizing the Gibbs free energy represents another way to obtain useful information about the present chemical systems. The thermodynamic data set was taken from the database of HSC CHEMISTRY 5.11 (for the present system Bi-H in the gas phase, refer to [5-10]), while we used the modeling software CHEMSAGE for the actual calculations. Various chemical reactions are conceivable using the data available for molecular and atomic hydrogen. The main reaction pathway is assumed the formation of the two hydridic species (BiH and BiH_3) in the gas phase. As seen in Fig. 1, these compounds are thermodynamically stable up to a temperature of approx. 1200 K. Changes in composition, pressure and the reactive hydrogen species lead to changed reactivities and thus to shifts in temperature of this quasi-equilibrium.

We report here on an experiment targeting the fast formation of $^{211}BiH_3$ using the reaction of recoiling ^{211}Bi (following radioactive decay from ^{211}Pb) in a gas phase composed of excited hydrogen species in a low temperature plasma. ^{227}Ac was used as an emanation source for ^{219}Rn ($t_{1/2} = 3.96$ s). The decay of this radioisotope of Rn leads over short-lived ^{215}Po to long-lived ^{211}Pb depositing on surfaces, which in turn β^--decays to the before mentioned ^{211}Bi recoiling partly into the gas phase.

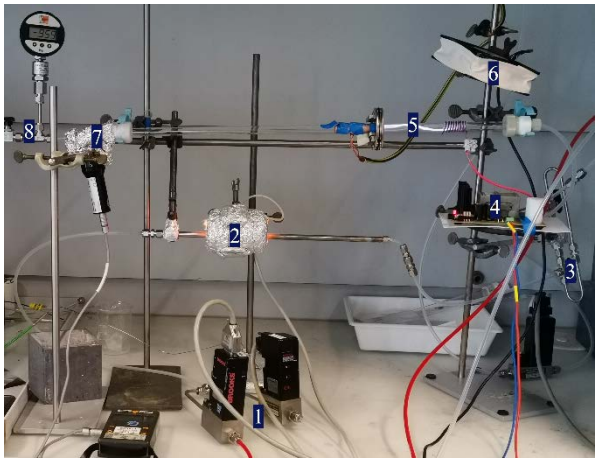

Fig. 2: Used experimental setup (see text for details).

The gas flow and composition was controlled using thermal mass flow controllers (1 in Fig. 2). Before being flushed through the ^{227}Ac-based ^{219}Rn-source (3), the reaction gas passed through a Ta getter oven kept at 950 °C to remove residual O_2 and H_2O (2). The gas mixture was then brought to the plasma state using a high-frequency/high-voltage generator (4), with the

plasma spreading from the copper coil to a grounded magnet (5). The generator required constant cooling with a fan (6). The assumed to be formed volatile Bi-H-species were transported to a charcoal trap and analyzed with a HPGe γ-detector after passing through a quartz glass tube ($\emptyset = 12$ mm, $l = 640$ mm). The pressure gradient was fine-tuned by a scroll pump (8).

The pressure in the reaction tube was adjusted to provide residence times of the carrier gas between $10 - 40$ s (e.g., 50 mbar and 10 ml/min $\rightarrow t = 20$ s) to allow most of the ^{219}Rn to decay before reaching the charcoal trap. The experiment was carried out at different pressures and various gas mixtures. The greatest difficulty proved to be the ignition of the plasma in the presence of hydrogen, which was improved by bringing a metallic object close to the copper coil. All experimental conditions are listed in Tab. 1. After each experiment the charcoal trap was exchanged and screened by γ-spectrometry.

Tab. 1: Applied experimental conditions

Gas composition (*Q*, ml/min)	Pressure *p*, mbar	Comment (d: distance coil – magnet)
H_2 (2) Ar (13,35±0,35)	40	d = 14 cm
H_2 (1,5) Ar (13,35±0,35)	40	d = 12 cm
Installation of the tantalum getter oven (900°C to 980°C)		
Ar (18,60±0,70)	40 60	Tube in water bath to produce H_2 *in situ* via oven
Ar (20)	40	Tube in water bath to produce H_2 *in situ* via oven
H_2 (15)	40	Plasma very unstable at high *Q*; d = 3.5 cm
Installation of a 2nd ^{219}Rn-source to obtain higher yields of ^{211}Bi in the plasma		
H_2 (15)	50	d = 3 cm
Ar (14,95±0,55)	50 100 150	Tube in water bath to produce H_2 *in situ* via oven.
He (20)	50	Tube in water bath to produce H_2 *in situ* via oven; d = 14 cm
H_2 (1,05±0,15) Ar (14,40±0,70)	40	
H_2 (1,05±0,15) Ar (13,00±1,40)	100 150 200	
H_2 (5) Ar (8,94±0,55)	50 100 150 200	
H_2 (7,40±0,10) Ar (8,94±0,55)	50 100 150 200	
H_2 (10,00±0,30) Ar (8,94±0,55)	100 150 200	
H_2 (1,00±0,10) He (20)	50	

Despite various experimental condtions, no ^{211}Bi was observed in the charocal that would have proven the transport of a volatile species of ^{211}Pb or ^{211}Bi. As an additional reactivity check chemical reaction occurring in cold plasma, a mixture of N_2 and H_2 was ignited. However, no formation of ammonia (NH_3) was detected either. By examining the entrance area of the tube more closely, ^{211}Pb/^{211}Bi-activity was found. This suggests an early adsorption of the radioisotopes in their respective elemental form before or in the plasma. Thus, the adsorption was obviously much faster than the actual formation of the hydride. Furthermore, the fast formation and immediate thermal decomposition of the hydride in the plasma (i.e., (electron-)temperatures up to 3000 K [11]) was ruled out, considering the above shown thermodynamic calculations.

In conclusion, an apparatus for the investigation of chemical reactions in a low-temperature plasma was developed. First experiments on the formation of bismuth hydride species were unsuccessful. Further optimization of the equipment is necessary in order to reproduce the formation of volatile hydrides, such as observed in combination with the heavy-ion-induced plasma in the recoil chamber during experiments at FLNR. Access to off-line, laboratory-scale expertiments would be very helpful to gain further insights in gas phase chemical reactions such as the investigated hydride formation. Therefore, we suggest using higher energy plasmas (e.g., a microwave plasma) for future experiments.

[1] N. A. Lange et al., Lange's Handbook of chemistry McGraw-Hill New York **13** (1985).

[2] D. R. Lide (Ed.) CRC Handbook of Chemistry and Physics, **84** (2003-2004).

[3] K. C. Sabat, J. Phys.: Conf. Ser. **1172**, 1 (2019).

[4] F. A. Holleman, N. Wiberg, E. Wiberg (Ed.) Anorganische Chemie, Vol. 2, De Gruyter, **103** (2016).

[5] V. P. Glushko, Thermocenter of the Russian Academy of Science - IVTAN Association (1994).

[6] I. Hurtado et al., Thermodynamic properties of inorganic materials, Springer (2006).

[7] O. Knacke et al., Thermochemical properties of inorganic substances, Springer, **1** (1991).

[8] C. L. Yaws, The Yaws handbook of thermodynamic properties for hydrocarbons and chemicals, Gulf Publishing Company (2007).

[9] M. Frenkel, Thermodynamics of organic compounds in the gas state, Thermodynamics Research Center, **1** (1994).

[10] Chase, M. W., Davies, C.A., J. Phys. Chem. Ref. Data **14**, 1 (1985).

[11] A. Alastuey et al., Phys. Rev. E **86**, 6 (2012).

OPTIMIZING THE IN-SITU FORMATION OF METAL CARBONYL COMPLEXES

Y. Wittwer (Univ. Bern & PSI), R. Eichler, D. Herrmann (PSI),
A. Türler (Univ. Bern)

Metal Carbonyl Complexes (MCCs) have been considered for the investigation of transactinide (TA) elements. All elements belonging to group 6 to 9 in the periodic table are forming volatile MCCs. The synthesis of $Sg(CO)_6$ by Even et al. in 2014 marks the first successful experiment with a TA-MCC compound [1]. Additional experiments performed in 2016 attempted to measure the first bond dissociation energy (FBDE) of $Sg(CO)_6$, a property that has never been measured before for a TA-compound. However, as already seen during the experiments presented in [1], the yields for formation and transport of the MCCs, produced under single-atom chemistry conditions, are very low [2]. This was found to be not only the case for $Sg(CO)_6$, but also for its homologues $W(CO)_6$ and $Mo(CO)_6$ as well as MCCs formed by other elements under similar conditions. This work is concerned with increasing these yields for future experiments using a variety of strategies.

In [3] we reported on the construction of the Fast On-line Reaction Apparatus (FORA) located at the University of Bern. This new setup allows for the optimization of experiments concerning the synthesis and transport of various MCCs under single-atom chemistry conditions [3]. In short, a ^{252}Cf-source is producing short-lived Mo, Tc, Ru and Rh radioisotopes by spontaneous fission, which are then serving as model system for their corresponding TAs. The radioisotopes are recoiling into a reaction chamber that is constantly flushed with a gas mixture containing CO. Depending on the reaction conditions, Mo, Tc, Ru and Rh react to form their corresponding MCCs, which are then volatile enough to be transported by the carrier gas. The formed MCCs are flushed out of the chamber along a PFA tube to a charcoal trap, where they are adsorbed. A HPGe γ-detector, positioned directly at the trap, is used to measure the radioactive decay of the adsorbed radionuclides. The overall yield of MCCs in the FORA-system is directly proportional to the obtained signal in the γ-spectrum for each isotope. The carrier / reactive gas is looped in the FORA system, employing various purification columns to ensure the purity of the used process gas.

Using this setup, we investigated the impact of various reaction parameters onto the formation and transport of MCCs. The adjusted parameters include the pressure of the used process gas, the gas-flow, as well as various impurities, e.g., O_2 and H_2O. The results of the corresponding measurements are currently prepared for publication. In 2018 [4], we reported that inserting freshly reduced nickel into the FORA-setup resulted in a fast and strong increase of the yield for all investigated MCCs. We assumed, that this might be associated with the formation of $Ni(CO)_4$, produced by the reaction of metallic nickel with the CO from the process gas. The macro amounts of $Ni(CO)_4$ might act as a catalyst favoring the formation of radioactive MCCs from ^{252}Cf fission products.

We decided to perform additional investigations on this matter. As $Ni(CO)_4$ is a very toxic substance, we decided to work with $Fe(CO)_5$ instead. The chemical compound was purchased with high purity (> 99.99%) from Sigma-Aldrich. At room temperature, $Fe(CO)_5$ is a liquid with a high vapor pressure. Thus, it could be added to the process gas of FORA by injecting it with a syringe through a membrane.

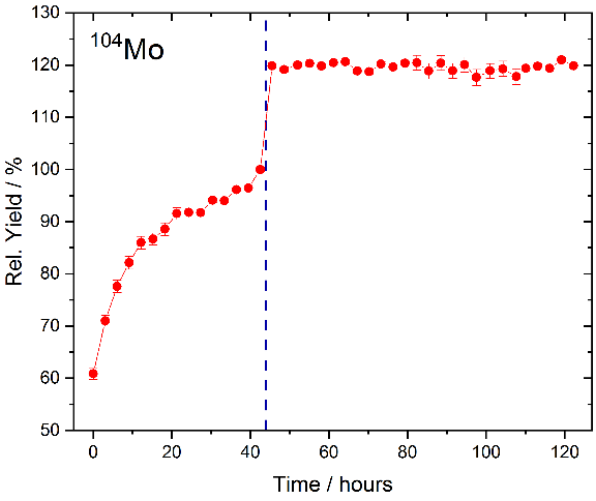

Fig. 1: Effect of 100 µL $Fe(CO)_5$ added to 100% CO at 1 bar and a gas flow of 1 l/min on the formation yield of $^{104}Mo(CO)_6$. A Sicapent®-column was used to remove moisture. The vertical blue line marks the point of $Fe(CO)_5$ addition. Continuous, three-hour-long measurements were performed. The data are normalized to the last point measured prior to $Fe(CO)_5$ addition. The red lines are plotted to guide the eye.

Figure 1 depicts the change in yield for $Mo(CO)_6$, produced from ^{252}Cf fission products, in 100% CO upon addition of 100 µL $Fe(CO)_5$. No other reaction parameters were changed. The formation of aerosol-particles upon $Fe(CO)_5$ addition can be excluded, as the obtained γ-spectra did not show any non-volatile fission products. Indeed, $Fe(CO)_5$ appears to have a similar effect regarding the MCC formation as in-situ synthesized $Ni(CO)_4$. Also visible in figure 1 is the FORA-typical increase in yield over time, especially pronounced during the first 12 hours after filling the setup with fresh process gas. This behavior was already discussed in [4]. According to our most recent studies, it is assigned to two causes. Firstly, the desorption of water from the internal surfaces of the FORA-loop and

its subsequent absorption by the corresponding purification columns. Secondly, the internal formation of $Fe(CO)_5$, $Ni(CO)_4$ and potentially other inactive MCCs by the interaction of CO with steel and metal-impurities in the charcoal-trap.
We performed additional experiments to further confirm the influence of $Fe(CO)_5$ and $Ni(CO)_4$ on the measured yield. These additional investigations included mass spectrometry, the usage of macro amounts of other inactive MCCs (other than $Ni(CO)_4$ and $Fe(CO)_5$), experiments in He instead of CO and the usage of purification columns, suitable for the removal of $Ni(CO)_4$ after its addition. All conducted experiments point towards a reaction of the fission products of ^{252}Cf with $Ni(CO)_4$ and similar inactive carbonyl species. Overall, this proved to be a much more efficient production route, than simply using the direct synthesis with pure CO.

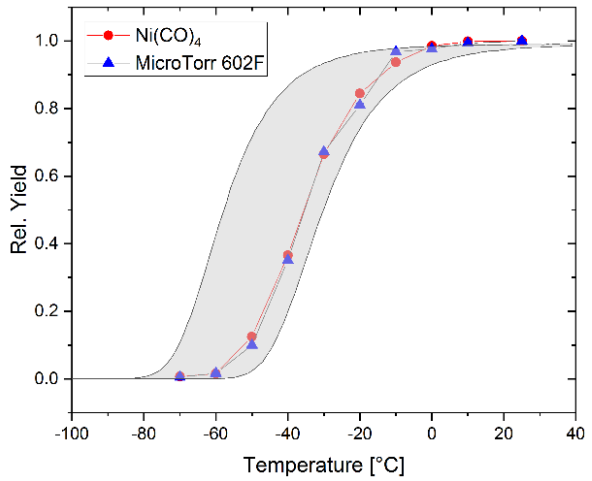

Fig. 2: Isothermal chromatography study using FORA filled with 100% CO at 1 bar and a gas flow of 1 l/min. The red points correspond to measurements with $Ni(CO)_4$ added to the process gas by the in-situ reaction between metallic nickel and CO. The blue points correspond to measurements using a MicroTorr 602F gas purification column instead (i.e., no $Ni(CO)_4$). The gray area corresponds to a $-\Delta H_{ads} = 42.5 \pm 2.5$ kJ/mol as determined by [5] for $Mo(CO)_6$. The lines are plotted to guide the eye.

An important question to answer concerned the speciation. By default, FORA allows to determine yields for volatile compounds, but not for the identification of the chemical state: The addition of $Ni(CO)_4$ simply increases the yield of volatile compounds of radioactive Mo. However, it cannot be excluded, that the interaction of Mo with $Ni(CO)_4$ produces a volatile product different from the intended $Mo(CO)_6$, e.g. a mixed carbonyl complex. Therefore, experiments assessing the speciation were necessary.
For this reason, we implemented an isothermal chromatography setup into the FORA system, i.e., between reaction chamber and charcoal trap. The chromatography setup consisted of a 2.4 m long quartz tube in a Dewar, which was cooled to different isothermal temperatures using a cooling bath of ethanol with dry ice and liquid N_2. Two isothermal gas-adsorption chromatography experiments were performed: Once using intense gas purification with a MicroTorr 602F column and once adding $Ni(CO)_4$ to the process gas. In both experiments, a Sicapent cartridge was used to remove moisture. The data are compared with each other in figure 2 as well as with reference data from Even et al. [5]. The unchanged adsorption interaction of the Mo-containing compound at both experimental conditions allowed for the conclusion, that the interaction of $Ni(CO)_4$ with Mo fission products indeed leads to pure $Mo(CO)_6$. In fact, $Ni(CO)_4$ seems to increases only the yield for the formation and transport of MCCs produced under single-atom chemistry conditions, but does not affect their chemical speciation.
We conclude that $Ni(CO)_4$ and $Fe(CO)_5$ can be used to increase formation and transport of MCCs produced under single-atom chemistry conditions in the FORA system. The approach is very effective and might prove extremely valuable for future investigations with carbonyl complexes of TA elements. However, additional studies will be necessary to confirm the observed effects with other experimental approaches and further MCCs from heavier elements.

We acknowledge funding from the Swiss National Science Foundation (Grant 200021_162769)

[1] J. Even et al., Science **345**, 1491 (2014).
[2] R. Eichler et al., EPJ Web of Conferences **131**, 07005 (2016).
[3] Y. Wittwer et al., LRC Annual Report 2016 (2017), pp. 5.
[4] Y. Wittwer et al., LRC Annual Report 2018 (2019), pp. 11.
[5] J. Even at al., Inorganic Chemistry **51**, 6431 (2012).

ESTABLISHMENT OF THE VOLATILITY TREND IN GROUP-5 ELEMENTS

N. M. Chiera, R. Eichler, R. Dressler (PSI), T. K. Sato, T. Tomitsuka, M. Asai, Y. Ito, H. Suzuki, K. Tokoi, K. Tsukada, Y. Nagame (JAEA), K. Shirai (Niigata Univ.)

With an expected $[Rn]5f^{14}6d^{3}7s^{2}$ ground state configuration, dubnium (Db, Z = 105) is placed among Group-5 elements of the periodic table, together with vanadium (V, Z = 23), niobium (Nb, Z = 41), and tantalum (Ta, Z = 73). Due to the strong tendency of these transition metals to form stable volatile pentahalide compounds, gas-phase studies with Db were mainly focused on the formation and on the chemical characterization of $DbBr_5$ and $DbCl_5$ complexes. However, in the experiments conducted to-date, discordant results were obtained, mostly due to 1) the formation of oxyhalides species with traces of oxygen / water in the carrier-gas, and 2) the modification of the chromatographic surface with the material of aerosol particles used to transport the radionuclides of interest from the production site to the chemical apparatus. In order to shed some light on the chemical behavior of Db in the gas phase, an Isothermal Gas-Chromatographic (IGC) setup - exclusively devoted to study the chemical interaction of oxy-chloride species with quartz surfaces - was developed at the Japan Atomic Energy Agency (JAEA) [1]. In on-line model experiments, the short-lived isotopes ^{88}Nb (E_γ = 1057 keV (100%); $t_{1/2}$ = 14.5 min) and ^{170}Ta (E_γ = 100.8 keV (20%); $t_{1/2}$ = 6.76 min) were simultaneously synthesized in the nuclear fusion reactions ^{nat}Ge(^{19}F, xn)^{88}Nb and ^{nat}Gd(^{19}F, xn)^{170}Ta, respectively, at the Tandem Accelerator facility (JAEA). The nuclear reaction products were swept out from the recoil chamber and directly injected into a heated quartz column (1000 °C) by the inert carrier gas. There, oxychloride compounds were synthesized by addition of $SOCl_2$ and O_2, and successively transported along the isothermal chromatographic column by the gas flow. The compounds leaving the chromatographic column were attached to KCl aerosol particles and transported to an aerosol-collection system. The activity of the collected aerosols was measured with an HPGe γ-ray spectrometer. The yields of $NbOCl_3$ and $TaOCl_3$ passing through the gas-chromatographic column as a function of the applied isothermal temperature were recorded (Fig. 1). The chromatographic behavior of $NbOCl_3$ and $TaOCl_3$ was analyzed with a Monte-Carlo simulation method based on a kinetic model of adsorption-desorption [2]. Their adsorption enthalpies (ΔH_{ads}) on quartz at zero surface coverage were determined as $-\Delta H_{ads}(NbOCl_3)$ = 102 ± 4 kJ/mol and $-\Delta H_{ads}(TaOCl_3)$ = 128 ± 5 kJ/mol [3]. The experimental ΔH_{ads} values were successively related to the macroscopic standard sublimation enthalpy, $\Delta H°_{subl}$, as a measure of the volatility of each substance, by applying an empirical correlation between ΔH_{ads} and $\Delta H°_{subl}$ for metal-oxychlorides, reported in [3]. The inferred sublimation enthalpies are in well agreement with tabulated thermochemical values, bolstering the suggested speciation. Under the same experimental conditions, the chemical exploration of $DbOCl_3$ in the temperature range from 350 to 600 °C was performed. For the purpose, ^{262}Db ($t_{1/2}$ = 34 s) was synthesized in the nuclear fusion reaction ^{248}Cm(^{19}F, 5n)^{262}Db at the Tandem Accelerator facility, using a ^{248}Cm-target of 800 µg/cm^2 thickness and a F^{+7} ion beam at an energy of 103 MeV in the middle of the target. For the detection of ^{262}Db and its daughter ^{258}Lr (see the chain decay pattern in Fig. 2 [4]), the IGC apparatus was connected to the detection system MANON (Measurement system for Alpha particle and spontaneous fissioN events ON-line) [5]. The result of the statistical analysis of the data for $DbOCl_3$ is presented, together with the ones for $NbOCl_3$ and $TaOCl_3$, in Fig. 1.

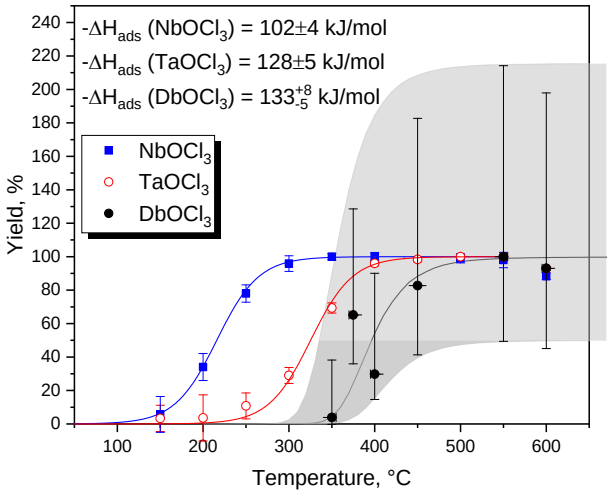

Fig. 1: Comparative isothermal chromatograms for $NbOCl_3$, $TaOCl_3$, and $DbOCl_3$.

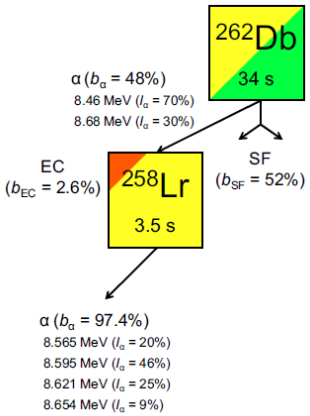

Fig. 2: Decay pattern for ^{262}Db [4].

Based on the periodic trends along Group-5 elements, a decreased relative volatility for $DbOCl_3$ in comparison to its lighter homologues (assuming the validity of a linear trend) is expected (Fig. 3).

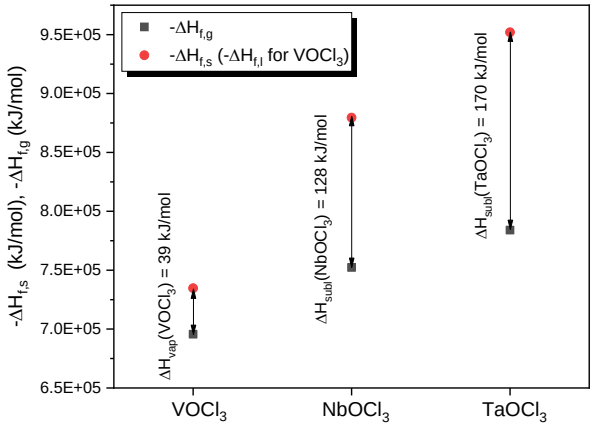

Fig. 3: Standard formation enthalpies in solid phase ($-\Delta H_{f,s}$) and in gas phase ($-\Delta H_{f,g}$) for group-5 oxychlorides [6]. Being the standard state of $VOCl_3$ liquid, its standard formation enthalpy in liquid phase ($-\Delta H_{f,l}$) is given. The inferred sublimation enthalpies ($\Delta H°_{subl} = \Delta H_{f,g} - \Delta H_{f,s}$) for each compound are reported. In case of $VOCl_3$, the vaporization enthalpy ($\Delta H°_{vap} = \Delta H_{f,g} - \Delta H_{f,l}$) is indicated.

Experimentally, a $NbOCl_3 > TaOCl_3 \geq DbOCl_3$ volatility sequence is observed, with an about 25% probability that $DbOCl_3$ is equally or even more volatile than its lighter homologue $TaOCl_3$. In fact, by performing Monte-Carlo simulations, an adsorption enthalpy of $-\Delta H_{ads}(DbOCl_3) = 133^{+8}_{-5}$ kJ/mol on quartz is deduced. From the above-mentioned empirical correlation for metal-oxychlorides [3], a $\Delta H°_{subl}(DbOCl_3) = 177^{+10}_{-7}$ kJ/mol is derived, in perfect agreement with the $\Delta H°_{subl}(DbOCl_3) = 180$ kJ/mol extrapolated in [7]. As suggested in [8], from the experimental $\Delta H_{ads}(DbOCl_3)$ value the standard formation enthalpy of single atomic Db in gaseous state ($\Delta H_{f,g}$) can be deduced. The inferred $\Delta H_{f,g}(Db) = 837^{+53}_{-50}$ kJ/mol is in agreement with selected predicted values for Db, i.e., $\Delta H_{f,g}(Db) = 821$ kJ/mol [7], and $\Delta H_{f,g}(Db) = 835 \pm 30$ kJ/mol [9].

Based on these results, theoretical calculations will be able to elucidate the impact of the relativistic effects on the electronic structure of Db, and hence, on its chemical behavior.

This project was funded by the JSPS Kakenhi Grant-in-Aid for Young Scientists (B) (Grant No. 20740152).

[1] N. M. Chiera et al., J. Radioanal. Nucl. Chem. **320**, 633 (2019).
[2] I. Zvara, Radiochim. Acta **38**, 95 (1985).
[3] N. M. Chiera et al., Inorg. Chim. Acta **486**, 361 (2019).
[4] H. Haba, EPJ Web of Conferences **131**, 07006 (2016).
[5] Y. Nagame et al., J. Nucl. Radiochem. Sci. **3**, A299 (2002).
[6] O. Knacke, O. Kubaschewski, K. Hesselmann (Eds.) "Thermochemical properties of Inorganic Substances II", Springer-Verlag, Berlin (1991).
[7] B. Eichler, et al., PSI Annual Report 1994/Annex FIIIA, p. 77 (1995).
[8] B. Eichler, R. Eichler "The Chemistry of Superheavy Elements (Ed. M. Schädel)", 375-413 (2014).
[9] G. V. Ionova et al., Radiokhimiya **37**, 307 (1995).

UPDATES AND MAINTENANCE AT SINQ-SECTORS 60/61: NEUTRON IRRADIATION SERVICES AND SINQ GAS-JET

A. Vögele, D. Herrmann (LRC/PSI), Ch. Stettler (LOG/PSI), R. Eichler, P. Steinegger (LRC/PSI)

The Laboratory of Radiochemistry runs sectors 60 and 61 at the Swiss Spallation Source SINQ. The Neutron Irradiation Service (https://www.psi.ch/en/nis), located at sector 60, operates two neutron irradiation facilities, i.e., NAA and PNA with their respective thermal neutron fluxes of $1 \cdot 10^{13}\ \mathrm{n/cm^2/s}$ and $4 \cdot 10^{13}\ \mathrm{n/cm^2/s}$ (see Fig. 1). In case of both positions, the samples are brought into place by a He-driven pneumatic rabbit system. Whereas the NAA irradiation facility is loaded and unloaded directly in the radiochemical laboratory WBGA/C41 (sample with lower activities up to 100 LA), the PNA facility includes a hot cell directly attached on the outside of the SINQ (sample with activities up to 10'000 LA). The Neutron Irradiation Service looks back on a long and successful history of about 23 years of operation, thereby assisting not only PSI-based activities, but also those from outside partners at universities and in industry. Due to its rather old age, the LRC staff used the SINQ-shutdown 2019/2020 for a long overdue revision of the two facilities NAA and PNA.

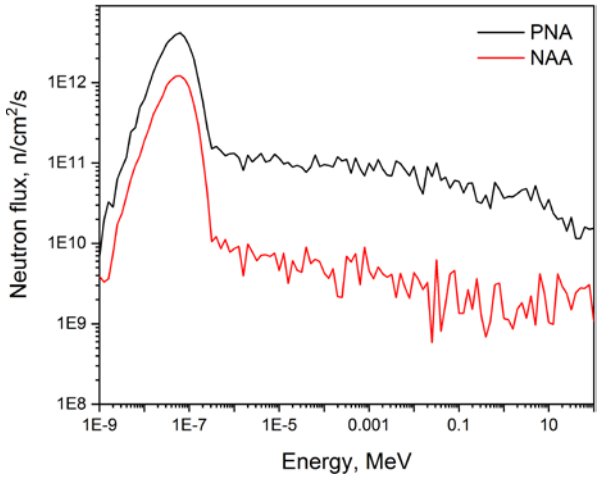

Fig. 1: Neutron fluxes at different energies for the neutron irradiation facilities NAA and PNA.

Meanwhile at sector 61, the SINQ Gas-Jet Facility is installed. The core of this facility is a target assembly consisting of three separate chambers, each with two individual ^{235}U-targets of masses below 1 mg (see Fig. 2). Connected over a gas-jet system, thermal-neutron-induced fission products of ^{235}U recoiling from the targets can be readily transported to the above mentioned radiochemistry lab WBGA/C41 by means of an aerosol-loaded carrier gas (non-volatile fission products) or *via* an inert carrier gas flow (volatile fission products). This 80 m long connection between the production site and the laboratory is established using PTFE-tubing inside a caldding tube, flushed on the outside with N_2 as a purging gas. The transported fission products are then used for example in gas chromatographic model experiments as preparatory studies for the chemical characterization of transactinide elements. This system was in operation from the end of the 1990s until mid-2010 [1] before it had to be shut-down due to technical difficulties with the real-time control system. In the following, it was decided to replace the latter with a state-of-the-art Siemens SPS control.

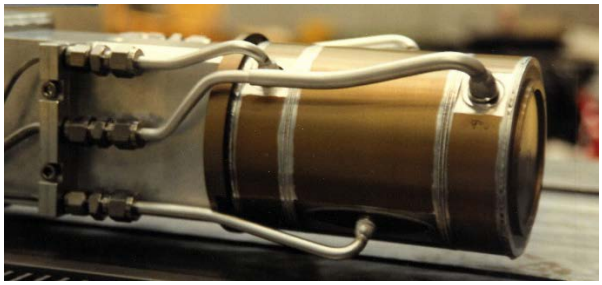

Fig. 2: Gas-jet target assembly, integrated at SINQ with six ^{235}U-targets ; the three separate chambers, each containing two ^{235}U-targets on either side, are individually flushed by an inert carrier gas or aerosol-loaded gas flows.

REVISON AND UPGRADE AT NAA & PNA

During the long SINQ-shutdown 2019/2020 the entire roof as well as the lead shielding between the irradiation facility in sector 60 and the outer wall of SINQ was removed (see. Fig. 3). This allowed access to vital parts of the NAA/PNA facilities, namely the gate valves, optical position sensors as well as pneumatic valves and tubing. During this first upgrade since the start of operation, a complete revision of all pneumatic cylinders and connected gate valves (including inside the hot cell) was carried out. These works included a complete disassembly of the components, their cleaning and subsequent MoS_2-polishing for dry lubrication. Furthermore, it was decided to exchange the entire optical positioning system for the irradiation capsules with a state-of-the-art solution due to the extended radiation damage of the optical fibers and the unavailability of old electronics. The existing components were replaced with fiber optic amplifiers of the FX-100 Series (*Panasonic*) in combination with a complete rewiring using polymethylmethacrylate (PMMA) plastic optical fibers. The latter was proven to be sufficiently stable for the used wavelength in high radiation fields [2]. Furthermore, all new electronics were repositioned; partly from predefined places inside the hot cell to a single point in sector 60, which allows constant access during operation of the SINQ. This

allows for diagnostics and if needed for the replacementof individual parts. On the control side, a hard- and software upgrade was carried out, thereby migrating to Windows 10. The update to the newest version 7.5 of the Siemens SIMATIC WinCC software package for the control of our pneumatic rabbit system was performed by our external partner *Bouygues E&S Prozessautomation AG*. All above described works are about to be finished and tested by the beginning of 2020, thus being all set for the upcoming SINQ-startup in June 2020.

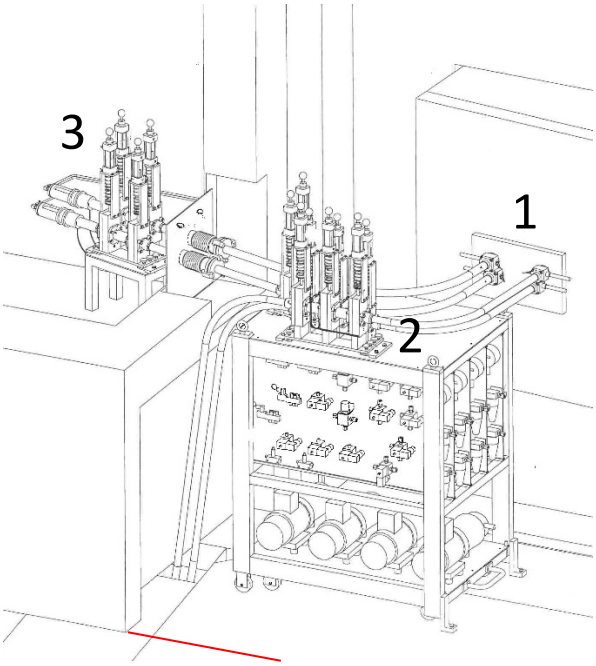

Fig. 3: Instrumentation for the operation of irradiation facilities NAA and PNA on the outside of SINQ (1); the main table on the right hand side (2) as well as connected parts are not accessible during SINQ-operation (lead wall at red line); the gate valves and further components on the left hand side are located inside the hot cell (3).

UPGRADING THE SINQ GAS-JET SYSTEM

After ceasing operation in 2006 due to the dysfunctional control system, the upgrade of the SINQ Gas-Jet system was thoroughly planned and finally executed during the SINQ-shutdown 2019/2020.

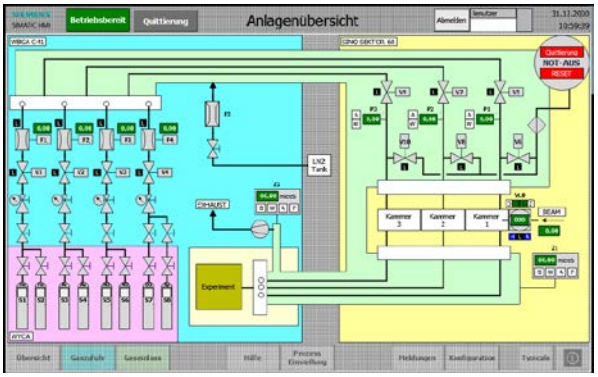

Fig. 4: Control panel in WGBA/C41 of the Siemens SPS control and monitoring system allowing for manual operation.

While some integral parts of the system, such as the target chamber (Fig. 2) and the over 80 m long gas-jet tubing between the SINQ and the radiochemistry lab WBGA/C41, did not require upgrading, the old control was fully replaced with a Siemens SPS control and monitoring system. This will allow for a manual operation of the gas-jet from WBGA/C41 using an enclosed assembly (German: Schaltgerätekombination SGK) in combination with a local control touch panel display (see Fig. 4). In addition to the upgrade of the control and monitoring system, the entire electrical wiring likewise needed replacement. Furthermore, all previous mass flow controllers were replaced with new units of the EL-FLOW Prestige series (*Bronkhorst*), which triggered the redesign of the gas distributor panel (see Fig. 5). In terms of safety, the current activity monitor and its sensor for monitoring the purge-gas-flow in WBGA/C41 were substituted with the new model, i.e., LB112 (*BERTHOLD*). Additionally, a new flow meter (KDG2251, *KOBOLD*) was implemented on the laboratory-side and was included together with the activity monitor in the new SPS control system. Thus, upon an activity increase in the purging gas of the cladding tube or in case of gas leakage, an interlock is triggered, which stops the product gas flow, closes the beam shutter in front of the ^{235}U-target assembly in the SINQ, and opens the pressure relief valves towards a filtered and monitored exhaust line. All system parameters and read-outs are constantly logged by a built-in archive function. The stand-alone control system for the beam shutter (VLD), located directly at the SINQ Sector 61, was implemented as it is at this point. A later upgrade is forseen, as its installation can proceed without further difficulties, since all required parts are accessible during normal SINQ operation.

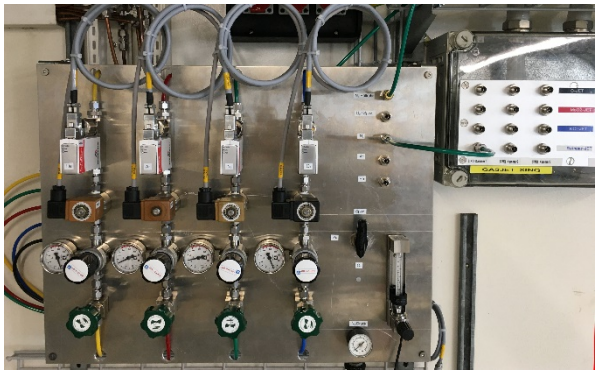

Fig. 5: Redesigned gas panel in WBGA/C41 for He, Ar, N_2, O_2, and a special gas (e.g., H_2/Ar-mixture); the feed to the target at Sector 61 at SINQ can be seen on the right hand side.

We highly acknowledge the internal technical support by LOG, NUM, and GFA, in particular, for their support of these revisions/upgrades.

[1] M. Wachsmuth et al., PSI Scientific Report 2000, Particles and Matter (2001), pp. 132.
[2] K. Toh et al., Proceedings of SPIE 6619 (2007).

DIRECT CATCH MEASUREMENTS AND RELATED CHALLENGES DURING CHEMISTRY EXPERIMENTS WITH THALLIUM

P. Steinegger (PSI), N. V. Aksenov, Yu. V. Albin, A. Y. Bodrov, G. A. Bozhikov, V. I. Chepigin, I. Chuprakov, S. N. Dmitriev, N. S. Gustova, A. V. Isaev, A. Sh. Madumarov, O. N. Malyshev, Y. Melnik, Yu. A. Popov, A. V. Sabelnikov, A. I. Svirikhin, M. G. Voronyuk, A. V. Yeremin (FLNR, JINR), T. K. Sato (JAEA), R. Dressler, R. Eichler, D. Herrmann, D. Piguet (PSI), P. Ionescu, B. Kraus (Univ. Bern & PSI), B. Gall, Z. Asfari (Univ. de Strasbourg)

Preparatory experiments for a future chemical characterization of Nh (Nh, $Z = 113$) are currently on-going at the Flerov Laboratory of Nuclear Reactions in Dubna, Russia. So far, three of these experiments were successfully carried out behind the velocity filter SHELS [1]. Details on the experimental setup as well as first results have been reported earlier [2]. The herein presented data regarding the conducted direct catch measurements were recorded in spring 2019.

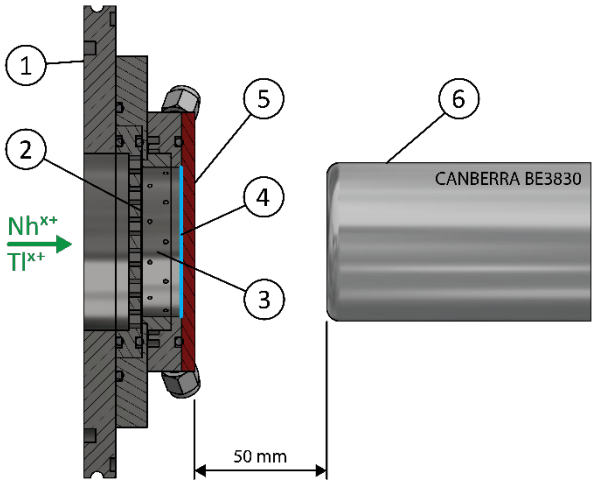

Fig. 1: Experimental setup used for the direct catch measurements, mounted in the focal plane of SHELS with the interface flange SHELS to gas-chromatographic setup (1), the 3.5 µm thin Mylar vacuum window (2), the evacuated area with the gas distributor ring (3), the position of the aluminum catcher foil marked in blue (4), the blind flange colored in red (5) and the HPGe γ-detector BE3830 (6) [not to scale] for the measurement of the equilibrium activities; the evaporation residues enter the setup from the separator side on the left side (see green arrow and labels) and were implanted in (4).

In order to establish the efficiency of the chemical synthesis, transport and subsequent characterization in using isothermal gas-adsorption chromatography, direct catch measurements were performed to determine the total delivered amount of the model isotope. These can be later compared against the collected fraction after the chemical separation stage for the chemical efficiency evaluation. ^{184}Tl was produced at the U400 accelerator facility of the Flerov lab in the heavy-ion-induced nuclear fusion evaporation reaction ^{141}Pr(^{48}Ti, 5n)^{184}Tl. The evaporation residues were separated from the primary ion beam as well as nuclear reaction byproducs using the above mentioned vacuum separator SHELS, passed through a 3.5 μm thin Mylar (*Goodfellow*) window and were finally implanted into a $\approx 11\ \mu$m thick commercial Al-foil (volume between vacuum window and blind flange evacuated). The collection foil was mounted directly after the gas-distributor ring on the blind flange (see Fig. 1). Thus, one collects the fraction of nuclear reaction producs, which are effectively available for the chemical experiment, mounted in the position of the red marked blind flange (see [2] for further details regarding the chemistry setup). By perfoming offline measurements of the collection foils regading the long-lived decay product ^{184}Ir ($t_{1/2} = 3.09$ h), the initially implanted amount of ^{184}Tl can be recalculated. However, cross section calculations for the above mentioned nuclear reaction (NRV-calculations, see [3] for more details) reveal possibly considerable cross-feeds from the 1p4n- and the 2p3n-channels (see Fig. 1), thereby populating directly the daughter nucleii ^{184}Hg and ^{184}Au in the ^{184}Tl decay chain (see Fig. 2). Whereas neutron evaporation channels can be predicted with rather good uncertainties for nuclear reactions such as the one used herein (good availability of experimental data), this does not hold for charged particle evaporation (larger uncertainties due to fewer experimental data). Even though the prediction might be not too reliable and possibly overestimate the production cross section for these proton/neutron-evaporations, the reaction channels need to be quantified nonetheless for the later inclusion in the calculation of the initially implanted ^{184}Tl.

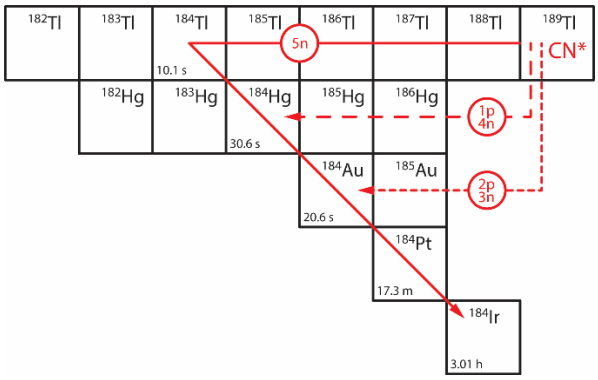

Fig. 2: Excerpt of the nuclide chart showing the different production pathways of ^{184}Tl (5n-channel), ^{184}Hg (1p4n-channel), and ^{184}Au (2p3n-channel), where the latter two feed the β^+-decay chain of ^{184}Tl to ^{184}Ir.

Therefore, a number of differently timed collections were performed. The ratios of the equilibrium activities of the short-lived radionuclides ^{184}Tl ($t_{1/2} = 10.1$ s),

^{184}Hg($t_{1/2}$ = 30.87 s), and ^{184}Au ($t_{1/2}$ = 20.6 s) were determined over online γ-spectroscopic measurements (portable broad energy Ge γ-detector BE3830, *CANBERRA*, see Fig. 1) directly behind the catcher foil (equilibrium conditions attained after ≈ 5 min, see Tab. 1). The additional activity input of ^{184}Hg and ^{184}Au from their respective, less reliably predicted reaction channels, can be then related to the one produced over the 5n-evaporation. These ratios served as crucial input for the data analysis (see below and Fig. 3) and can be used to derive relative cross section values for the 1p4n as well as 2p3n reaction channels (Tab. 1).

Tab. 1: Summary of the measured equilibrium activities A_{eq} as averaged value of five different direct catch measurements for the main contributors to the β^+-dacay along the isobar $A = 184$; σ_{rel} indicates the estaimated cross sections in [mbarn] for the direct production of ^{184}Hg (1p4n) and ^{184}Au (2p3n) relative to the cross section for the 5n evaporation channel leading to ^{184}Tl.

Radionuclide	A_{eq}, Bq	σ_{rel}, mbarn
Tl-184	600 ± 16	1.0 ± 0.0
Hg-184	2092 ± 53	7.3 ± 2.9
Au-184	3926 ± 88	2.0 ± 1.3

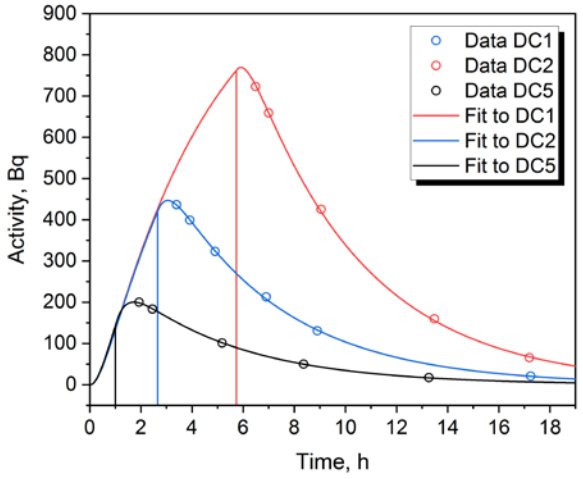

Fig. 3: Fits (lines) to the sequential offline measurements of long-lived ^{184}Ir (circles) of direct catch samples DC1 (t_{EOB} = 2.65 h), DC2 (t_{EOB} = 5.73 h), and DC5 (t_{EOB} = 1 h); statistical uncertainties are smaller than the symbols. The vertical lines indicate the different times for the end of bombardement (EOB) of the three direct catch measurments DC1, DC2, and DC5; $t = 0$ s marks the start of collection.

After the end of bombardment (EOB), the implantation foils were folded to a defined geometry and sequentially measured offline using γ-spectrometry (standard electrode coaxial HPGe γ-detector GC2018, *CANBERRA*). The sequentially obtained data points for each direct catch measurement were finally fitted using an analytical solution of ingrowth and decay of all involved radionuclides (see Fig. 3); the nuclear decay characteristics were taken from [4]. The herein presented direct catch measurements were carried out at almost equal ^{48}Ti^{20+}-ion beam intensities of around 3.6 μA.

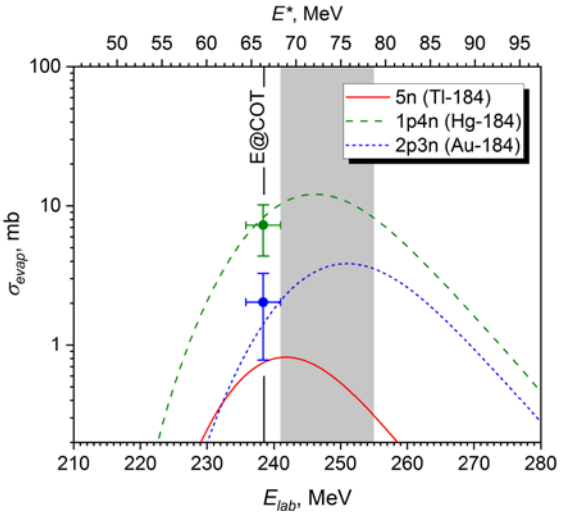

Fig. 4: Cross section calculations using the NRV web knowledge base on low-energy nuclear physics [3] for the nuclear reaction ^{141}Pr(^{48}Ti, 5n)^{184}Tl, showing the 5n-channel to ^{184}Tl (solid red line), the 1p4n-channel to ^{184}Hg (dashed green line), and the 2p3n-channel to ^{184}Au (dotted blue line); the vertical black line indicates the center of target energy, while the shaded region highlights the energy loss in the 2 μm thin titanium target backing. The two points represent (y-error at 68% c.i., half the target thickness as x-error) an estimate of the relative cross sections for the production of ^{184}Hg and ^{184}Au over the 1p4n-channel (green) and the 2p3n-channel (blue) respectively; both are calculated relative to the 5n evaporation channel.

The above determined relative cross section values and therewith calculated equilibrium activities of ^{184}Tl from the ^{184}Ir offline measurements can be later on used to estimate the efficiency of the chemistry setup (synthesis and chemical separation). However, due to the on-going data analysis, we refrain to discuss actual efficiencies any further. As for the up-coming beam time in April/May 2020, we will complement the applied procedure with direct catch measurements at different beam intensities. This will allow us to extrapolate to the typically increasing beam intensities over the course of the experiment. In addition we will perform a second set of measurements at the very end of the beam time (instead of at the beginning only) to consider the target stability throughout the duration of the experiment.

We acknowledge funding from the Swiss National Science Foundation (Grant P2BEP2 165403).

[1] A. G. Popeko et al., Nucl. Instrum. Meth. B **376**, 140 (2016).
[2] P. Steinegger et al., LRC Annual Report 2017, (2018), pp. 12-13.
[3] A. V. Karpov et al., Nucl. Instrum. Meth. A **859**, 112 (2017).
[4] C. M. Baglin, Nucl. Data Sheets **111**, 275 (2010).

FIRST RESULTS 2018/2019 FROM PREPARATORY EXPERIMENTS WITH THALLIUM

P. Steinegger (PSI), N. V. Aksenov, Yu. V. Albin, A. Y. Bodrov, G. A. Bozhikov, V. I. Chepigin, I. Chuprakov, S. N. Dmitriev, N. S. Gustova, A. V. Isaev, A. Sh. Madumarov, O. N. Malyshev, Y. Melnik, Yu. A. Popov, A. V. Sabelnikov, A. I. Svirikhin, M. G. Voronyuk, A. V. Yeremin (FLNR, JINR), T. K. Sato (JAEA), R. Dressler, R. Eichler, D. Herrmann, D. Piguet (PSI), P. Ionescu, B. Kraus (Univ. Bern & PSI), B. Gall, Z. Asfari (Univ. de Strasbourg)

Preparatory experiments for a future chemical characterization of Nh are currently on-going at the Flerov Laboratory of Nuclear Reactions in Dubna, Russia. The experimental setup as well as first conclusions have been presented earlier [1]. Therein, the authors reported on a relatively volatile chemical species, being readily transported under ambient conditions. At the same time, the synthesis and transport of thallium species according to the offline experiments from A. Serov et al. [2] were unsuccessful. The latter observation was explained by the different starting states in offline and online experiments, respectively. Unlike in offline-experiments with the release of elemental Tl from a metal matrix at high temperatures (oxidation state 0), an online approach is confronted with highly ionized evaporation residues from nuclear fusion evaporation reactions. This might lead to an unexpected formation of thallium species with the metal in an oxidation state +III instead of the dominant one +I. So far unknown chemical compounds such as $Tl(OH)_3$ or TlOOH might form under the applied conditions and thus, could explain the observation of a relatively volatile Tl-species during all previous beamtimes. In order to identify this chemical compound, further experiments as well as state-of-the-art theoretical calculations are needed. During the two follow-up experiments in Spring 2018 and 2019, we focused on the following points:

- Unambiguous synthesis and characterization of TlOH by using admixtures of reducing agents (i.e., H_2) in order to promote reduction from $Tl^{3+} \rightarrow Tl^{+}$.
- Further characterization of the observed relatively volatile Tl-species.

The application of H_2 comes with the disadvantage of less stopping power and thus a possible loss of incoming nuclear reaction products due to implantation into the walls of the recoil transfer chamber (RTC). A full depletion of almost any nuclear reaction products has been shown using only H_2 as a carrier gas (see Fig. 1). Therefore, only small admixtures of H_2 to the main carrier gas Ar were used. A sufficient stopping range was ensured *via* simulations with the SRIM-2013 software package [3] in combination with the correction factor for the stopping of ions in gases [4]. As a further admixture to the carrier gas, O_2 was used, acting as oxidizing atmosphere. Regarding the synthesis and characterization of TlOH in accordance with earlier studies presented in [2], the past experiments remained unsuccessful. The addition of H_2 as a reducing agent to the otherwise inert carrier gas did not lead to the intended reduction of the presumed case of $Tl^{3+} \rightarrow Tl^{+}$. Thus, for the fourth campaing taking place in April/May 2020, we plan to employ an additional oven section in front of the isothermal chromatography oven, which can be run at temperatures above 1000°C. In this way we will force the in the RTC thermalized and from there flushed out Tl-species over a Ti/Ta-foil at temperatures in excess of 1000°C (i.e., for an efficient desorption from the foil after reduction). In this way, we ensure the unambiguous reduction of thallium from a higher oxidation state to the aimed at elemental state, which was shown in [2] to react inevitably with quartz surfaces to form TlOH.

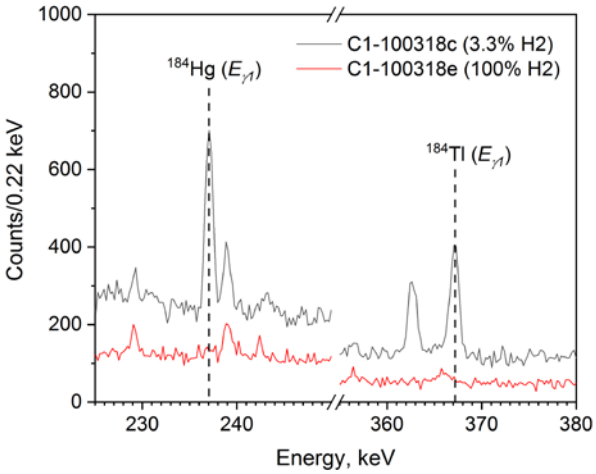

Fig. 1: Proof-of-principle γ-spectrometric measurements, showing the full depletion of the nuclear reaction products ^{184}Tl and ^{184}Hg by switching from a 3.3%-vol. admixture of H_2 to Ar (black excerpt of spectrum) to a 100% H_2 carrier gas (red excerpt of spectrum); due to the lower stopping force of a pure H_2 carrier gas, the in-coming nuclear reaction products are implanted into the walls of the recoil transfer chamber.

Concerning the further characterization of the observed volatile thallium species, a series of experiments at different gas compositions (i.e., different redox potentials) were conducted (see Fig. 2). For this purpose, the RTC as well as the isothermal chromatography section were kept at room temperature. First results show, that the relative yield after the isothermal chromatography stage shows a clear response to the applied chemical conditions and can be thus attributed to a chemical effect rather than a physical one, such as, e.g., different stopping ranges or aerosol transport. As it was shown, the addition of H_2O (see green right-hand scale in the upper panel of Fig. 2) as well as small admixtures of O_2 (see underlying bar plots, left-hand scale, upper panel in Fig. 2) proved to be beneficial for the transport of the synthesized, so far

unidentified, chemical compound of thallium. The observed effect has been studied in more detail. The data analysis is on-going and the results are prepared for publication.

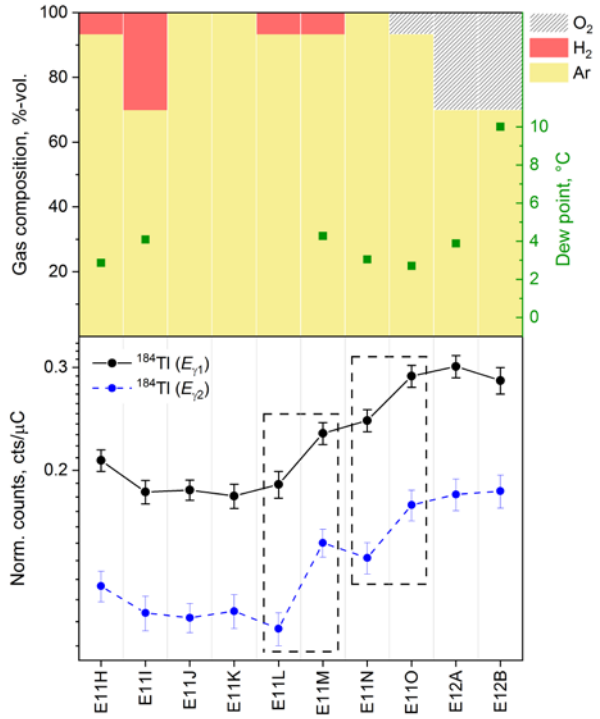

Fig. 2: Different experiments applying different gas compositions (O_2, H_2, and Ar) as well as H_2O-admixtures (top) and the correspondingly obtained production-normalized yield after the chemical separation stage for the two main γ-lines of ^{184}Tl (bottom); areas of interest have been edged with a dashed line (i.e., beneficial addition of H_2O and O_2).

We acknowledge funding from the Swiss National Science Foundation (Grant P2BEP2 165403).

[1] P. Steinegger et al., LRC Annual Report 2017, (2018), pp. 12-13.
[2] A. Serov et al., Radiochim. Acta **101**, 421 (2013).
[3] J. F. Ziegler et al., Nucl. Instrum. Meth. B **268**, 11 (2010).
[4] D. Wittwer et al., Nucl. Instrum. Meth. B **268**, 28 (2010).

NEUTRON CAPTURE CROSS SECTION OF ^{10}Be

M. Volknandt, A. Endres, P. Erbacher, M. Fix, K. Göbel, J. Glorius, T. Heftrich, E. Hrivula, C. Langer, R. Reifarth, S. Schmidt, B. Thomas, D. Veltum, M. Weigand, C. Wolf (Univ. Goethe), K. Eberhardt, C. Geppert, N. Wiehl (Univ. Mainz), N. Kivel, D. Schumann (PSI), S. Heinitz (SCK-CEN), A. Junghans (Helmholtzzentrum Dresden), F. Käppeler (KIT), A. Mengoni (CERN)

INTRODUCTION

The main goal in nuclear astrophysics is the explanation of the origin of the elements and to reproduce isotopic and elemental abundances we observe in the solar system and in the universe. Various processes assigned to different astrophysical scenarios are involved. The big bang nucleosynthesis and nuclear reactions contribute to the interstellar medium. Hence, for a successful reproduction of the observed abundances, there is a need for extensive experimental data on involved reaction rates [1].

In the scope of this article, neutron capture reactions on ^{10}Be have been studied by the means of the activation method [2] at the TRIGA reactor in Mainz, Germany. In 2014 the cross section of the reaction ^{10}Be(n,γ) was determined for the first time. To understand the differences of theoretical models to the first activation experiment, another activation experiment with improvements to the sample material and the method was performed in September 2016 at the TRIGA reactor in Mainz

Astrophysical aspects on the ^{10}Be(n,γ) reaction

The pattern of the solar abundances of nuclides features a conspicuous minimum in the region of the light elements Li, Be, and B. The main origin of these scarce elements are thought to be spallations of C, N and O in the interstellar and circumstellar matter by cosmic gamma rays. It is referred to as interstellar nucleosynthesis [3,4]. However, it is essential for the understanding of how the big bang nucleosynthesis and nuclear reactions in stars contributed to the observed abundances, to determine the involved capture reaction cross sections in this mass area. One of those, which has not been measured so far, is the ^{10}Be(n,γ) cross section. Figure 1 depicts the area of the lightest elements in the chart of nuclei along with the reaction of interest (black arrow) and the decay of the product (red arrow).

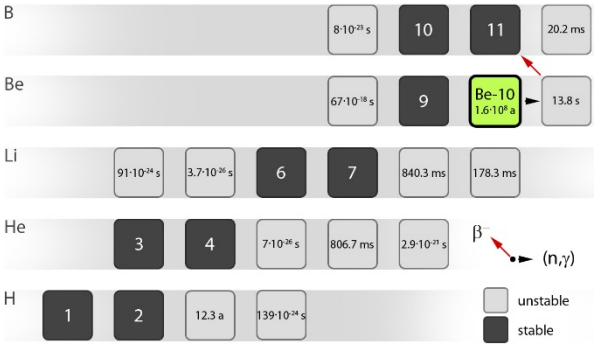

Fig. 1: Chart of the nuclides from hydrogen to boron. Stable isotopes are depicted as dark, unstable isotopes as light grey boxes. A neutron capture on ^{10}Be leads to ^{11}Be, which has a half-life of 13.8 s only and decays to ^{11}B.

The ^{10}Be sample

The BeO sample has been produced at PSI. Its weight was 8.93 mg including 6.6×10^{19} particles of ^{10}Be in the sample. It was produced at the PSI muon production facility via proton spallation in polychrystalline graphite and extracted using pyrolysis and chemical purification. The amount of ^{10}Be was determined via mass spectrometry and confirmed by total activity measurements [9]. Originally it was foam-like and after the first activation it turned to a white small-grained powder.

The activation experiment

The activation was performed at the TRIGA reactor in Mainz. In the permanent mode the reactor delivers a maximum of 10^{13} cm^{-2}s^{-1}. In the pulse mode of the reactor, for a time period of 30 ms, a thermal fluence of 10^{15} cm^{-2}s^{-1} can be reached. Using the pneumatic rabbit system, the sample can be transported into the reactor and back within seconds.

The sample was irradiated in a cyclic activation. The neutron fluence has been determined using monitors with well-known cross sections. In this case, gold and scandium were used together with the sample in a sandwich configuration. The thermal neutron fluences were in the order of 1×10^{14} and 8×10^{13} in case of the epithermal neutron fluences.

The number of produced ^{11}Be particles were identified by γ-ray spectroscopy using two $LaBr_3$ detectors in a head-to-head setup. Using the cadmium differential method, the thermal neutron capture cross section as well as the resonance integral could be determined. The analysis results in a preliminary thermal neutron capture cross section of

$$o_{therm} = 1.309 \text{ mb}$$

and a resonance integral of

$$I_{res} = 1.005 \text{ mb}.$$

The data evaluation is currentliy ongoing. Uncertainties of less than 10% are expected. Figures 2 shows the new experimental results.

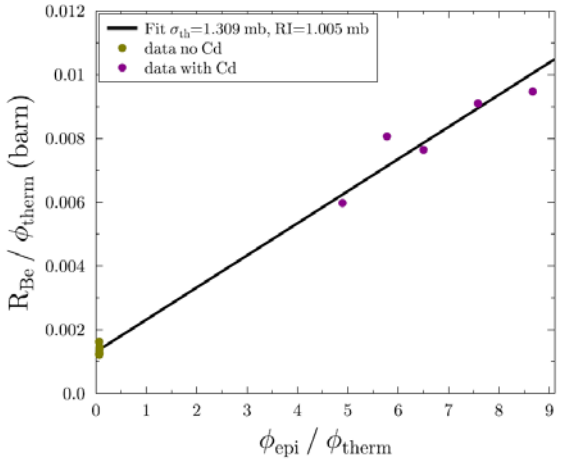

Fig. 2: The activation ratio over the integrated thermal flux plotted against the epithermal to thermal flux ratio. The resulting linear fit provides both cross sections as its variables. The activations without cadmium shielding can be seen in green, those with cadmium shielding in purple.

SUMMARY

An activation experiment was performed to determine the neutron capture cross section of ^{10}Be. The first measurement in 2014 showed a discrepancy between theory and experiment. However, the thermal cross-section and the resonance region could not be disentangled. A new ^{10}Be sample with a higher purity and higher number of ^{10}Be particles was produced by S. Heinitz at PSI. In 2016 the new sample was additionally exposed to a higher neutron flux and thus it was finally possible to determine the thermal neutron capture cross section and the resonance integral of the reaction ^{10}Be(n,γ).

[1] E. M. Burbidge, et al. Rev. Mod. Phys. **29**, 547 (1957).
[2] F. Käppeler et al., Rev. Mod. Phys. **83**, 157 (2011).
[3] D. Thomas et al., arXiv preprint astro-ph/9206002 (1992).
[4] A. Coc et al., Astrophys. J. **744**, 158 (2012).
[5] S. Heinitz et al. Appl. Radiat. Isot. **130**, 260 (2017).

DEVELOPMENT OF AN INTENSE ^{10}Be RADIOACTIVE BEAM

E. A. Maugeri (PSI), P. Figuera, L. Cosentino (INFN-LNS Catania), A. Di Leva (INFN Napoli), A. Di Pietro, M. Fisichella (INFN-LNS Catania), L. Gialanella (INFN Napoli), S. Heinitz (PSI & SCK-CEN), M. Lattuada, C. Marchetta, S. Marletta, D. Mascali, A. Massara (INFN-LNS Catania), D. Schumann (PSI), F. Tudisco (INFN-LNS Catania)

This manuscript reports on the development of an intense ^{10}Be beam at the LNS Tandem accelerator in Catania, Italy.

The beam was obtained "off-line" accelerating high purity ^{10}Be, previously separated via radiochemical methods. ^{10}Be beams will be used in several relevant experiments, which could shed light on different long lasting issues of nuclear structure and nuclear reaction dynamics, see e.g. [1].

The Isotope and Target Chemistry group at PSI was responsible for the preparation of the ^{10}Be cathodes to be used in the LNS Tandem sputter source. Specifically, ^{10}Be was extracted from a decommissioned polycrystalline graphite target, previously used at the SμS muon source for the production of muons, following the method developed in our laboratory and described in [2]. The resulting solution of $Be(NO_3)_2$, with a specific ^{10}Be activity of 0.25 kBq μL^{-1}, was used to prepare two different kind of ^{10}Be cathodes, with 100 kBq and 200 kBq of ^{10}Be, respectively. In particular, concentrated NH_4OH (anhydrous, ≥ 99.98, Sigma-Aldrich) was added to a $Be(NO_3)_2$ solution, with the needed ^{10}Be activity, in a 1:1 molar ratio. The resulting solution, $Be(OH)_2$, was then heated at 500 °C for 10 hours to obtain BeO. The obtained BeO was recovered, mixed with Ag in order to enhance electric and thermal conductivity, placed in a copper cathode and compacted applying a force of two tons by means of a manual hydraulic press (Specac, Atlas Manual Hydraulic Press).

Several preliminary tests were performed to optimise the ^{10}Be production efficiency at the Tandem sputter source (860C from High Voltage Engineering). These tests were performed with ^{9}Be in the same amount as foreseen for ^{10}Be.

The first tests were devoted to optimize the cathode geometry, resulting in a copper cylinder 13 mm long with a diameter of 9.5 mm. A small hole, 2 mm large and 2 mm deep, was drilled on one side of the cylinder to contain the BeO-Ag mixture. A very important improvement in terms of beam current stability was achieved covering the surface of the copper cathode with a thin layer of gold, which probably inhibits the potentially deleterious diffusion of beryllium into the copper bulk.

Tests were also performed changing the mass ratio BeO:Ag. In these tests it was found out that the best results were obtained by adding Ag in mass ratio BeO:Ag= 1:10. In particular, 1/3 of the Ag mass was added before the thermal treatment at 500 °C, while the remaining 2/3 was added in a second moment, before the final pressing.

After these preparatory tests, ^{10}Be cathodes, resulting from this implementation process, were used to perform the first tests aimed to accelerate $^{10}Be^{+4}$ at an energy of 54.4 MeV. This energy was achieved with a terminal voltage of about 12.5 MV. In these tests, the extracted molecular ions $^{10}BeO^{-}$ were injected into the Tandem and broke up crossing the stripper foil in the Tandem HV terminal, forming ^{10}Be and ^{16}O positive ions with different charge states. The $^{10}Be^{+4}$ beam of interest was then selected by using the analysing magnet after the Tandem and found to be 25% of the total ^{10}Be amount in the different charge states. In order to investigate on the beam purity, we reduced the intensity down to about 100 ^{10}Be/s and sent the beam onto a DE(17μm)-E(500 μm) Si telescope. This measurement showed a pure ^{10}Be beam with a ^{10}B contamination of about 0.15%.

^{10}Be beams, obtained with the described developed method, have already been successfully used to perform two experiments to investigate the cluster structure in ^{14}C and ^{15}C. In these experiments we used $^{10}Be^{+4}$ beams, with an average intensity of 1.7 enA after a collimation system consisting of a first square collimator of 4x4 mm followed by a circular collimator of 3 mm diameter placed 1.5 m downstream the first one. To obtain the above intensity the cathodes (containing 200 kBq of ^{10}Be) were changed every 4 days during the data taking. To our knowledge, this is the most intense accelerated ^{10}Be beam developed worldwide for nuclear physics studies

ACKNOWLEDGEMENT

The authors wish to thank Tanja Wieseler for her help in preparing the ^{10}Be samples and Niko Kivel for the analysis of the sample content.

---

[1] M. Freer et al., Phys. Rev. C **90**, 054324 (2014).

[2] S. Heinitz et al., Appl. Radiat. Isot. **260**, 130 (2017).

PREPARATION OF A ^{10}Be TARGET ON A CARBON BACKING FOR NUCLEAR STRUCTURE MEASUREMENTS

L. Tetley (Univ. York), E. A. Maugeri (PSI), M. Petri (Univ. York), D. Schumann (PSI), A. Lagoyannis (NCSR Demokritos)

Understanding nuclear structure and dynamics in terms of the fundamental interactions between protons and neutrons is one of the overarching goals of nuclear science. To this end, nuclear theory is developing chiral effective field theory (EFT) [1,2], an unified approach to nuclear forces, where two-nucleon (NN), three-nucleon (3N) and higher-body forces are derived within a consistent, systematically improvable framework. Neutron-rich oxygen isotopes are particularly fruitful candidates to test ab initio theory. First valence-space calculations with NN+3N forces were able to explain, for the first time, the location of the oxygen dripline at ^{24}O [3]. More recently, large-space ab initio calculations, where all nucleons are treated as explicit degrees of freedom, have confirmed those early results [4-6]. An important next step is to benchmark these calculations and the role of 3N forces against other observables, which are sensitive to physics beyond what is relevant for excitation energies alone. Indeed, previous work on the structure of ^{21}O has demonstrated the sensitivity of the 3N forces to spectroscopic observables such as level lifetimes [7]. We will perform an ambitious measurement of lifetimes of excited states in ^{22}O, populated via the ^{10}Be(^{14}C,2p)^{22}O fusion-evaporation reaction, employing a radioactive ^{10}Be target [8].

The production and characterisation of the ^{10}Be target, represents the last challenge to the experiment going forward. In addition, the successful production of this ^{10}Be target could lead to a greater experimental accessibility to the light neutron-rich region, for future nuclear structure experiments.

^{10}Be targets will be produced at PSI, where ^{10}Be is chemically extracted and purified from decommissioned SμS muon sources consisting of proton irradiated polycrystalline graphite targets [9].

The first test targets were prepared depositing a drop of ^{nat}Be$(NO_3)_2$ ICP-standard solution (1000 mg/L Be in in 2% nitric acid,) doped with ^{7}Be (produced and purified at PSI [10]) onto 75 μm thick graphite backing. The ^{7}Be ($t_{1/2}$ = 53.22 days) activity was monitored by means of a coaxial HPGe-detector, to evaluate material lost during all the steps of the target preparation. The concentration of the $Be(NO_3)_2$ initial solution was adjusted to obtain a 500 μg/cm^2 thick beryllium layer deposited on the backing. The ideal target should contain only carbon and beryllium atoms, thus it was necessary to remove the nitrate groups and to reduce considerably the concentration of oxygen and water.

The $Be(NO_3)_2$ drop was treated with small amounts of elemental sodium for reducing the water contents ($2H_2O + 2Na \rightarrow 2NaOH + H_2$) and converting $Be(NO_3)_2$ in Be and $NaNO_3$. However, beryllium reacts with water and/or oxygen forming BeO. The resulting solution, standing onto the backing, was placed in a tubular furnace and heated under dry hydrogen flux (25 ml/min) up to 70 °C for 1 hour and after up to 900 °C for two hours, then the temperature was fast reduced to 25 °C. All the products of the redox reactions are evaporated during the thermal treatment but BeO, which diffuses into the first layer of the carbon backing bulk. No variation of the ^{7}Be activity was measured before and after each step. The resulting samples consisted in graphite backing with a layer of BeO incorporated near to their surface. The carbon layers standing above the beryllium layer, will prevent lost and/or contamination of ^{10}Be during the envisaged experiment.

A Nuclear Reaction Analysis (NRA) experiment was carried out at NCSR "Demokritos" in Athens, to characterise the beryllium target and carbon backing, Figure 1. Using the Tandem 5.5 MV accelerator, a 1.35 MeV deuteron beam, with a beam current of ~2 nA, was impinged upon the target and backing. The deuterons undergo a neutron transfer reaction with the nuclei in the target, emitting protons with energies up to 10 MeV, which were detected by a silicon detector at 170^o to the beam axis. The energy of the detected protons allows for the determination of the target atoms, as well as their depth within the target. The beam was focussed on three different positions on the target surface, on three identically prepared samples. This not only allowed for the spatial and depth profiling of the target atoms, but also provided a way of testing the consistency of the production method.

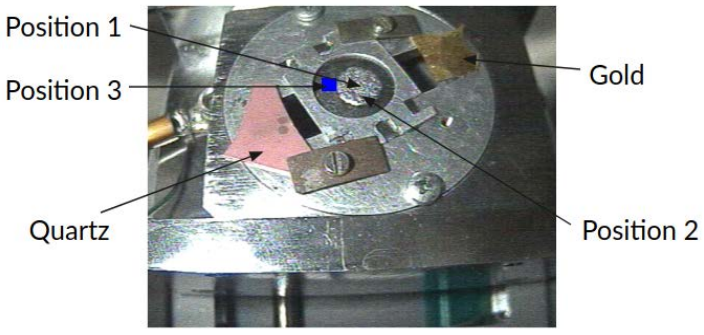

Fig. 1: Beryllium target and carbon backing on the target holder. The measurement positions are highlighted as are the gold and quartz used for calibration.

The analysis was carried out using SimNRA to reproduce the proton spectra by defining a series of layers of different materials. Each layer corresponds to a certain amount of material in the target, with the first layer being the target surface and the last layer being the target back (the position when the beryllium concentration goes to zero). In this way, the elemental concentrations and depths within the target were

determined. Figure 2 displays the material depth distribution of the target atoms for sample 1 position 1 (centre of the target).
Comparing the distribution plots corresponding to the other positions and samples, we see a high degree of consistency, not only between the positions on the same sample, but also between samples. Between the centre and the edge of the target (positions 1 and 2 respectively), the amount of beryllium varies by about ~1 μg/cm^2, with a slightly higher concentration of beryllium on the edge of the target. The increased concentration of beryllium at position 2 was likely due to the dynamics of the droplet, where the centre of the droplet collapses pushing the residue to the edges.

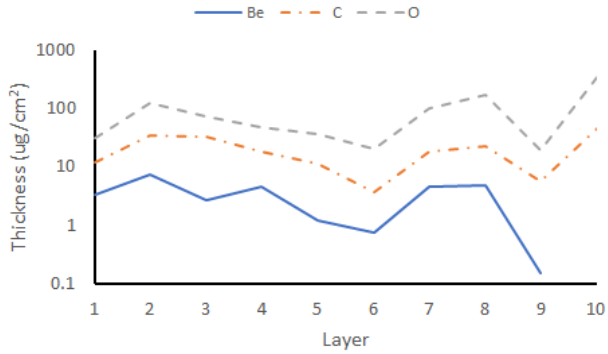

Fig. 2: The material density profile of carbon, beryllium and oxygen for the centre of sample 1.

In all three of the samples, the amount of beryllium at position 3 (outside the target) was below any reasonable analytical limit. This confirms that diffusion of the beryllium out of the target during production is minimal. In addition, from Figure 2 we can determine that the amount of carbon detected when the beryllium concentration goes to zero is ~200 ug/cm^2. This is about ~2% of the carbon in the backing, suggesting that the beryllium is confined to the surface of the carbon backing. The spectra also provide evidence of the purity of the target-backing setup, with only oxygen, carbon and beryllium present. There is no evidence of any nitrogen from the $Be(NO_3)_2$ solution or of any contamination from the target synthesis procedure.
The concentration profile of oxygen is also included in Figure 2. However, these data points have a large associated uncertainty, as the energy of the deuteron beam was selected to enhance the detection of beryllium and carbon. The sharp increase in oxygen concentration towards the back of the target is likely due to the oxygen already present on the surface of the carbon backing before the $Be(NO_3)_2$ solution was deposited.
In summary, the targets produced and tested here look promising for the ^{22}O lifetime measurement. The key properties required of the target i.e. homogeneity, purity and the confinement of the beryllium on to the surface of the carbon backing are all met.

---

[1] E. Epelbaum et al., Rev. Mod. Phys. **81,** 1773 (2009).
[2] R. Machleidt et al., Phys. Rep. **503**, 1 (2011).
[3] T. Otsuka et al., Phys. Rev. Lett. **105**, 032501 (2010).
[4] H. Hergert et al., Phys. Rev. Lett. **110**, 242501 (2013).
[5] A. Cipollone et al., Phys. Rev. Lett. **111**, 062501 (2013).
[6] K. Hebeler et al., Ann. Rev. Nucl. Part. Sci. **65**, 457 (2015).
[7] S. Heil, et al., arXiv:1912.02884, submitted to Phys. Lett. B.
[8] M. Petri, experiment #1732, Argonne National Laboratory (2020).
[9] S. Heinitz et al., Appl. Radiat. Isot. **260**, 130 (2017).
[10] D. Schumann et al., Radiochim. Acta **101**, 509 (2013).

^{32}Si SEPARATION AND PURIFICATION FROM PROTON IRRADIATED METAL VANADIUM MATRIX

I. Mihalcea (PSI), M. Veicht, A. Pautz (EPFL & PSI), D. Schumann (PSI)

INTRODUCTION

The SINCHRON project has one main goal, the half-life ($t_{½}$) redetermination of ^{32}Si. Previous experimental attempts gave $t_{½}$ values that suffer from high dispersity among each other and high uncertainty [1]. Accurate determination of this specific constant would turn ^{32}Si into a perfect isotopic dating tool for environmental samples, filling the dating gap between 100 and 1000 years back.

One of the major challenges of the project is the separation and purification of silicon from the complex vanadium matrix. From the variety of Si specific separation methods, only two fitted our matrix constraints. First was Si distillation as a SiF_4 volatile specie. After experimenting on it, this method was discarded due to low yields (25% average) and due to tritium contamination of the final solution. The second method was ion exchange chromatography (EC). A modified method from the literature [2] was used together with other techniques to build a functional separation scheme (figure 1). The method employs the binding properties of SiF_6^{2-} on strong anion exchange resins and relies, as well, on non-ionic properties of hydrolyzed silica.

EXPERIMENTAL

For all the experimental steps required in assessing the feasibility of the method, inactive model solutions were used. The main analytical method in matrix components analysis was Inductively Coulped Plasma – Optical Emission spectroscopy (ICP-OES) conducted on an Agilent 5110 spectrometer. The initial matrix was constituted by dissolving a pure vanadium disc (Goodfellow 0.41 g on average, 1.0 mm thickness, 9.2 mm diameter) in 5 ml 1:1 HCl/HNO_3 8M solution followed by the addition of a reducing agent (N_2H_4) and of standard ICP solutions (Sigma Aldrich) of the remaining matrix constitutents. The last step is a dilution to a final volume of 100 ml. The employed ion exchange resins were DOWEX® 50WX8-200 H^+ as a strong cation exchanger and AG® 1-X8 F^- as a strong anion exchanger.

From the initially obtained solution, aliquots of 10 ml were taken and subjected to the separation steps for parameters optimization. After dissolution, vanadium is present in two oxidation states: +4 and +5 from wich the later, regardless of pH, has a very low retention on strong cation exchangers. To reduce V^V, hydrazine was chosen as an optimal reducing agent. It has a strong reducing capacity (4 electrons per molecule), reaction kinetics is fast and resulting decomposition products do not influence further procedures. The initial twenty-fold dilution is required to bring down the solution acidity to a point where the cation exchanger can optimally trap all the cationic elements of the matrix. By its molecular nature $Si(OH)_4$ passes through with no retention.

The second step of separation is tritium removal. This consists in an evaporation to dryness followed by three successive additions of water and re-evaporations, all under nitrogen flow. No losses of silicon were observed after this step.

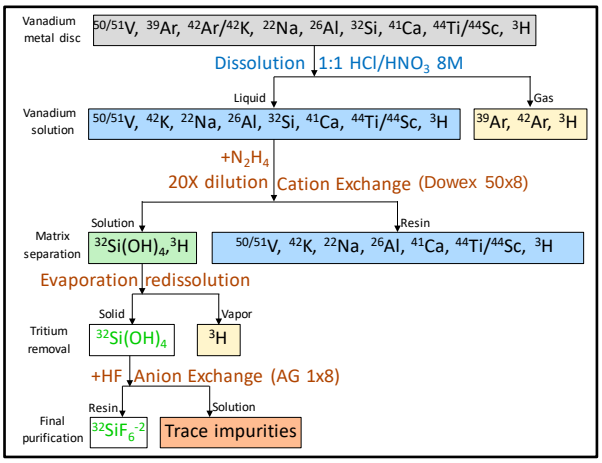

Fig. 1: Overview of ^{32}Si separation and purification from a complex vanadium matrix.

The final purification consists in dissolution of silica in 1M HF solution followed by an anion exchange separation:

$$Si(OH)_4 + 6HF \rightarrow H_2SiF_6 + 4H_2O$$

Under these conditions, the only anionic radioactive species are $HSiF_6^-$ and $H_2PO_4^-$. Both ^{32}Si and its daughter ^{32}P are retained on the strong anion exchange resin in the F^- form and both are easily eluted as pure fraction with a 0.5M HNO_3 solution.

RESULTS AND DISCUSSION

Once full optimization was done, the method has been applied to the active discs, containing ^{32}Si. This isotope was generated by proton irradiation of vanadium discs through spallation: $^{51}V(p,x)^{32}Si$. The irradiation conditions were described in a previous report [3].

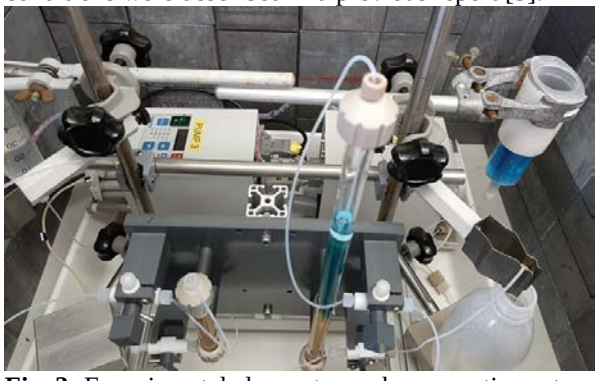

Fig. 2: Experimental chromatography separation setup: cation exchange column (right) and anion exchange column (left).

The dissolution process, this time took place in a nitrogen purge, open loop, system that ends with a water bubler for ^{3}H capture, followed by a charcoal trap for $^{39}Ar/^{42}Ar$. Gamma spectroscopic analysis of the trap, following the experiment shows the presence of ^{42}K, daughter of ^{42}Ar.
After the cation exchange separation, the active matrix is eluted from the resin with 3 M HNO_3 solution and stored for further processing of other nuclides of interest such as $^{44}Ti/^{44}Sc$ pair.
In the anion exchange separation step, both Si and P are anionic and do bind with different strengths to the resin, resulting in a partial separation of the two. Since ^{32}P, the daughter of ^{32}Si is only partially separated; certain activity measurements such as liquid and plastic scintillation can only be performed after the time reachieving equilibrium has passed. Other atom counting measurements such as ICP-MS and AMS can be performed immediately since there are no interferences with ^{32}P. A picture of the separation apparatus, containing both cation and anion exchange chromatography columns is presented in figure 2.

CONCLUSION AND OUTLOOK

The proposed method for separation and purification of ^{32}Si from a complex vanadium matrix was tested and optimized on model inactive solutions. Analytical results were obtained by ICP-OES. Further on, the same method was applied to the active sample resulting in a pure $^{32}Si/^{32}P$ fraction.
Since on the final solution, multiple activity and atom counting measurements will be performed, the properties of this solution should include no volatility, no loss of Si on drying the sample and long time solution stability (no polymerization, no precipitation). Currently in the final fraction, ^{32}Si is present as a hexafluoride anion, which is both volatile and unstable upon heating; hence, the future focus of our work is sample conditioning for long-term storage stability.

ACKNOWLEDGEMENT

This project is funded by the Swiss National Science Foundation (SNSF) as part of SINERGIA (No.177229).

This project has received funding from the European Union's Horizon 2020 research and innovation programme under the Marie Skłodowska-Curie grant agreement No 701647.

---

[1] L. K. Fifield & U. Morgenstern, Quaternary Geochronology, 400-405 (2009).
[2] R. D. Schink, Radiochemistry of Silicon, U. S. Atomic Energy Commission (1968)
[3] M. Veicht, M. Mihalcea, D. Schumann, A. Pautz, PSI Annual Report, Laboratory of Radiochemistry, (2018), pp. 38-39.

DEVELOPMENT OF A WET-CHEMICAL SEPARATION PROCESS FOR THE DETERMINATION OF THE REACTION CROSS SECTIONS OF ^{26}Al, ^{41}Ca AND ^{32}Si FROM PROTON-IRRADIATED VANADIUM SAMPLES

M. Veicht (EPFL & PSI), S. Chen (ETHZ & PSI), I. Mihalcea, D. Schumann (PSI), R. Michel (Leibniz Univ. Hanover), E. Strub (Univ. of Cologne), H.-M. Prasser (ETHZ)

INTRODUCTION

A wet-chemical separation process for ^{26}Al ($t_{1/2}$ = 7.17×10^5 years), ^{41}Ca ($t_{1/2}$ = 9.94×10^4 years), and ^{32}Si ($t_{1/2}$ = 1.44×10^2 years) from proton-irradiated vanadium samples is presented. ^{26}Al and ^{32}Si are continuously produced by cosmic-ray-induced spallation of argon in the atmosphere. In contrast, ^{41}Ca is produced by neutron activation of ^{40}Ca. Therefore, most of its production is in the upper metre of the soil column, where the cosmogenic neutron flux is still sufficiently strong.

On the one hand, all three radioisotopes are cosmogenic nuclides and thus are widely present on Earth due to their natural occurrence; however, only in very little amounts. On the other hand, certain nuclear production routes allow the artificial production of these nuclides, in order to faciliate a variety of applications. In this regard, with the development of new, large-scale facilities for several scientific purposes, like spallation neutron sources (SINQ | Switzerland, ESS | Sweden, CSNS | China), but also new energy production and waste mangement concepts such as accelerator driven systems (ADS), the characterization of accelerator waste is more and more in the spotlight of research (MYRRHA, Belgium) [1]. Different from the treatment of waste from nuclear power plants, where the radionuclide inventory is well-known, the situation in the case of activated material from accelerators is much more complicated regarding the composition of the nuclide inventory. To access information of such an inventory, a separation method of the bulk matrix is needed in order to obtain the different chemical elements in a pure state.

EXPERIMENTAL

Measurement techniques

The determination of radionuclides with very long half-lives and/or hard-to-measure radiation is very challenging. Therefore, techniques based on counting atoms instead of decays like accelerator mass spectromery (AMS) proved to be the better approach. Favourable for a chemical separation process, AMS does not require the knowledge of chemical yields, because an isotopic ratio is eventually determined.

Chemical separation techniques

The sample preparation is described elsewhere [2]. Generally, before the chemical separation, 2 mg of each element, stable aluminium, calcium, and silicon in form of ICP-Standard solutions (Merck KGaA, Germany) were added to each sample solution in order to adjust an isotopic ratio conveniently measureable by AMS. For the separation procedure, tailor-made PMMA-columns were utilized, with a total length of 200 mm (Dowex® 50WX8-200) and 100 mm (for DGA), respectively.

For the development of the separation process, inactive model solutions with similar concentrations and molarities were used to mimic the sample`s composition. To evaluate the separation process, obtained fractions of all previous experimental approaches were analyzed with inductively coupled plasma optical emission spectrometry (ICP-OES) using an Agilent 5110 (Agilent Technologies Inc., U.S.A.).

Separation Step I: ^{32}Si-Fraction

The initial sample solution was diluted to 200 mL (≈0.4 M [H^+]) and 2 mL of 1 M L-ascorbic acid (Merck KGaA, Germany) were added to reduce vanadium(V) to vanadium(IV). This solution was passed through the strongly acidic cation exchange resin Dowex® 50WX8-200 (Merck KGaA, Germany) in H^+-form. To quantitatively recover Si, the column was washed with additional 30 mL of ultrapure water.

Separation Step II: ^{41}Ca-Fraction

After the silicon fraction was gathered, all elements that were bound to the cation exchange resin, were eluted with 50 mL 3 M HNO_3. To separate calcium, the non-branched DGA (*N*,*N*,*N'*,*N'*-tetra-n-octyldiglycolamide) resin (TrisKem International SAS, France) was used. With 20 mL of 3 M HNO_3, the column was cleaned from remaining matrix-components, so that the finally gathered fraction comprised 70 mL 3 M HNO_3. Subsequently, the elution of calcium from the DGA-column was achieved using 30 mL of 3 M HCl.

Separation Step III: ^{26}Al-Fraction

Upon the addition of 7 mL H_2O_2 (30% w/v, Merck KGaA, Germany) to the 70 mL solution, its color turned red. Subsequently, this solution was heated in a hot water bath (≈70 °C) to facilitate the decomposition of surplus hydrogen peroxide. Afterwards, the heated solution was placed into an ice bath to prevent further disintegration of H_2O_2. In order to separate aluminium from the bulk vanadium, this solution was diluted to 310 mL (≈ 0.75 M [H^+]). After the initial solution passed through, a gradual elution was achieved by a step-wise use of 0.75 M / 1 M / 3 M HNO_3 in which aluminium was finally collected with 30 mL of 3 M HNO_3.

RESULTS AND NEXT STEPS

Figure 1 summarizes the separation procedure, which allowed the selective removal of aluminium, calcium, and silicon. With the demonstrated procedure, it was possible to obtain very pure fractions of Al and Ca with a reliable high recovery yield (> 95%) and basically no further impurities. Silicon was recovered as neutral $Si(OH)_4$ and hence not retained on Dowex® 50 (Fig. 2).

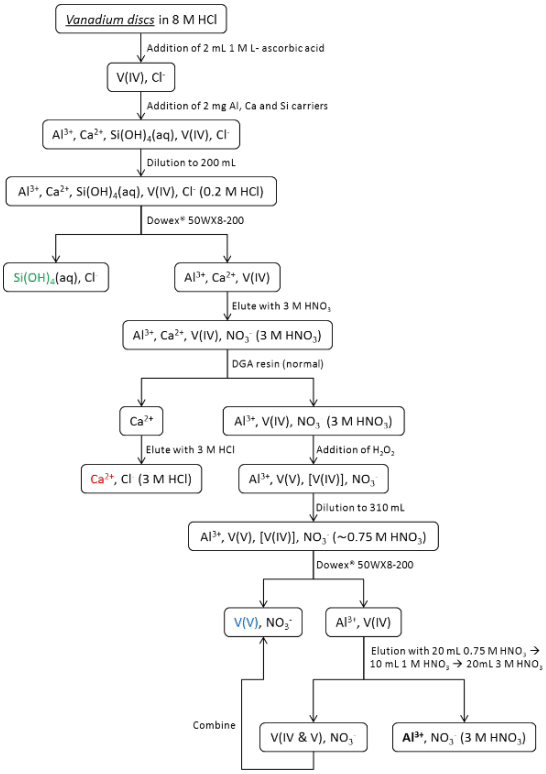

Fig. 1: Tree diagram of the wet chemical separation process. Aluminum is shown in bold, calcium, silicon and vanadium fractions are shown in red, green and blue, respectively.

The separation of calcium was achieved on DGA (Fig. 3), as calcium shows a very high affinity in 3M HNO_3 [3]. A cleaning step (3M HNO_3, from 50 to 70 mL) was introduced to keep the Ca fraction reliably clean from vanadium(IV,V) traces. Finally, Ca was eluted with 30mL of 3M HCl. In order to separate aluminium, the initial addition of H_2O_2 to the matrix turned vanadium mostly into vanadium(V) and concurrently into the oxoperoxo species ($[VO(O_2)]^+$). Vanadium(V) shows only a very low retention in 0.75M HNO_3 on Dowex® 50, whereas Al is still retained. To remove also traces of V(IV), a gradual increase of the HNO_3-concentration was necessary and thus allowed to achieve a complete separation. In a next step, AMS measurements will be carried out, once all the samples are prepared. This will cover the experimental procedures in order to obtain Al_2O_3 (s), CaF_2 (s), and SiO_2 (s), respectively. Finally, the results will be used to determine production cross-sections of those isotopes, which will in turn address the lacking excitation functions $^{nat}V(p,x)^{26}Al$, $^{nat}V(p,x)^{41}Ca$ and $^{nat}V(p,x)^{32}Si$ in previous studies [4].

ACKNOWLEDGEMENT

This project has received funding from the European Union's Horizon 2020 research and innovation programme under the Marie Skłodowska-Curie grant agreement No 701647.

[1] H. A. Abderrahim et al., Nucl. Instrum. Meth. **463**, 487 (2001).

[2] S. Chen, Master`s thesis, ETHZ (2019).

[3] C. Dirks-Fandrei, PhD thesis, University of Marbug (2014).

[4] R. Michel et al., Nuclear Physics A, **441**, (1985).

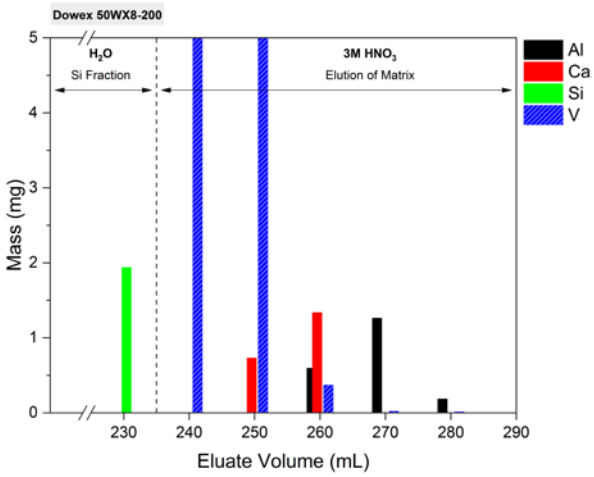

Fig. 2: Exemplary elution profile of the initial separation to obtain the Si-Fraction (green).

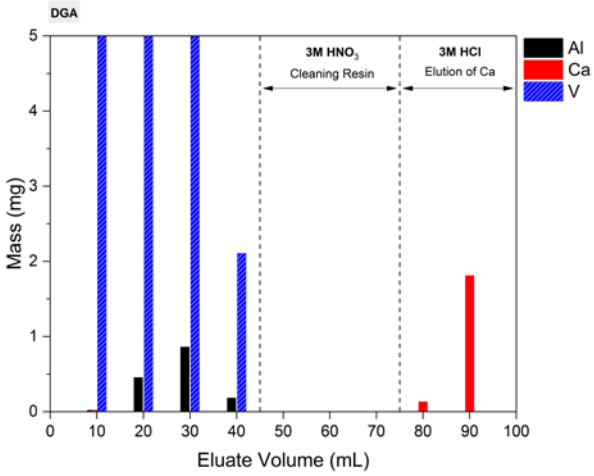

Fig. 3: Exemplary elution profile for the calcium fraction (red).

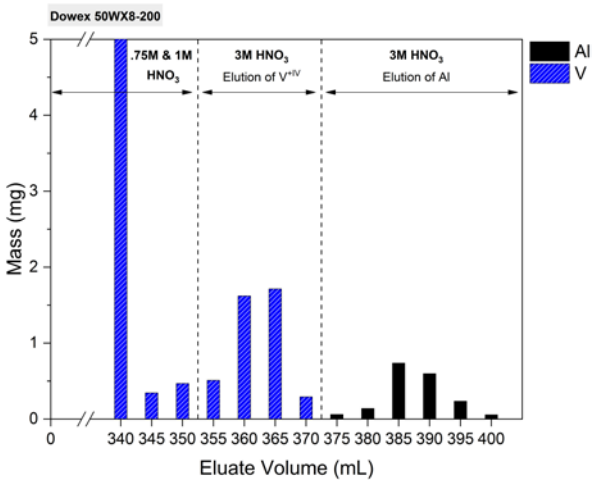

Fig. 4: Exemplary elution profile for the aluminium fraction (black).

EXTRACTION AND SEPARATION OF Sm, Gd, Tb AND Dy FROM PROTON IRRADIATED Ta SAMPLES

N. M. Chiera (LRC/PSI), Z. Talip (CRS/PSI), D. Schumann (LRC/PSI), A. Fankhauser, P. Sprung (AHL/PSI)

In the framework of the ERAWAST[1] initiative, a stepwise procedure for the extraction and recovery of purified lanthanides from highly activated metallic tantalum pieces from STIP II [1] was developed. The ultimate goal of this project is to perform high precision half-life ($t_{1/2}$) measurements of ^{146}Sm, ^{148,150}Gd, ^{157,158}Tb, and ^{154}Dy. As a project follow-up, half-life measurements of ^{137}La, ^{145}Pm, and ^{163}Ho are envisaged as well. For isotopes with $t_{1/2}$ of considerably more than 100 years, the so-called «direct method» is applied. This consists on the determination of the number of atoms of interest (N) using MC-ICP-MS, followed by the measurement of its actitivy (A). From $t_{1/2} = N*\ln 2/A$, a reliable half-life value, with an uncertainty below 5%, can be obtained. For radionuclides with $t_{1/2} \leq 100$ years, decay measurements can be performed. In this case, a source with the radionuclide of interest is prepared (e.g., *via* molecular plating), and its decay is monitored with periodic measurements over a time span of at least a year. Also with this method, uncertainties below 5% can be reached.

Here, the development of a separation method of lanthanides (Lns) fractions (specifically, Sm, Gd, Tb, and Dy) from Ta irradiated samples is presented. In a previous work [2], a method for the isolation of Lns from the Ta matrix material *via* formation of aqueous insoluble fluoride salts (LnF_3) was developed. During the LnF_3 precipitation process, insoluble HfF_4 and BaF_2 were formed as well. The fluoride precipitate was rinsed, separated from the surnatant, and successively dissolved in a mixture of 6 M HNO_3 and 0.5 M H_3BO_3. Then, two different procedures (Method A and Method B, depicted in Fig. 1) using cation exchange resins were applied for the sequential separation of each lanthanide fraction from the fluoride precipitate.

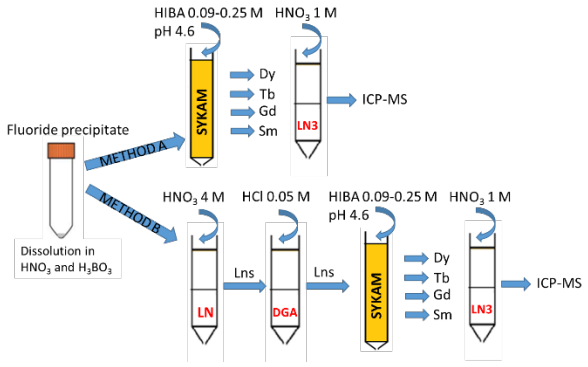

Fig. 1: Method A: two-steps separation procedure (SYKAM+LN3 resins); Method B: four-steps separation procedure (LN+DGA+SYKAM+LN3 resins).

Chemical separations were monitored by γ-spectroscopy. For the purpose, ^{166m}Ho, ^{159}Dy, ^{153}Gd, and ^{145}Sm were added as γ-tracers. An example of the separation profile with SYKAM resin and HIBA as eluent (pH = 4.6) is presented in Fig. 2. Due to the lack of Nd and La γ-emitter tracers, these elements were included in the Pm fraction.

The Dy, Tb, Gd and Sm fractions separated with the two different methods were analyzed by Inductively Coupled Plasma Mass Spectrometry (ICP-MS). Only signals above the limit of detection (LOD) were considered. In all the fractions, the disruption of the natural isotopic abundance of each element, with a predominance of neutron-deficient isotopes, is observed. The presence of the exotic nuclides ^{146}Sm, ^{148,150}Gd, ^{154}Dy, and ^{157,158}Tb is confirmed.

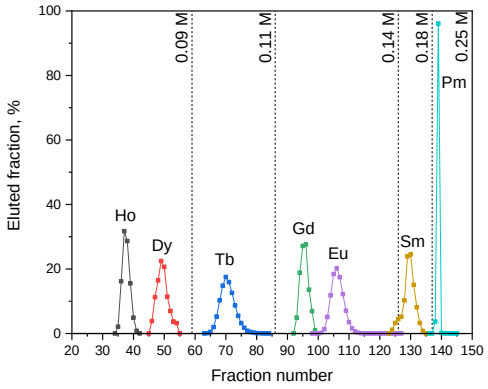

Fig. 2: Fractional separation of Ho, Dy, Tb, Gd, Eu, Sm, and Pm fractions *via* a gradient elution with HIBA at pH = 4.6 on SYKAM resin. The concentration of the load solution is fixed at 0.05 M HCl.

Whereas the Gd and Sm fractions obtained with Method A appear devoid of contaminants, the Dy and Tb ones suffered from a significant Lu interference (Fig. 3 and 4). Furthermore, isobaric interferences were detected in the Dy (^{162}Dy-^{162}Er; ^{163}Ho-^{163}Dy; ^{164}Dy-^{164}Er) and in the Tb (^{157}Tb-^{157}Gd; ^{158}Tb-^{158}Gd-^{158}Dy) fractions. A removal of Hf and Lu at the beginning of the process is thus necessary not only to minimize the overall dose rate exposure (in the mSv/h range), but also to obtain pure Dy and Tb final fractions. By applying Method B, no isobaric interference is detected in the Sm, Gd, and Dy fractions. The isotopic composition of each fraction is elucidated in Table 1. However, presence of Dy (1% in mass fraction) was identified in the Tb sample (Fig. 5). The contribution of ^{158}Dy to the ^{158}Tb-^{158}Dy isobaric interference was calculated being less than 5%. Despite the slight contamination of the Tb fraction with Dy, the separated sample can be used for the preparation of γ-

[1] https://www.psi.ch/en/lrc/erawast

sources for ^{158}Tb decay measurements. In fact, the Tb fraction does not contain any γ-interferents (e.g., Lu γ-emitters) that might increase the Compton scattering or emit in the same energy region as ^{158}Tb. The Dy, Gd, and Sm fractions obtained with Method B are suitable for the preparation of samples for half-life measurements, with an expected uncertainty on the final value below 5%.

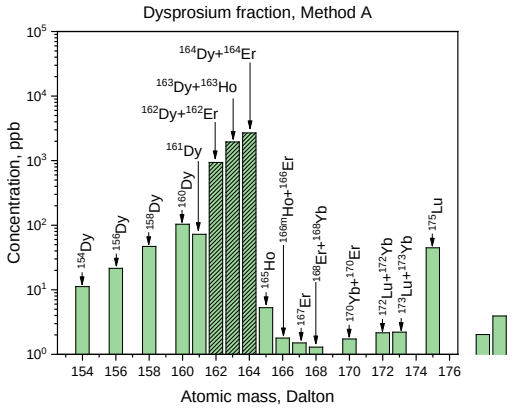

Fig. 3: Results of the ICP-MS analysis of the Dy fraction obtained with Method A. Isobaric interferences in the detection of Dy nuclides are indicated (patterned bars). Further contaminants (Yb and Lu) are identified as well.

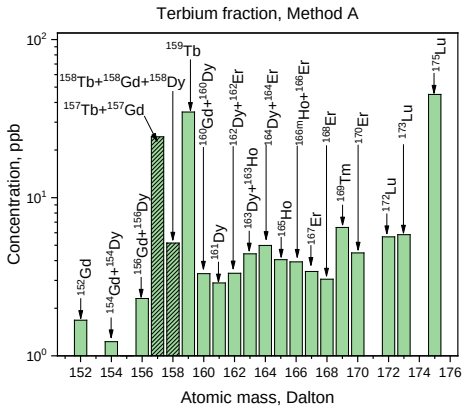

Fig. 4: Results of the ICP-MS analysis of the Tb fraction obtained with method A. Isobaric interferences in the detection of Tb nuclides are indicated (patterned bars). Further contaminants (Er, Ho, Tm, and Lu) are identified as well.

Tab. 1: Isotopic abundances in the Dy, Tb, Gd, and Sm fractions obtained by applying the separation Method B. Detected lanthanide impurities above LOD are reported.

Fraction	Lns impurities > LOD, (mass fraction, %)	Isotopic abundance, (mass fraction, %)
Dy	None	^{154}Dy (7); ^{156}Dy (12); ^{158}Dy (18); ^{160}Dy (28); ^{161}Dy (29); ^{162}Dy (4); ^{163}Dy (1); ^{164}Dy (1)
Tb	Dy (1)	^{157}Tb (39); ^{158}Tb (5); ^{159}Tb (56)
Gd	none	^{148}Gd (2); ^{150}Gd (5); ^{152}Gd (22); ^{154}Gd (19); ^{155}Gd (5); ^{156}Gd (39); ^{157}Gd (7); ^{158}Gd (1); ^{160}Gd (not detected)
Sm	none	^{144}Sm (5); ^{146}Sm (6); ^{147}Sm (58); ^{148}Sm (8); ^{149}Sm (6); ^{150}Sm (13); ^{151}Sm (<1); ^{152}Sm (3); ^{154}Sm (<1)

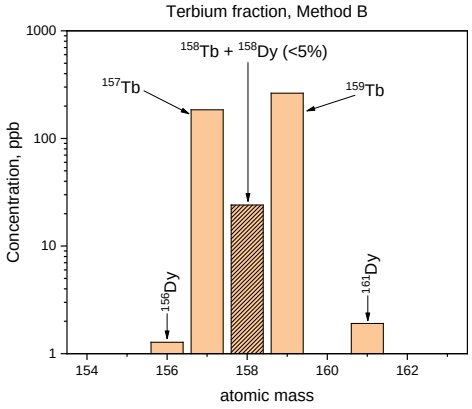

Fig. 5: Results of the ICP-MS analysis of the Tb fraction obtained with Method B. Isobaric interference (i.e., ^{158}Dy, < 5% in mass fraction) in the detection of ^{158}Tb is indicated (patterned bar). The overall amount of Dy was calculated being 1% in mass fraction.

During the separation process, fractions containing Ba, Hf, Lu, Ho, Eu, and Pm were collected. Further separation procedures, where necessary, are envisaged.

ACKNOWLEDGMENT
This project is funded by the Swiss National Science Foundation (SNF grant no 200021-159738).

[1] Y. Dai et al., J. Nucl. Mat. **343**, 33 (2005).
[2] Z. Talip, Ann Rep. Lab. of Radiochem. (2019).

THE INFLUENCE OF PLATING TIME, ACIDITY, INITIAL CONCENTRATION, AND CATHODE MATERIAL ON THE ELECTRODEPOSITION OF Dy

N. M. Chiera, D. Schumann (PSI)

For the determination of the half-lives ($t_{1/2}$) of radionuclides, different methods can be applied, depending on the order of magnitude of the expected $t_{1/2}$. In case of long-lived radionuclides such as ^{146}Sm, ^{150}Gd, and ^{154}Dy (i.e., with $t_{1/2}$ ~10^6 years) the so-called "direct method" is the only applicable one. An exemplary description of this methodology is given in [1]. For radionuclides with an expected $t_{1/2}$ of less than 100 years (e.g., ^{148}Gd) the "decay method", as described in [2], can be used. In both cases, high precision measurements of the activity of the radionuclides of interest are essential. For the quantification of the activity of α-emitting nuclides, thin and homogeneous sources, in order to get high-resolution spectra, are required. When only low amounts of the desired material (i.e., 10^{-9}-10^{-6} mol range) are available, the most efficient method is the molecular plating technique (also called electrodeposition) [3]. With this method, thin layers can be prepared by applying a constant DC voltage (or a constant current) in an organic media (e.g., iPrOH). Despite being a widely applied technique, only few studies treated the molecular plating of the rare-earth elements Sm, Gd, and Dy [4-6]. Furthermore, all the mentioned works were performed with amounts of material in the milligram range.

Here, the influence of plating time, acidity of the electrodeposition solution, initial concentration, and cathode material on the deposition yield of nanomol of Dy is discussed.

A description of the electrodeposition cell can be found in [7]. In order to maintain a constant deposition temperature, the cell was implemented with a Peltier cooler at the cathode. Before each test, a cleaning procedure (stepwise rinsing in 1 M HNO_3, MilliQ water, and iPrOH) was applied to the cell, to the spiral Pt wire (anode), and to the deposition foil. Electrodeposition test solutions were prepared by transferring an aliquot of a 0.0033 M $DyNO_3$ stock solution to a HDPE 20 ml vial, and diluting it in 5 mL 1 M HNO_3. 2 µL of the ^{159}Dy tracer solution were added in order to quantify the deposition yield *via* γ-spectrometry. Successively, the solution was evaporated to dryness (70 °C under N_2 flow) and re-dissolved in 10 ml iPrOH (WVR AnalR NORMAPURE® grade, >99.7%). Then, the solution was transferred into the electrodeposition cell and plated at 550 V with an anode-cathode distance of 10 mm on an Al deposition foil (thickness thk: 15 µm, diameter of deposition area: 20 mm). The foil was maintained at 15 °C during the entire plating. For a constant initial amount of Dy (75 µL = 250 nmol) deposition yields ≥ 90% were reached for continuous plating times above 120 minutes (Fig 1).

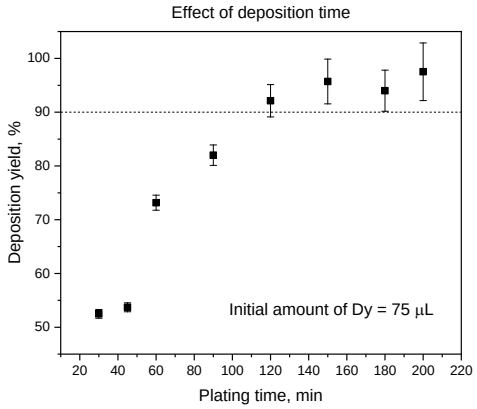

Fig. 1: Effect of the plating time on the deposition yield of 250 nmol of Dy on an Al foil. No HNO_3 was added to the plating solution. Voltage applied = 550 V.

A similar methodology (i.e, starting solution in HNO_3, evaporation to dryness, and re-dissolution of the precipitate in iPrOH) was applied in [7]. In that work, high deposition yields of Be layers were reached under strict control of the acidity of the plating solution. However in [8], deposition yields above 90% of Tm were achieved by addition of diluted HNO_3 in the plating solution. A similar procedure was used in [4-6], and more recently, in [9]. Hence, in this work, the effect of the acidity of the initial solution on the deposition yield of Dy was explored. The plating efficiency was drastically decreased when HNO_3 0.01 M was added to the electroplating solution (Fig. 2).

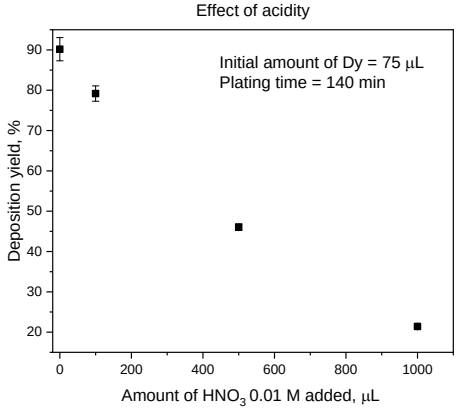

Fig. 2: Effect of acidity (i.e., amount of 0.01 M HNO3 added to the plating solution) in the deposition yield of 250 nmol of Dy on an Al foil. Plating time = 140 min, voltage applied = 550 V.

The most likely explanation is a competitive reduction of H^+ at the cathode at the applied voltage. Even though release of H_2 was observed only when 1 mL of 0.01 M HNO_3 was added, microscopic H_2 development at the interface between the solution and the deposition foil cannot be excluded. The apparently contradicting behavior observed in previous works - besides the different typology of elements electroplated - might be related to the initial amounts of material in the plating solution. In the nanomol range the addition of acid media decreases the deposition yield at high voltages. Whereas, in the case of micro- or even millimol amounts of material an addition of HNO_3 might help: 1) for the dissolution of the precipitate prior to iPrOH addition, and 2) for the solvatation of the species to be deposited, preventing other complexation, or in extreme cases, agglomeration/precipitation. It has to be pointed out as well that in the above-mentioned works different voltages and diverse amounts of organic media in the electroplating process were used. This renders a direct comparison of the obtained yields misleading. Hence, in order to understand the relation between the amount of initial material in the plating solution and its acidity on the deposition yields, a systematic study at a constant voltage and with the same amount of organic media needs to be performed. Future experiments, extending perhaps this study to other elements besides the lanthanides, can be envisaged.

Intuitively, an increase of the initial Dy amount corresponds to an increase of the required plating time to reach deposition yields >90%. The trend is linear under the applied electroplating conditions, at least for Dy amounts below 2 µmol (Fig. 3).

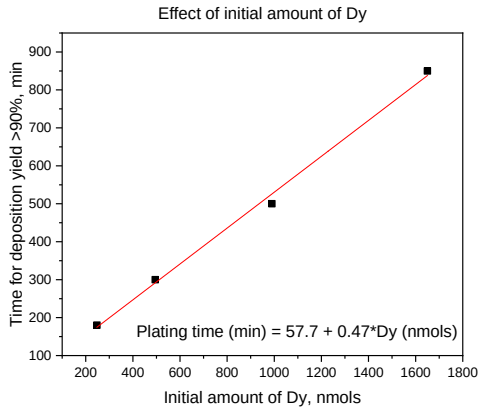

Fig. 3: Relation between the initial amount of Dy (250-1650 nmol range) and the time needed to obtain a deposition yield > 90% on an Al foil. No HNO_3 was added to the plating solution. Voltage applied = 550 V.

Lastly, four different types of deposition foils were tested, namely glassy C (thk: 15 µm), Ta (thk: 50 µm), Cu (thk: 15 µm), and Ag (thk: 15 µm). In the cleaning procedure, the Cu and Ag foils were rinsed in 1 M citric acid instead of HNO_3. Contrary to [1], the type of cathode material did not affect the deposition yield at the applied conditions.

In a future work, the same parameters will be tested for the electrodeposition of nanomole amounts of Gd and Sm.

---

[1] Y. Nedjadi et al., Appl. Radiat. Isot. **70**, 1990 (2012).
[2] K. F. Flynn et al., Nucl. Sci. Eng. **22**, 416 (1965).
[3] W. Parker et al., Nucl. Instr. Methods. **16**, 355 (1962).
[4] W. Parker et al., Nucl. Instr. Methods. **26**, 55 (1964).
[5] K. Eberhardt et al., Nucl. Instr. Methods. **521**, 208 (2004).
[6] A. Vascon, Dissertation Thesis, Mainz Universität (2013).
[7] Maugeri et al., J. Instrum. **12** 1 (2017).
[8] S. Heinitz et al., Radiochem. Acta **105** 801 (2017).
[9] Z. Talip et al., Anal. Chem., **89**, 13541 (2017).

TOWARDS THE DETERMINATION OF THE HALF-LIFE OF ^{148}Gd VIA DECAY METHOD

N. M. Chiera (LRC/PSI), Z. Talip (CRS/PSI), R. Dressler, D. Schumann (LRC/PSI)

Long-lived lanthanides are of great interest in several research domains, including astrophysics, geophysics, and fundamental physics. Astonishingly, nuclear properties (e.g., half-lives - $t_{1/2}$) of a considerable number of these radionuclides are still poorly known. A prominent example is ^{148}Gd, for which different $t_{1/2}$ values were measured (Table 1). The $t_{1/2}$ = 74.6 y value currently reported in the ENDF/B VIII-0 database was recently supported - within the indicated uncertainties - by the work of Fülöp et al. However, the latter was given only as a preliminary result. A re-measurement is needed, in order to confirm or even improve the accuracy and precission of the $t_{1/2}$ value for ^{148}Gd.

Tab. 1: Half-life ($t_{1/2}$) values for ^{148}Gd.

$t_{1/2}$, years	Author	Year	Adopted in
84 ± 9	A. Siivola [1]	1962	
97.5 ± 6.5	A. M. Friedman [2]	1966	
74.6 ± 3.0	R. J. Prestwood [3]	1981	ENDF/B VIII-0
70.9 ± 1.0	Zs. Fülöp [4]	2003	Nubase 2016
71.1 ± 1.2	averaged value [5]	2017	KNCO++

^{148}Gd (α-branching ratio: 100%; Eα = 3182.8 keV - ENDF/B-VIII.0 and JEFF-3.1 databases) was retrieved via liquid phase separation from proton irradiated Ta targets (99.988% ^{181}Ta, 0.012% ^{180}Ta) [6]. For the $t_{1/2}$ measurements, two different ^{148}Gd samples (Ta-S3-Gd and Ta-S5-Gd) were prepared with the molecular plating technique. As backing material, commercially available glassy carbon (0.075 mm thickness) was used. For both samples, the deposited ^{148}Gd material (2.5 μm thickness, 20 mm diameter) was coated with a 30 nm Au layer in order to avoid contamination of the alpha detector *via* sputtering. The stopping of alpha particles by absorption in the sample or in the detector's dead layer is negligible. Efficiency calibration was performed by a certified ^{241}Am source of the same diameter (539±14 Bq, PTB). All the measurements were performed with the samples kept at a fixed position. The standard deviation in the solid angle, due to the inhomogeneous activity distribution of the samples and the reference source, was calculated as less than 1%. Both samples (i.e., Ta-S3-Gd and Ta-S5-Gd) were measured simultaneously for 15 times, during a consecutive period of 7 months. Each alpha measurement was performed for 14 days. Measurements interrupted before the planned 1.21E+6 seconds are indicated in Table 2.

Tab. 2: Summary of the alpha measurements of samples Ta-S3-Gd and Ta-S5-Gd. L.T. = life time; R.T. = real time.

Meas. #	Ta-S3-Gd		Ta-S5-Gd	
	L.T. (*10^6 s)	R.T. (*10^6 s)	L.T. (*10^6 s)	R.T. (*10^6 s)
1	1.21	1.21	1.21	1.21
2	1.21	1.21	1.21	1.21
3	1.21	1.21	1.21	1.21
4	1.21	1.21	1.21	1.21
5	1.21	1.21	1.21	1.21
6	1.21	1.21	1.21	1.21
7	1.21	1.21	1.21	1.21
8	1.21	1.21	1.21	1.21
9	1.21	1.21	1.21	1.21
10	1.03	1.03	1.03	1.03
11	1.21	1.21	1.21	1.21
12	666328	666346	666302	666315
13	200355	200361	200343	200347
14	1.21	1.21	1.21	1.21
15	1.22	1.22	1.22	1.22

In the alpha spectra an increasing counting rate below 1.5 MeV due to noise contribution is observed (Fig. 1).

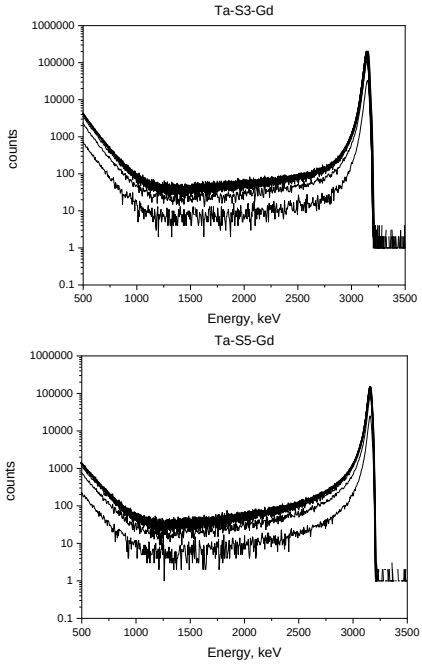

Fig. 1: Alpha spectra of 15 consecutive measurements of samples Ta-S3-Gd (top) and Ta-S5-Gd (bottom).

Hence, for the counting rate evaluations, the alpha energy range 1.5-3.3 MeV is selected. In both samples, a sensible decrease of the counting rate during the measuring period of 7 months is observed (Fig. 2).

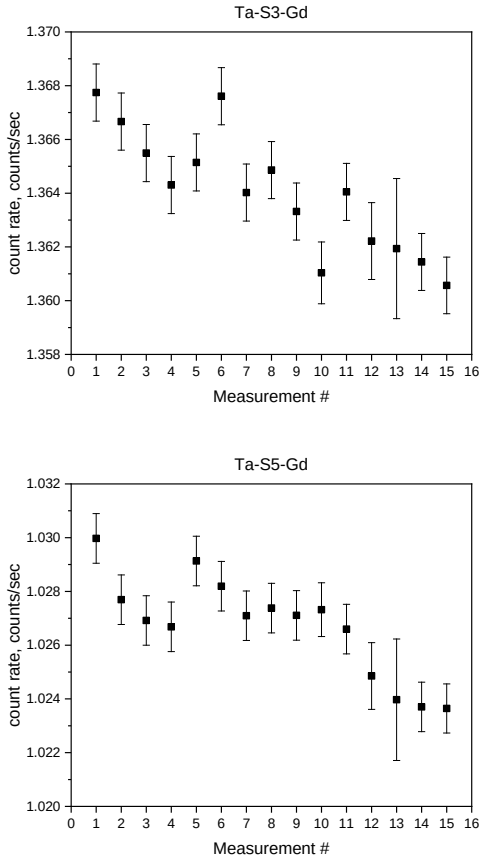

Fig. 2: Alpha counting rate (counts/sec) in the 1.5-3.3 MeV range per each of the 15 measurement for sample Ta-S3-Gd (top) and Ta-S5-Gd (bottom). A significant decrease of the counting rate along the measurement period is observed.

The difference between the count rate recorded at the beginning of the alpha measurements (time t_0) and the count rate at a given time t, normalized to the count rate at t_0, is plotted in Figure 3. By applying a linear regression, the following values for the decay constant (λ) and its uncertainty are found:

Ta-S3-Gd: λ = 2.43E-5 s uncertainty = 4.0E-6 s

Ta-S5-Gd: λ = 2.42E-5 s uncertainty = 4.9E-6 s

From $t_{1/2} = \frac{\ln(2)}{\lambda}$, an estimation of the $t_{1/2}$ value of ^{148}Gd can be deduced:

Ta-S3-Gd: $t_{1/2}$ = 78.1 ± 12.7 years

Ta-S5-Gd: $t_{1/2}$ = 78.6 ± 15.8 years

These preliminary results may suggest a higher $t_{1/2}$, in comparison to the values reported in [4] and [5]. An uncertainty below 10% on the measured $t_{1/2}$ value can be achieved by performing the same typology of sequential measurements for an extended period.

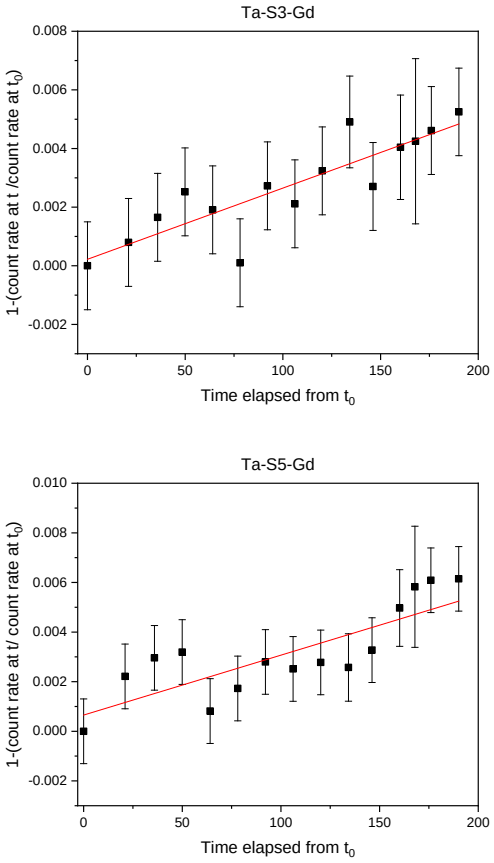

Fig. 3: Difference between the initial count rate (at time t_0) and the count rate at time t, normalized by the initial count rate. The linear regression fit line is indicated in red.

ACKNOWLEDGEMENT

This project was partially funded by the Swiss National Science Foundation (SNF grant no 5201.24003.808).

[1] A. Siivola et al., Ann. Acad. Sci. Fennicae, Ser. A VI Physica **109**, 1 (1962).

[2] A. M. Friedman et al., Radiochim. Acta **5**, 192 (1966).

[3] R. J. Prestwood et al., Phys. Rev. C **24**, 1346 (1981).

[4] Zs. Fülöp et al., Nucl. Phys. A **718**, 688 (2003).

[5] N. Nica. Nuclear Data Sheets, **117**, 1-229 (2014).

[6] Z. Talip et al., Anal. Chem. **89**, 6861 (2017).

^{35}Cl(n,γ) CROSS SECTION MEASUREMENT AT N_TOF (CERN)

S. Bennett (Univ. Manchester), I. Porras (Univ. Granada), T. Wright (Univ. Manchester), E. A. Maugeri (PSI) and the n_TOF Collaboration

The nuclear reaction ^{35}Cl(n,γ) has a double interest, in medical physics and nuclear fission applications. Firstly, chlorine is present in the brain at 3% and this reaction accounts for 10% of the radiation dose in Boron Neutron Capture Therapy of brain tumors. In addition to this, it is also present in the materials of fission reactors so is important for criticality calculations and predictions of the build up of the long-lived radionuclide ^{36}Cl. The previous experimental data available in the resonance region comes from a single capture measurement, which covers the neutron energy range 0.1 to 500 keV [1]. The behavior at low energies was fitted to a thermal value obtained from a different experiment [2]. The n_TOF facility allows performing a new measurement that can improve the knowledge of the cross section from thermal up to MeV neutron energies.

For this reason, a proposal for the measurement of this reaction at the n_TOF facility (EAR1) was presented and approved by the INTC committee in February 2018 [3]. The experiment was carried out in August of the same year.

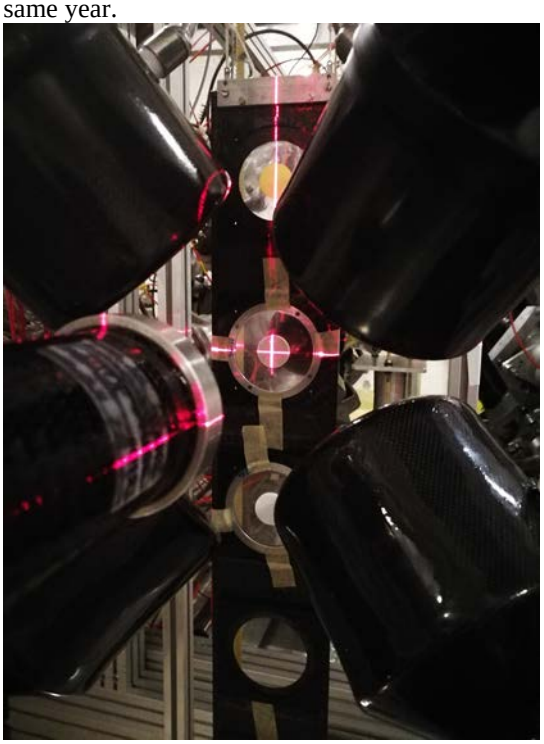

Fig. 1: Experimental set-up for the measurement of the ^{35}Cl(n,γ) cross section.

The experimental set-up is displayed in Fig. 1. The chlorine samples are placed veritically facing the neutron beam and four liquid scintillators of deuterated benzene C6D6 are placed out of the beam for measureing the gamma radiation coming from the sample. This material has a low sensitivity to the neutron background and has proven to be very useful for this kind of measurement [4], so the same set-up was used in all the campaign of measurement of (n,γ) cross sections.

A sample of 99% enriched Na^{35}Cl was prepared at PSI with a delicated high pressure sintering procedure. This was a critical part of the experiment because this material is very rare and expensive. Futhermore, the sample material had to be purified from contaminats, e.g. alluminum scraps, coming from a previous unsuccessful attempt of target preparation. The obtained target, shown in Fig. 2, is a 2 cm diameter disk with a mass of 960 mg.

Fig. 2: Sample of Na^{35}Cl used in the experiment inside a Mylar bag.

PSI produced an additional and more massive sample of very pure Na^{nat}Cl that was used in the experiment for improving the reaction rate.

This measurement is still under analysis. The response of the detector can be related to the total energy from the gamma cascade by means of the Pulse Height Weighting Technique (PHWT) [4] for which Monte Carlo simulations of the whole set-up have been perfomed with the Geant4 toolkit. Different corrections, including background subtraction, to the results obtained from the raw data are in progress. This will provide data on the low-energy region as well as in the resonance one. In Fig. 3 illustrates the analysed counts from the two samples mentioned.

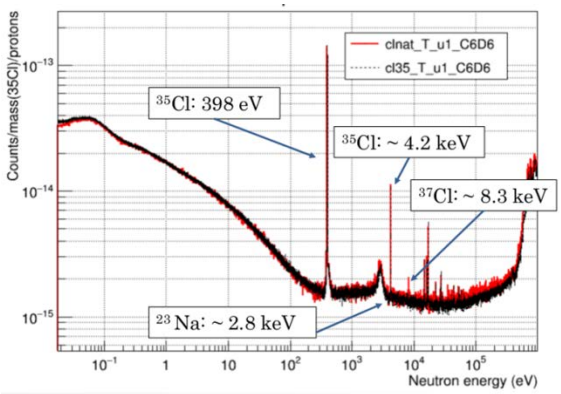

Fig. 3: Spectra produced at all detectors from the gammas emitted from neutrons colliding in the samples (enriched (black line) ^{35}Cl and natural (red line) Cl) as a function of neutron energy, obtained by time of flight.

---

[1] K. H. Guber et al., Phys. Rev. C **65**, 058801 (2002).

[2] G. L. Molnár, et al., Nucl. Instrum. Meth. Phys. Res. B **213**, 32 (2004).

[3] I. Porras et al., CERN Document Server: http://cds.cern.ch/record/002299695

[4] A. Borella et al., Nucl. Instrum. Meth. Phys. Res. A **577**, 626 (2007).

MEASUREMENT OF THE ^{140}Ce(n,γ) CROSS SECTION AT n_TOF

S. Amaducci (INFN-Catania, Univ. Catania), E. A. Maugeri (PSI), M. Barbagallo (CERN), L. Cosentino (INFN-Catania), N. Colonna (INFN-Bari), S. Cristallo (INFN-Perugia), P. Finocchiaro (INFN-Catania), C. Massimi (INFN-Bologna, Univ. Bologna), M. Mastromarco (Univ. Manchester), A. Mazzone (INFN-Bari, CNR-Bari), A. Mengoni (INFN-Bologna, ENEA-Bo) and the n_TOF Collaboration

PHYSICAL MOTIVATIONS

One of the main mechanisms driving the elements' nucleosynthesis is the so-called *s*-process, namely a sequence of slow neutron captures alternated by rapid beta decays. Its large contribution to the production of elements heavier than ^{56}Fe is well-established since the 1950s [1], and the evolution of Asymptotic Giant Branch (AGB) stars, where the *s*-process occurs, is nowadays well described in stellar models. Neutron capture cross sections are the most relevant nuclear physics input, so that taking advantage of the increasing quality of the nuclear data, most of the stellar models can predict the evolution of each elemental abundance with growing precision. The comparison between model predictions and astronomical observations, in particular when averaged on a large number of stars as in ref. [2,3], is a well-suited test to validate the stellar models and highlight possible discrepancies between theories and experimental evidences.

In the case of cerium, a large discrepancy emerges when the astronomical observations and the abundance predicted by recent stellar models are compared [4]. On the contrary, the same model shows an excellent agreement for all the elements with an atomic number close to cerium, proving its reliability at this stage of the *s*-process. Since the final abundance is very sensitive to the neutron capture cross section, the discrepancy might have a nuclear origin, in particular due to the cerium destruction channel, namely the neutron capture reaction on ^{140}Ce. Only a few experimental cross section data of this reaction in the energy region of interest are present in literature, in particular, because of the difficulty in producing high purity samples of ^{140}Ce and the small value of the cross section itself (^{140}Ce has a closed neutron shell).

In order to overcome this lack of data, by improving the nuclear data quality and thus try to solve the abundance discrepancy, a high precision measurement of the ^{140}Ce(n,γ) cross section has been performed at n_TOF [5].

TARGET AND EXPERIMENTAL SETUP

The measurement was performed at the n_TOF facility located at CERN. Here a pulsed neutron beam is produced with a high instantaneous flux and an excellent energy resolution (up to 10^{-4}, thanks to the time-of-flight technique). Four C_6D_6 detectors [6] were used to measure the gamma rays produced by the capture reaction. These are customized liquid scintillators with a very low neutron sensitivity to ensure a high background rejection.

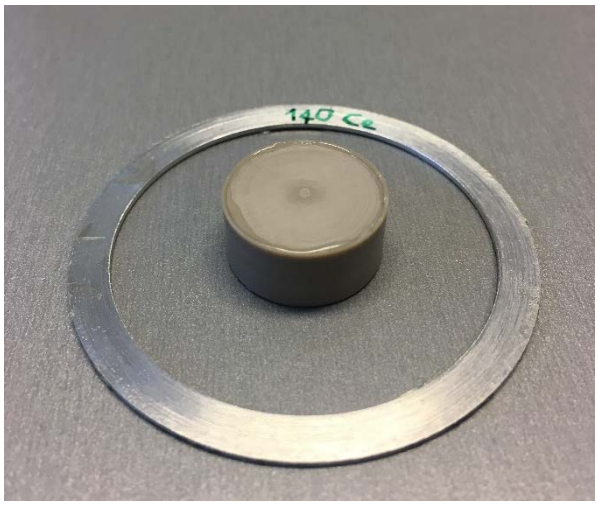

Fig. 1: Cerium target fixed on the Mylar frame.

The original sample was made of 12,318 grams of $^{140}CeO_2$ powder. According to the producer it was enriched at 99.4% in ^{140}Ce, with only a 0.6% of ^{142}Ce as relevant contamination (the natural cerium presents a 11% of ^{142}Ce). The target was produced at PSI by pressing CeO_2 powder applying a force of 7 tons by *means of a manual hydraulic press (Specac, Atlas Manual Hydraulic Press). The obtained sample* was then enclosed in a cylindrical PEEK capsule 1 mm wall thickness, and heated at 100 °*C for 4 hours in a glove box with a controlled inert atmosphere (O_2 and H_2O content in Ar lower than 1 ppm).* This capsule was sealed using as less glue as possible and then fixed to a Mylar frame, being careful in minimizing the material surrounding the target and consequently reducing the background during the measurement. The target was successfully used for the measurement in June 2018 at n_TOF.

PRELIMINARY RESULTS

In Figures 2 and 3 the preliminary neutron energy spectra are shown, together with the ^{140}Ce(n,γ) cross section evaluated by ENDF-B/VIII (right-handed axis). The main aim of this measurement is to evaluate the MACS (Maxwellian Average Cross Section), namely the capture cross section convoluted with the neutron thermal population at stellar temperature. In case of cerium at T = 8 keV, i.e. the typical temperature at which the cerium is destroyed in AGBs, the MACS mainly depends on the resonances below a few tens of keV.

Figure 2 shows a preliminary wide neutron energy spectrum. It is clear that, even though the signals are

dominated by the background in the valleys, the resonances are well separated from the background and their parameters may be extracted. All the resonances included in the ENDF-B/VIII evaluation are present in the experimental data as well. Furthermore, the only trace of contaminants above the background is due to the large resonance at 1.153 keV. This resonance is attributable to ^{142}Ce, as foreseen by the libraries, although the cross section is not large enough to justify its magnitude and further investigation is needed.

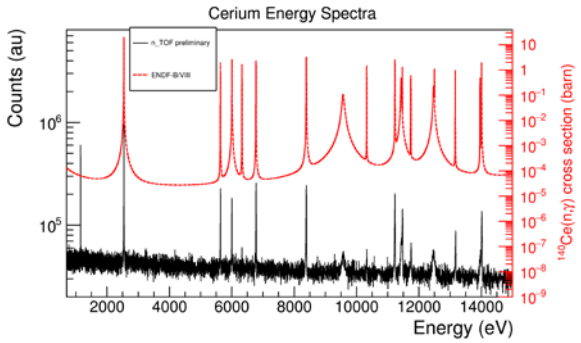

Fig. 2: Preliminary n_TOF cerium energy spectra from 0.8 to 15 keV compared with ENDF-B/VIII.

The correspondence of the resonances energies included in ENDF-B/VIII is clearer in Figure 3, where the spectrum between 2 and 9 keV is enlarged. The data are not normalized and many experimental effects are not yet included in the analysis, among which the more relevant are the resolution function and the Doppler broadening. The preliminary results demonstrate the good quality of the collected data, well promising for the resonance analysis that is in progress. This analysis is being carried out using the software SAMMY, with the aim to extract all the resonance parameters up to the neutron energy of 100 keV.

CONCLUSION

An accurate measurement of the ^{140}Ce(n,γ) cross section has been performed at n_TOF facility, in order *to shed* light on the discrepancy found between the cerium abundance predicted by stellar modelling and the astronomical observations. The careful preparation of the highly enriched sample by PSI resulted to be of a key importance for the measurement. Indeed, preliminary results demonstrate that during the target preparation no relevant contaminants, which could affect the analysis, were included in the sample. The analysis is currently ongoing, and it will be completed with fitting of resonance parameters and computation of the MACS.

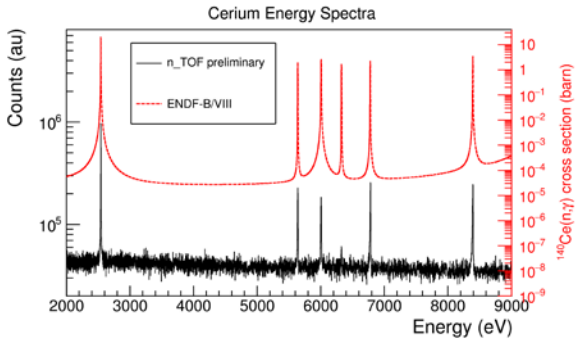

Fig. 3: Enlargement of Figure 2 from 2 to 9 keV

ACKNOWLEDGEMENT

The cerium oxide material for this measurement has been provided by Prof. T. Katabuchi, of the Tokyo Institute of Technology.

---

[1] E. M. Burbidge et al., Rev. Mod. Phys. **29**, 547 (1957).
[2] I. Roederer et al., ApJ **742**, 37 (2011).
[3] D. Yong et al., ApJ **689**, 1031 (2008).
[4] O. Straniero et al., ApJ **785**, 77 (2015).
[5] https://ntof-exp.web.cern.ch/ntof-exp/
[6] P. Mastinu et al., Tech. rep., Cern (2013).

PREPARATION OF ^{78}Se AND ^{79}Se TARGETS FOR MEASURING THE ^{79}Se(n,γ) CROSS SECTION WITH DIRECT AND INDIRECT METHODS

I. I. Danilov, N. M. Chiera, E. A. Maugeri (PSI), S. Heinitz (SCK-CEN), J. Balibrea, C. Domingo Pardo, J. Lerendegui (IFIC/CSIC-Univ. Valencia), U. Köster (ILL)

MOTIVATION

The measurement of the ^{79}Se(n,γ) neutron capture reaction cross section in a wide range of energies is extremely important for both nuclear astrophysics and nuclear safety applications.

In the first case, knowledge on this reaction may help to better understand the *s*-process nucleosynthesis, since ^{79}Se is a branching point in the *s*-process path. On the other end, ^{79}Se is one of the seven long-lived fission products [1]. Thus, knowledge of its neutron capture cross section is very important for evaluating its transmutation into a short-lived or a non-radioactive nuclide, in order to reduce the radiotoxicity of the nuclear spent fuel in geological disposal.

Two complementary approaches are going to be followed to measure this cross section, namely a direct method where a ^{79}Se target will be used for a direct (n,γ) cross section measurement via the TOF technique at the CERN n_TOF facility, Geneva, and a surrogate ratio method consisting in studying the (2n) transfer reaction ^{78}Se(^{18}O,^{16}Oγ)^{80}Se at the Piave-Alpi INFN facility, Legnaro, Italy. The direct approach will provide accurate information on the weak *s*-processes occurring at neutron energies below 100 keV, characteristic of core-He burning in massive stars. The surrogate approach will provide instead valuable information for shell C-burning, which operates in the higher energy range (100-300 keV) before the star explodes as supernova.

This manuscript reports on the ^{79}Se enriched target preparation and characterization and on the first implementations for the production and characterization of the ^{78}Se target, performed at PSI.

^{79}Se TARGET: PREPARATION AND CHARACTERIZATION

^{79}Se can be obtained by neutron irradiation of ^{78}Se at the high flux reactor of the Institut Laue-Langevin (ILL). However, macroscopic amounts of elemental selenium cannot be directly irradiated in the reactor due to γ-ray heating which would bring the sample close to or above its melting point (T_m = 220 °C). For this reason, it was proposed to use a PbSe target, which has a much higher T_m (1079 °C). Enriched ^{208}Pb was required for this purpose to considerably reduce interferences from neutron capture on ^{207}Pb in the future measurement at n_TOF.

A ^{208}Pb^{78}Se sample was produced as follows: a quartz tube (L = 200 mm, ID = 10 mm) with a NS29 socket joint sealed on one side was thoroughly cleaned with conc. H_2SO_4 to remove any inner surface contaminant. Then it was rinsed with ethanol first and distilled water after. The tube was then introduced into an argon-saturated glovebox and filled with 3.0073 g of elemental ^{208}Pb (ORNL, 99.1% enrichment) and 1.1027 g of ^{78}Se (Campro Scientific, 99.39% enrichment) using a plastic spatula. The tube was then closed with a NS29 metal cone joint, evacuated, and transferred into a fume hood. The evacuated tube was flame-sealed using a H_2/O_2 torch approx. 10 cm above its lower end. The resulting ampoule was subsequently placed inside a furnace set to 1200 °C to allow the reaction between Pb and Se. The quartz ampoule was periodically shaken to favour a homogeneous reaction between the two elements. After 24 hours, the ampoule containing the ^{208}Pb^{78}Se sample was retrieved from the furnace and rapidly cooled in a water bath. Afterwards, the ampoule was carefully broken in a plastic bag, the PbSe extracted, weighed, and enclosed in a pure 0.5 mm thick aluminium capsule (Goodfellow, 6N purity). The latter was laser-welded at CERN, enclosed into an aluminium irradiation shuttle, and irradiated in the V4 beam tube of the ILL high flux -reactor. The irradiation lasted for 40.4 days at a neutron flux of ~1.3×10^{15} cm^{-2} s^{-1} followed by an additional 11 days at a flux of ~ 9×10^{14} cm^{-2}s^{-1} to a total neutron fluence of about 5×10^{21} cm^{-2}. After a year of decay, the sample was shipped to PSI, where it was characterized by means of γ-ray spectrometry using a high-resolution HPGe detector. The accurate knowledge of the sample mass and of the amount of contaminants is crucial to calculate the expected counting rates and background in the upcoming measurement at n_TOF, and to be able to optimize the experimental setup in advance. Preliminary results of the γ-measurements indicate that the amount of contaminants in the ^{208}Pb^{79}Se target (^{75}Se, ^{60}Co, ^{110}Ag, ^{65}Zn) agrees or is below the expected values and no activation of the aluminium casing was observed, see Table 1 reporting the data extracted from the spectrum depicted in Fig. 1. However, the high concentration of Pb might compromise the ^{79}Se (n,γ) measurement. Evaluation of chemical removal of Pb, and eventually of other contaminants, from the produced target is ongoing.

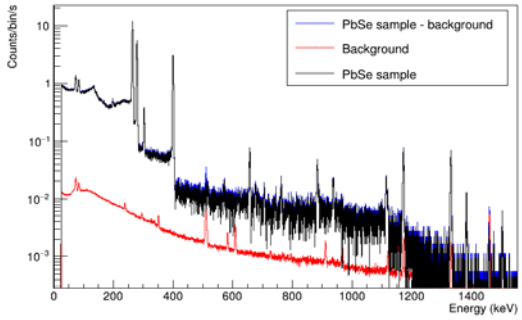

Fig. 1: High-resolution γ-ray spectrum of the $^{208}Pb^{79}Se$ target compared to the background.

Tab. 1: Preliminary results for the activities of the main contaminants identified in the $Pb^{79}Se$ sample.

Isotope	Activity (MBq)
^{75}**Se**	338(4)
^{110}**Ag**	29(1)
^{65}**Zn**	1.89(9)
^{60}**Co**	2.77(6)

^{78}Se TARGET: PRELIMINARY TESTS OF PREPARATION AND CHARACTERIZATION

Also for the surrogate ratio experiment, PbSe is going to be used as target material, instead of elemental Se. Again, the higher melting temperature is favorable to withstand the target heating by the ^{18}O beam current.

The ^{78}Se target is going to be produced *via* a three-step method: 1 - synthesis of $Pb^{78}Se$; 2- purification of the synthesized $Pb^{78}Se$; and 3- Physical Vapor Deposition (PVD) of $Pb^{78}Se$ onto a graphite backing.

The synthesis of $Pb^{78}Se$ is similar to the one described in the previous section.

A preliminary test was carried out using metallic Pb shots (Alfa-Ventron, 1.3 mm diameter) and black Se powder (Merck, purity ≥ 99.0%) in a 1:1 Pb:Se molar ratio as starting material, placed in a 6 mm quartz tube. The obtained PbSe was characterized by X-ray diffraction (XRD). XRD analysis (Figure 2, red line) show clearly the presence of a small fraction of unreacted Pb. This problem was solved using an excess of Se in the starting material (1:1.22 Pb:Se molar ratio), and a larger quartz tube, i.e. 15 mm. The XRD analysis of the resulting PbSe sample (Figure 2, black line), shows a complete reaction of the entire Pb. The relation between the initial amount of Pb-Se and the diameter of the quartz ampoule is crucial, since the synthesis in smaller quartz tubes does not allow for a complete mixing of the single reactants.

The second step of the method consists in the purification of the synthesized PbSe from the excess of Se. In fact, the presence in the final sample of unreacted Se in amorphous form cannot be excluded since it would not be detected by XRD. Hence, a gas-phase purification was performed. PbSe was grinded and placed in the middle of a quartz tube, and heated up to 450 °C under a He gas flow (20 mL/min) in a tubular furnace. At this temperature, the not-reacted Se is evaporated, whereas PbSe remains in solid phase. After purification, the sintering of the PbSe powder at 850 °C under an Ar/H_2 (3%) flow for 4 h, as reported in [2], is envisaged. In the second part of this project, PVD experiment using the produced PbSe will be performed. For the purpose, an Univex 450 (Leybold vacuum) thermal evaporation station (operational vacuum 10^{-4}-10^{-6} mbar), equipped with a mechanical shutter and a quartz crystal microbalance, will be used. PbSe will be placed in a Ta boat coated with Al_2O_3, which will be in contact with a Type-K thermocouple to monitor the temperature at the applied current. Thermal evaporation of PbSe will be conducted at ~500 °C, at an evaporation rate of 0.15 nm/s.

A comparison of the stoichiometric Pb:Se, by means of X-ray fluorescence, of the PbSe sample previous and after PVD, will allow to check if the vaporization is congruent, i.e., $PbSe_{(s)} \rightarrow PbSe_{(g)}$.

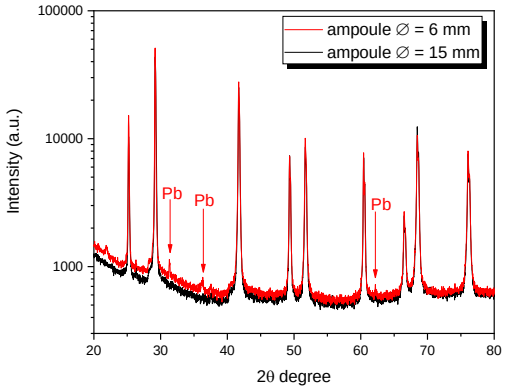

Fig. 2: XRD of PbSe synthesized in a 6 mm diameter quartz ampoule (red line) and in a 15 mm diameter one (black line). The unreacted Pb peaks are indicated.

ACKNOWLEDGEMENT

We would like to thank Dr. E. Pomjakushina (NUM, PSI) for the XRD measurements.

Advanced Nuclear Fuel Cycles and Radioactive Waste Management (2006).

[1] OECD-NEA. Advanced Nuclear Fuel Cycles and Radioactive Waste Management (2006).

[2] H. Unuma et al., J. Am. Ceram. Soc. **81**, 444 (1998).

DILUENT EFFECTS IN SOLVENT EXTRACTION WITH DIGLYCOLAMIDES

I. Kajan (LRC/PSI), M. Florianova (CVUT, Prague)

Organic diluents are the major constituent of the organic phase in the solvent extraction systems. It has been shown in many studies that the diluent has a substantial effect on the outcome of the extraction with respect to both excess of extraction as well as separation factors between the different elements [1-3]. However, exact mechanisms for those effects are still not well understood. The family of diglycolamides is known as extracting agents in solvent extraction for trivalent lanthanides and actinides, with expected application in partitioning and transmutation of nuclear fuel [4]. While the behavior of diglycolamides with respect to equilibrium distribution ratios, acid extraction and kinetics was extensively evaluated [5-6], the effect of diluent on the extraction was targeted only in a few studies [7-9].

In order to bring deeper insight into the diluent effect we performed studies on the diluent effect on solvent extraction of americium and europium by N,N,N′,N′-Tetraoctyl diglycolamide (TODGA) from nitric acid media. Three different groups of diluents were used consisting of alkanes, long chained alcohols and ketones. The effect of carbon chain length was systematically evaluated from 5 to 10 carbons except for alkane diluents.

The distribution coefficients for trace amounts of Eu and Am were determined from system where 1ml of aqueous phase was contacted with 1ml of organic phase consisting of selected diluent and TODGA. For the primary and secondary alcohols as well as ketones, the TODGA concentration in the organic phase was 20mM. For the alkane diluents, the TODGA concentration was 2mM. The organic and aqueous phases were contacted for 120 min in a shaking machine with a thermostated setup. After shaking, the samples were allowed to settle by gravity for 60 min and sampled. The distribution coefficients were determined by measuring the count-rate of ^{152}Eu (122keV line) and ^{241}Am (59.6keV line) isotopes in each phase by a p-type HPGe detector. The distribution coefficients were calculated as a ratio of equilibrium solute concentration in the organic phase over its concentration in the aqueous phase represented by its radioactivity (Eq 1.).

Eq. 1 $$D_M = \frac{[M]_{(org)}}{[M]_{(aq)}} = \frac{A_{M(org)}}{A_{M(aq)}}$$

Separation factors were consequently calculated as a ratio of distribution coefficients of europium and americium as presented in Eq. 2.

Eq. 2 $$SF_{Eu/Am} = \frac{D_{Eu}}{D_{Am}}$$

The distribution ratios of both europium and americium in polar diluents showed significant dependence on the carbon chain of the diluent. A significant increase of the distribution ratio was observed in 5 carbon chains regardless of the diluent type. The obtained distribution ratios for Eu in different diluents at temperature of 298K are presented in Figure 1 and the separation factors for Eu/Am are presented in Figure 2.

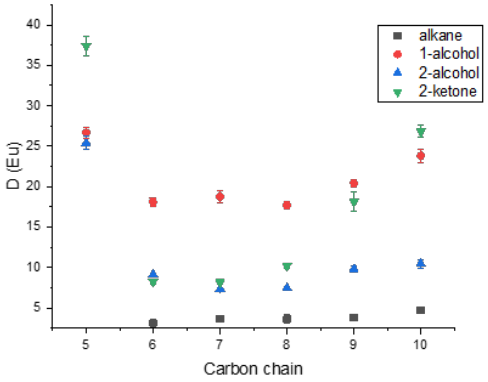

Fig. 1: Distribution ratios of Eu(III) dependence on diluent type and its carbon chain.

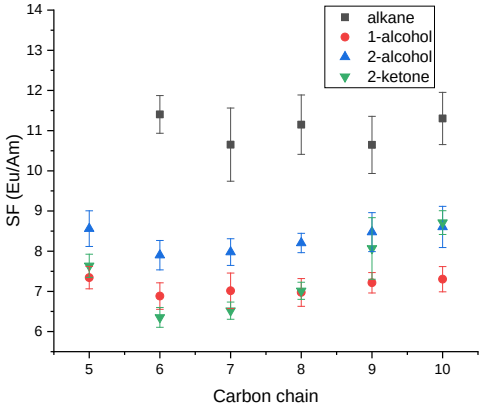

Fig. 2: The dependence of separation factors between Eu(III) and Am(III) on the diluent type and its carbon chain length.

From Figure 1 it is clearly visible that the type of diluent as well as the length of carbon chain have a substantial effect on the distribution coefficient of europium. Generally, it was observed that the distribution ratio in polar diluents increases with the increase of the carbon chain length except for 5 carbon chain. In the case of alkane diluents, the distribution ratios were increasing only slightly with the increase of the carbon chain length.

As showed in Figure 2, the effect of carbon chain length on the separation factor was pronounced strongest in the

ketone diluents. The observed separation factors in the secondary alcohols were higher for all carbon chain lengths when compared to primary alcohols despite lower distribution coefficients. We observed the significant increase in the separation factors in the alkane diluents when compared to the polar ones. In the alkane diluents, the separation factor did not show statistically significant variations with the increase of carbon chain unlike in the other diluent types.

In order to determine the thermodynamic properties of extraction, each diluent stoichiometry of the extracted complexes needed to be determined. The stoichiometry of extracted complexes with respect to TODGA complexation was determined by the slope analysis of the log-log plots of distribution coefficients against the TODGA concentration in the organic phase. This was performed according to the proposed extraction mechanism in Eq.3:

Eq. 3 $$M^{n+}_{(aq)} + nNO^{-}_{3(aq)} mL_{(org)} \overleftrightarrow{K_{ex}} M(NO_3)_n L_{m(org)}$$

Where K_{ex}, the equilibrium extraction constant is defined as :

Eq. 4 $$K_{ex} = \frac{[M(NO_3)_n L_{m\,(org)}]}{\left[M^{n+}_{(aq)}\right] * \left[NO^{-}_{3\,(aq)}\right] * [L_{(org)}]^m}$$

After obtaining stoichiometry of extracted complexes, enthalpy and entropy changes of extraction reactions could be determined by variating the temperature during the contacting of the phases and utilizing Vant Hoff's equation (Eq. 5).

Eq. 5 $$lnK_{ex} = -\frac{dH^0}{RT} + \frac{dS^0}{R}$$

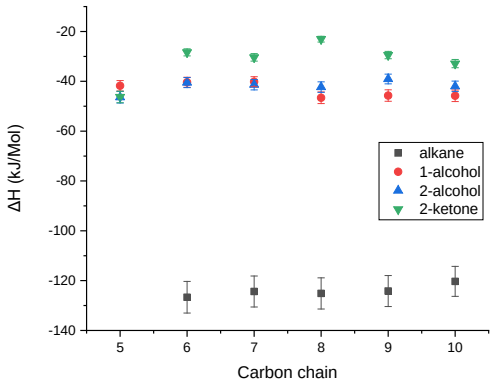

Fig. 3: Dependence of the enthalpy change plotted against the length of carbon chain in different diluents.

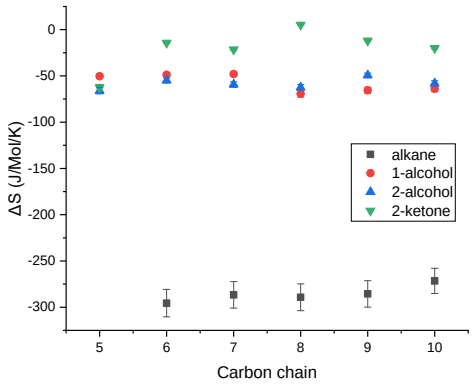

Fig. 4: Dependence of the entropy plotted against the length of carbon chain in different diluents.

From the Figures 3 and 4 it is obvious that the extraction reaction in alkane media is much more exothermic than in polar diluents, while at the same time the change of entropy of the system is significantly more negative.

We have shown in this study that the choice of diluent in the solvent extraction has a significant effect on the outcome of the reaction with respect to both distribution coefficients, separation factors and basic thermodynamic properties of extraction. This is valid for both choices of diluent groups as well for the carbon chain length.

Follow-up studies are ongoing on the changes diluent undergoes during the extraction process and effect of those on the dielectric properties of diluent phase.

---

[1] D. Dyrssen et al. Acta Chem. Scand. **14**, 1100 (1960).

[2] T. V. Healy, J. Inorg. Nucl. Chem. **19**, 328 (1961).

[3] R. K. Jyothi et.al. Korean J. Met. Mater. **56**, 763 (2018).

[4] G. Modolo et.al. Radiochim. Acta. **715**, 100 (2012).

[5] Y. Sasaki et.al. Solvent Extraction and Ion Exchange **19**, 91 (2001).

[6] Z.-X. Zhu et. al. Anal. Chim. Acta **527**, 163 (2004).

[7] Y. Sasaki et.al., Solvent Extr. Ion Exc. **25**, 187 (2007).

[8] S. A. Ansari et.al., Radiochim. Acta. **94**, 307 (2006).

[9] P. N. Pathak et.al, Spectrochim. Acta A **73**, 348 (2009).

Cs-REMOVAL FROM HIGHLY ACIDIC SPENT FUEL SOLUTIONS: COLUMN TESTS

M. Lin (Univ. Bern & PSI), I. Kajan, D. Schumann (PSI), A. Türler (Univ. Bern)

Previous studies in batch mode showed that AMP (ammonium molybdophosphate), AMP_PAN (AMP immobilized in polyacrylonitrile) and AMP/SiO_2 (AMP immobilized on SiO_2) are very selective towards Cs in 4 M HNO_3, the preferred medium for conditioning several liters of spent nuclear fuel solution from the PSI Hot laboratory [1].
In this report, the performance of AMP_PAN was tested in Column mode. The Cs adsorption profiles in dependence on the Cs concentration and flow rates were determined as well as the capacity for Cs in the designed column. In addition, the influence of U, the matrix element in the spent nuclear fuel solutions, on the Cs adsorption was tested, and the effect of U on Cs adsorption was evaluated.

EXPERIMENTAL

The scheme of column extraction system is presented in figure 1. Two glass columns were utilized: column A (Φ5mm×14.5cm) and column B (Φ5mm×7.2cm). The volume of the mobile phase of the column system was measured by the following method: 1) loading the column system (including connecting tubes) with sorbent and water; 2) full removal and collection of the water from column system; 3) weighting the collected water and calculating the volume. These procedures were repeated five times and the average value was used in the experiment (further called "dead volume of the system"). The volume of the mobile phase was ca. 2.6ml and 1.7ml for column A and B, respectively.

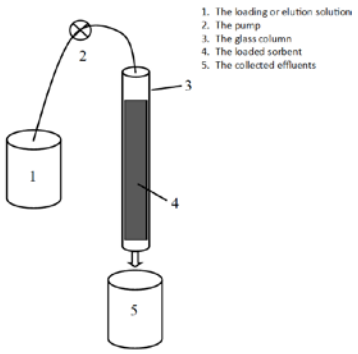

Fig. 1: The scheme of the column extraction system.

AMP_PAN (Triskem) was preconditioned with about 10 ml of 4 M HNO_3 and loaded in the column. Then, the sorbent was washed by 10-15 ml of 4 M HNO_3 before loading the stock solution.
Four stock solutions, shown in the Table 1, were prepared by dissolving $UO_2(NO_3)\cdot 6H_2O$ (Merck) or (and) $CsNO_3$ (Sigma-Aldrich) into 4 M HNO_3 and spiked with ^{137}Cs tracer.

After reaching the radioactive equilibrium of ^{137}Cs and ^{137m}Ba, the ^{137}Cs content in the collected fractions was measured by γ-spectrometry (Canberra EFPC 25, Gamma Analyst Canberra Lynx with software Genie2000) and the Cs content was calculated.
The count rates of U (^{238}U, ^{234}U and ^{235}U) in the collected fractions were determined by liquid scintillation counting (LSC) system (Tri-Carb 3110 TR, Perkin Elmer). The samples for LSC measurement were prepared by mixing 20 µl of the fraction with 15 ml of scintillation-cocktail (Ultima Gold AB) in a 20 ml scintillation vial (Zinsser Analytic GmbH).

Tab. 1: Detail of prepared stock solutions.

Stock solution	Content	Solute concentration
No.1	$CsNO_3$, Cs-137, 4M HNO_3	Cs: 50mMol/L
No.2		Cs: 10mMol/L
No.3		Cs: 1mMol/L
No.4	$CsNO_3$, Cs-137, $UO_2(NO_3)_2\cdot 6H_2O$, 4M HNO_3	Cs: 1mMol/L; U: 600mMol/L

1. Cs loading and washing process

For Cs loading, 2 g of AMP_PAN were preconditioned and loaded in the column A and set of experiments with the stock solutions No.1 – No.3, respectively, was performed. The dead volume of the system was separately collected. The stock solution was pumped through the column at preset flow rate (0.2 – 1 ml/min), and the fractions were collected. Details of the sample collection procedure are summarized in Table 2. The washing process started immediately after reaching the initial Cs concentration in the collected fractions. In the Cs washing process, 4M HNO_3 was pumped through the column. Again, the dead volume of the system was collected separately and then the fractions were collected as follows: 1 ml/sampe for the first 10 fractions; 5 ml/sample for the second 10 fractions; 45 ml/sample for the last 3 fractions.

Tab. 2: Detail of sample collection during loading.

Stock solution	Flow rate (ml/min)	Volume of collected fractions during loading process in column A
No.1	0.2	1ml/sample (0 - 5 ml); 0.2 ml/sample (5 - 7.6 ml)
	0.6	
	1	
No.2	0.2	17 ml/sample (0 - 17 ml); 0.2 ml/sample (17 -24 ml);
	0.6	17 ml/sample (0 - 17 ml); 0.2 ml/sample (17 -24 ml);1 ml/sample (24 - 32 ml)
	1	15ml/sample (0 -15 ml); 0.2ml/sample (15 -20 ml);1ml/sample (20 - 24 ml)
No.3	0.2	25ml/sample (0 - 125 ml); 1 ml/sample (125 - 155 ml)
	0.6	25ml/sample (0 - 125 ml); 1 ml/sample (125 - 175 ml)
	1	45 ml/sample (0 - 90 ml); 1ml/sample (90 - 155 ml); 5 ml/sample (155 - 195 ml)

Stock solution	Flow rate (ml/min)	Volume of collected fractions durings loading process in column B
No.3	0.6	5 ml/sample (0 - 45ml); 1 ml/ sample (45 - 75 ml)
No.4		1 ml/sample (0 - 10 ml); 5 ml/sampe (10 - 45 ml); 1 ml/ sample (45 - 75 ml)

2. Effect of U

0.8 g of AMP_PAN were preconditioned and loaded in the column B and stock solutions No.3 and No.4 were used for the experiments, respectively. Fractions of 1-5 ml were collected after release of the dead volume of the system at a flow rate of 0.6ml/min (table 2).

RESULTS

1. Cs loading and washing process

The Cs loading and washing profiles are shown in figure 2. The retained Cs concentrations in AMP_PAN under different conditions are presented in table 3.

Table 3. The retained Cs concentrations in AMP_PAN after washing with 195 ml of 4 M HNO_3, the uncertainty is stated as 1 sigma.

Stock solution used for Cs loading	Flow rate (ml/min)	Retained Cs in AMP_APN (g/g) after washing
No.1	0.2	(9.0 ± 0.3)E-3
	0.6	(8.5 ± 0.4)E-3
	1	(9.2 ± 0.3)E-3
No.2	0.2	(8.6 ± 0.2)E-3
	0.6	(9.5 ± 0.2)E-3
	1	(7.5 ± 0.2)E-3
No.3	0.2	(8.1 ± 0.5)E-3
	0.6	(8.1 ± 0.2)E-3
	1	(8.4 ± 0.1)E-3

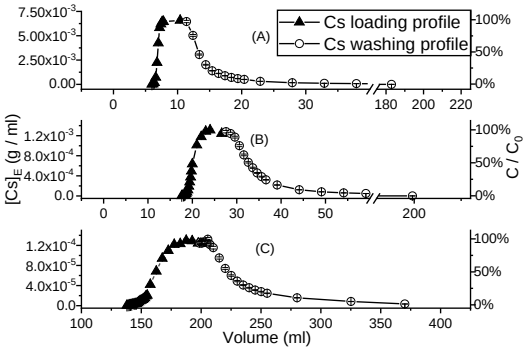

Fig. 2: The Cs loading and washing profiles with the same flow rate (1ml/min) but different Cs concentrations. (A) Cs: 50mM/l (B) Cs: 10mM Cs/l (C) Cs: 1mM/l

No dependence of the loading and washing performance on the flow rates was observed. Therefore, the results obtained for 1ml/min flow rates are shown as representative example in figure 2. After washing with 195 ml of 4 M HNO_3, only around 8 mg/g of Cs are retained in the system, pointing to a lower practical capacity than obtained in the batch studies (33 mg Cs/g AMP_PAN). This finding has to be considered when designing the setup for the processing of the real spent nuclear fuel solutions.

2. Effect of U

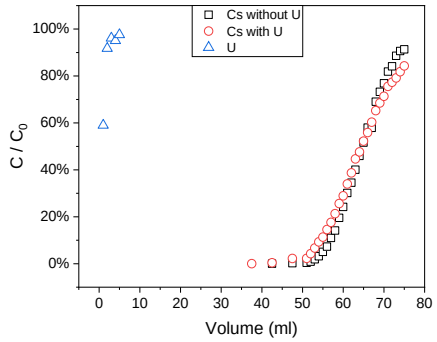

Fig. 3: Adsorption profiles of U and Cs.

Breakthrough curves of Cs and U are shown in figure 3. This figure illustrates that the breakthrough of U occurred immediately when starting to pump stock solution. The Cs breakthrough behavior is not influenced by the presence of U, which can be deduced from the nearly identical shape of the curves for Cs without U (black squares) and Cs with U (red circles).

CONCLUSION

The chromatography extraction system using AMP_PAN shows high capability for Cs-removal from highly acidic solutions. The Cs loading and washing profiles show similar trend with variation of flow rate and Cs concentration. The retained Cs after washing with 195 ml of 4M HNO_3 amounts to ca. 8 mg / g. The immediate breakthrough of U reveals insignificant adsorption of U by the column system, thus Cs adsorption is not influenced by U. We conclude that the separation system is feasible for selective Cs removal from highly acidic spent nuclear fuel solutions containing up to 0.6 Mol/L U.

We acknowledge funding from the Swiss Nuclear project “Waste treatment and Isotope Reclamation (WIR)”.

[1] M. Lin et al. Radiochim. Acta, accepted (2019).
[2] F. Sebesta et al. Phase II report. (1996). https://digital.library.unt.edu/ark:/67531/metadc670512/m2/1/high_res_d/231361.pdf
[3] T. A. Todd et al. J.Radioanal. Nucl. Chem. **254**, 47 (2002).

ADSORPTION BEHAVIOR OF IODINE RELEASED FROM IRRADIATED TELLURIUM IN VARIOUS ATMOSPHERES

E. Karlsson (Univ. Bern & PSI), J. Neuhausen (PSI), I. I. Danilov (Univ. Bern & PSI), A. Vögele, R. Eichler (PSI), A. Türler (Univ. Bern)

INTRODUCTION

To assess the safety of lead-bismuth eutectic (LBE) cooled reactors with regard to release of radioactive iodine, thermochromatographic experiments have been performed [1]. The methodology of sample preparation in these experiments was based on doping LBE with tellurium (2%). This was required to produce samples of sufficient activity as no other way of introducing carrier free ^{131}I into the LBE was available. From these experiments it was concluded that iodine behaves in a similar way on steel and fused silica surfaces in inert and reducing gases (He, H_2). In oxygen gas, the iodine was observed to be significantly more volatile [1]. To examine the influence of the presence of significant amounts of tellurium in the LBE on the speciation it is desirable to perform analogous experiments under variation of the LBE and tellurium content. As a first step in this direction we performed experiments were iodine doped natural Te was produced by n-irradiation and the iodine was evaporated from these samples and deposited in fused silica gradient tubes. Additional experiments were performed where the iodine was separated from the Te prior to the experiment. The results were then compared with the ones obtained when evaporating the iodine directly from LBE. As a next step, we plan to investigate I-containing LBE samples containing much lower amounts of Te compared to those used in [1].

EXPERIMENTAL

Thermochromatography is a method used to determine the affinity of a nuclide species to the surface of a particular material. This is of importance when performing calculations on potential releases in an accident scenario. To quantify the strength of this interaction, the nuclide species was evaporated and carried in a gas stream inside a column of the material to be evaluated.

The experimental setup used for this featured a gas loop for purification as well a starting furnace to evaporate the sample. To ensure low moisture content in the carrier gas, a Sicapent® moisture absorber cartridge was introduced to remove H_2O as well as dew point meter (Michell PuraOEM) to monitor the remaining amount. With this gas cleaning system a water content of between 0.1 – 14 ppm was achieved. This was set up in the same way as for the experiments on tellurium doped LBE to replicate the conditions as close as possible [1]. The column was made of fused silica and had dimensions of 120 cm length and an inside diameter of 5 mm. Carrier gases used were H_2, He and O_2 with flow rates between 25-45 ml/s. The fused silica column was inserted into a gradient tube furnace, which applied a thermal gradient to it from 700°C down to room temperature. For the case the nuclide species had a very low surface affinity and thus would escape the column, a charcoal trap was introduced at the exit of the column to avoid contaminations.

Sample preparation was performed by irradiating natural tellurium granules (5-25 mg) with neutrons to produce ^{131}I from neutron capture and subsequent β-decay of ^{131}Te. The irradiation was conducted in the SINQ irradiation source with 10^{13} n/s·m^2 for 3 hours. This produced an initial activity of approximately 3 kBq/mg which proved to be sufficient for the three month experimental campaign. The sample was placed in a small (approx. 15 mm x 5 mm) 316L stainless steel boat before being inserted into the setup. To reduce aerosol transport a piece of quartz wool was placed downstream from the sample. Additional experiments were also performed in helium after first having evaporated the iodine onto a silver foil to reduce the amount of tellurium in the system. The silver foil was then placed at the sample point and heated which evaporated the iodine. To treat the data, the method described in [1] is applied to obtain the adsorption enthalpy (ΔH_{ads}) to quantify the affinity of the species in the system to the surface in question.

RESULTS AND DISCUSSION

To evaluate the results of these experiments, they were compared to their LBE counterparts with differences and similarities pointed out and discussed.

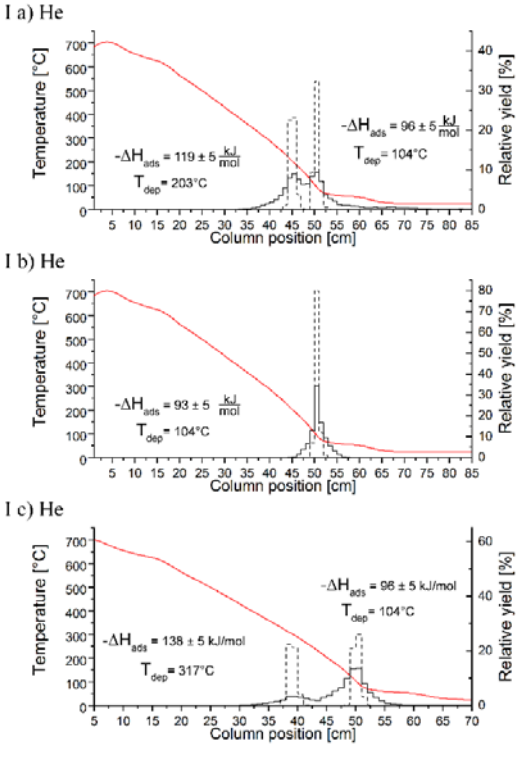

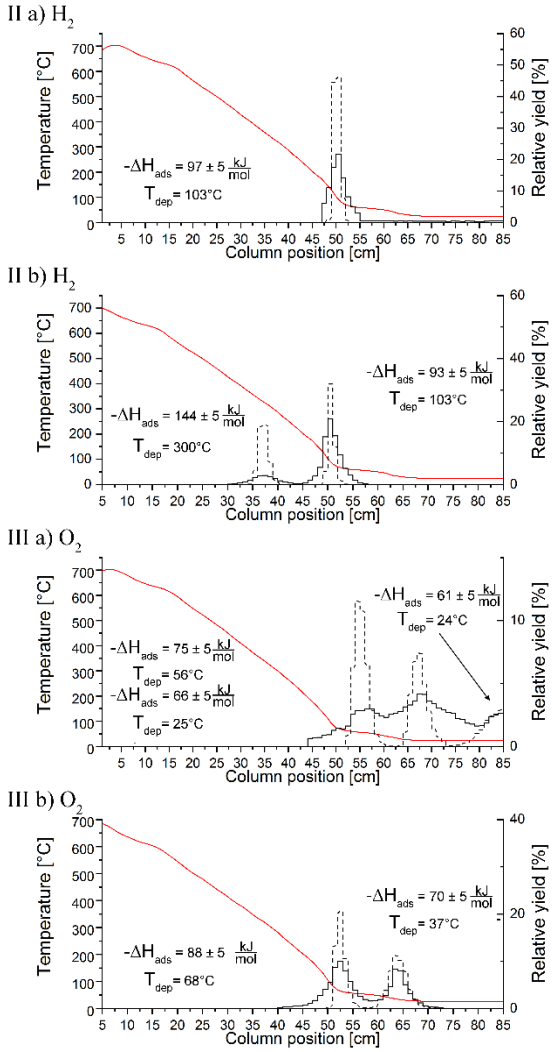

Fig. 1: Experimental results of thermochromatography on irradiated tellurium (a) and LBE doped with 2 wt% tellurium (b), with carrier gases I) helium II) hydrogen III) oxygen. Included is also one experiment with pre-separated iodine evaporated from a silver foil designated Ic). Measured deposition patterns are displayed as black solid line. The red line shows the temperature gradient in the column and the dashed black line is the results from the Monte Carlo simulations.

While the thermochromatograms in Fig. 1 may seem quite similar at first glance, there are some considerations to be factored in before one can make conclusions based on them. The samples used in these experiments contained approximately mole fractions of 10^{-10} to 10^{-11} with respect to iodine. To form polyiodic tellurium iodides beyond TeI and Te_2I, higher concentrations of iodine are needed. Additionally, chalcogen halides follow a trend of decreasing dissociation energy (MF > MCl > MBr > MI, M = S, Se, Te..) [2]. Furthermore, the stability of Pb and Bi-tellurides [3] indicates that in the system with LBE tellurium will tend to be associated to Pb and/or Bi rather than iodine. Thus, in the LBE-experiments the formation of BiI and possibly small amounts of PbI (high temperature peak in Fig. 1 IIb) is more likely. In the experiments with pure tellurium, the tellurium would instead form gaseous compounds with the iodine. In inert gas (Fig. 1, Ia) two clear depositions are formed, likely TeI and Te_2I supported by the previous reasoning. The results of the experiments using pre-separated iodine evaporated from a silver foil in helium (Fig. 1, Ic) showed disappearance of the peak at 203 °C, possibly because the amount of tellurium available in the system is not sufficient for the formation of Te_2I. This procedure did however introduce a peak at 317 °C of yet unknown origin. The single peak in hydrogen carrier gas could be explained by the instability of the Te_2I-species in reducing conditions. For oxygen the situation is more complex. There are possible tellurium oxyiodide species however literature shows no formation of monoiodic species in such a system [4]. Similar to the LBE containing system, the assumed likely species are I, IO_x and the family of HIO_x acids with the hydrogen coming from water impurities. These impurities are present either in the carrier gas or as silanol groups on the silica surface.

CONCLUSIONS

While iodine evaporated from LBE does at a glance share adsorption characteristics with iodine evaporated from tellurium one must consider the chemistry. With thermodynamical data and reasoning it is possible to deduce where similarities are present and where they are merely apparent. In the carrier gases helium and hydrogen, in the LBE-containing system the speciation alternative which includes tellurium is less likely from a thermodynamic standpoint than the bismuth monoiodide. Similarities in the chemical behaviour of the iodine from irradiated tellurium doped LBE compared with the irradiated natural tellurium is considered as limited to species that are shared between them, for example the species of oxygen, iodine and hydrogen postulated in the case of oxygen carrier gas. Thus we suggest the observed overlaps in the chromatograms in Fig. 1 (I and II) are not due to similarities in speciation but are caused by similar adsorption characteristics of the bismuth and tellurium monoiodide.

The system of LBE doped with other elements must continue to be probed in ways like this to properly understand the influence of the added chemical components. Additionally, impurities and dissolved gases in the LBE complicate the chemistry involved in such an investigation.

ACKNOWLEDGEMENT

This work was funded by the project MYRTE under EURATOM HORIZON2020 Grant Agreement No. 662186.

[1] E. Karlsson, et al., LRC Ann. Rep. 2016, p. 11, PSI (2017).
[2] Y.-R. Luo, Comp. Handbook of Chem. Bond Energies, CRC Press: Boca Raton, Fl, USA, (2007).
[3] I. Barin, Thermochemical data of pure substances, 3rd ed., VCH, Weinheim, (1995).
[4] H. Oppermann et al., Anorg. Allg. Chem. **461**, 165 (1980).

SILVER AS A POTENTIAL FILTERING MATERIAL FOR ADSORBING GAS PHASE IODINE EVAPORATED FROM LBE

E. Karlsson (Univ. Bern & PSI), J. Neuhausen (PSI), I. I. Danilov (Univ. Bern & PSI), A. Vögele, R. Eichler (PSI), A. Türler (Univ. Bern)

INTRODUCTION

In the context of Gen IV reactor research this study focused on the fission product chemistry of lead-bismuth eutectic (LBE) cooled reactors. Investigations have been done on the evaporation and deposition behaviour of iodine in an LBE system. These have shown that the chemical species of iodine present in such a system have a relatively high volatility and consequently low affinity to both stainless steel and silica surfaces at conditions both with and without water present [1]. The volatility is further increased when oxygen is introduced resulting in high mobility at temperatures near room temperature. This highlights the need for efficient filtering solutions to immobilize the iodine species.

Iodine being reactive and highly volatile, as well as having a large fission yield needs to be closely controlled in a nuclear reactor system. For light-water reactors a lot of research has been performed, resulting in innovative systems for filtering out gaseous iodine from the containment atmosphere during operation and particularly, in the event of an accident. [2]. Fortunately, iodine has a high affinity towards caesium which is another high yield fission product, with which it forms CsI if available in macroscopic amounts. This relationship limits the amount of iodine released. However, a large amount is still available to form $I_xO_yH_z$ species which are volatile or can be otherwise transported with aerosol particles. The remaining iodine is dealt with through for example scrubbing the atmosphere inside the containment by releasing it through a burst-disc into an external venturi scrubber system containing specially designed alkaline scrubbing solutions. This system filters out remaining iodine species with a very high efficiency, with the exception of organic iodine [3]. These available systems are based on an aqueous chemistry, whereas the cover gas system of an LBE-cooled reactor should ideally operate at extremely low moisture content. Some suggestions for gas purification systems fulfilling this criterion are based on gas adsorption of the iodine to a solid. Most of these are based on some form of activated charcoal being used to capture the iodine [4, 5]. This works well as long as the amount of iodine is not too large when a significant heat load from the decay of the shorter-lived iodine isotopes is expected. The temperature can reach levels high enough for the filter to ignite if enough oxygen is present [6]. To avoid this issue we must look for materials that can handle higher heat stresses such as for example metals. Proposed systems are often based on some form of inorganic framework into which silver is dispersed, for example zeolites [7]. This introduces adsorption sites to which iodine has a strong affinity with high capacity due to the large surfaces. To investigate the iodine silver interaction a simple system was constructed where the iodine was allowed to evaporate from LBE before being transported in a carrier gas and deposited on a silver foil inside a tube of fused silica exposed to a temperature gradient.

EXPERIMENTAL

The experimental setup used was analogous to the setup used for determining iodine behaviour and affinity to fused silica and steel surfaces in various conditions through thermochromatography (TC). For a detailed description of parts of the setup, their function and the performance of the experiments refer to [1]. For the moisture controlled experiments, the level of water in the carrier gas was measured to be 5-100 ppm. The difference between the experiments performed here and the ones using empty columns is the addition of an inserted rolled up silver foil reaching from the hottest section of the column continuing 45 centimetres along the gas flow direction (see Figure 1). The temperature along the silver stretches from 700°C down to 50°C in the water saturated setup and 700° to 180°C in the moisture controlled setup. Pilot experiments were performed to determine the temperature range most appropriate for the placement of the foil. Initial attempts had all activity adsorbed on the first centimetre as the column was not clad with silver up to the highest temperatures. The position of the silver foil was marked on the outside of the column prior to the experiment to ensure that any movement of the foil would be noticed easily. To prevent any movement, pieces of quartz wool were placed before and after the foil. The quartz wool had a secondary function as an aerosol filter to prevent transport of small amounts of LBE, which may change the surface and transport unwanted activity.

RESULTS AND DISCUSSION

Moisture-controlled experiments

In moisture-controlled conditions, good retention of iodine was observed (Fig.1). To compare, iodine species evaporated from LBE adsorb to stainless steel and fused silica at temperatures of about 110°C or lower [1]. Here, the deposition peaks on silver are all above 450°C, which is indeed equivalent to the approximated highest coolant temperature allowed in an LBE-cooled reactor due to corrosion issues [8].

Water-saturated experiments

For the water-saturated case, the situation looks very similar revealing high adsorption temperatures of volatilized iodine species (Fig.2). The highest deposition temperature is found in hydrogen in both

setups, this may be due to surface reduction of the silver occurring at increased temperatures.

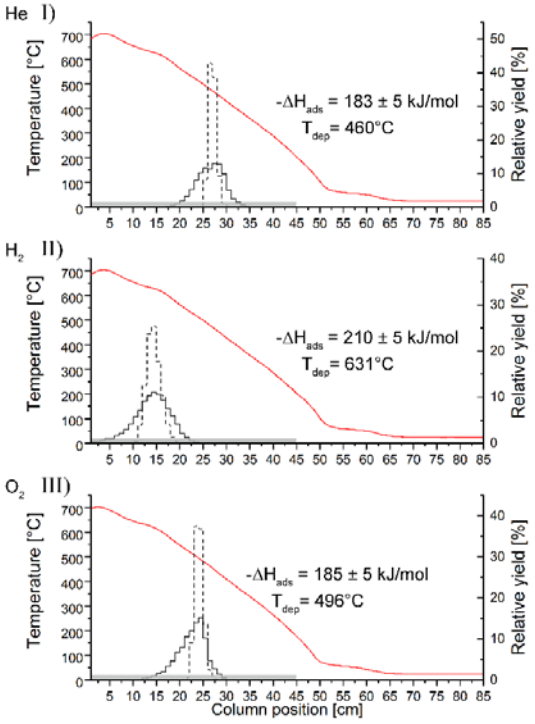

Fig. 1: Experimental results of TC with LBE doped by 2 wt% Te in a moisture controlled system with carrier gases I) He II) H_2 III) O_2. The measured deposition pattern is displayed as a black solid line. The red line shows the temperature gradient in the column and the dashed line is the results from the Monte Carlo simulations. Given in the figure is also the deposition temperature and calculated adsorption enthalpy (ΔH_{ads}). The position of the silver foil is indicated by the grey line.

CONCLUSIONS

The performed series of experiments indicate that silver surfaces provide an adequate filtering solution for iodine species evaporated from an LBE-coolant.

In all three gases the deposition pattern features a single peak, however there may be multiple chemical species adsorbing with similar adsorption enthalpies giving the illusion of a single peak. This is a likely reason for the broadening on for example the left hand side of the peak in Fig. 1 III).

The adsorption is relatively strong and the resulting deposition temperatures high enough to ensure lasting retention with a safety margin in case of the presence of decay heat. Surface modifications including high temperature reduction of the silver foil with hydrogen as well as the removal of potential inorganic as well as organic impurities contribute to a stronger adsorption.

One reason for the strong adsorptions observed compared to the stainless steel or fused silica experiments may be the transition from weak physisorption to strong chemisorption. The iodine adsorbs on the silver surface where it reacts, forming a strong Ag-I bond.

The cost of silver used as a filtering material are mitigated by regeneration using off-line high temperature desorption of the iodine connected, e.g., to a well established capturing procedure in aqueous solutions.

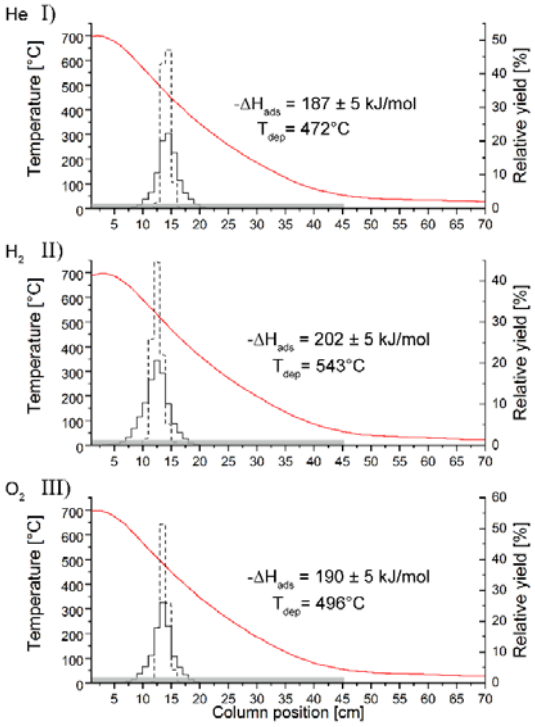

Fig. 2: Experimental results of TC with LBE doped by 2 wt% Te in a water saturated (~2 vol%) system with carrier gases I) He II) H_2 III) O_2.The measured deposition pattern is displayed as a black solid line. The red line shows the temperature gradient in the column and the dashed line is the results from the Monte Carlo simulations. Given in the figure is also the deposition temperature and calculated adsorption enthalpy (ΔH_{ads}). The position of the silver foil is indicated by the grey line.

ACKNOWLEDGEMENT

This work was funded by the project MYRTE under EURATOM HORIZON2020 Grant Agreement No. 662186.

[1] E. Karlsson, et al., LRC Annual Report 2016, p. 11, PSI, (2017).
[2] L.E. Trevorrow et al. ANL-83-57 Part I, Argonne National Laboratory, Argonne, Illinois, USA (1983).
[3] R.O. Schlueter, et al., Nucl. Eng. Des. **103**, 93 (1990).
[4] R.T. Jubin et al., ORNL/TM-10477, Oak Ridge National Laboratory, Oak Ridge, Tennessee, USA (1988).
[5] H. Sun et al., J. Hazardous Mater. **321**, 210 (1980).
[6] R.A. Lorenz et al., CONF-740807--P2, Oak Ridge National Laboratory, Oak Ridge, Tennessee, USA (1975).
[7] J. Wilhelm et al., Patent No. EP332964A3, Kernforschungszentrum Karlsruhe GmbH, Karlsruhe, Germany (1989).
[8] G. Müller et al., J. Nucl. Mat. **335**, 163 (2004).

RADIAL DISTRIBUTION OF RADIOTRACERS IN N-IRRADIATED Te-DOPED LBE SAMPLES

J. Neuhausen (PSI), I. I. Danilov (Univ. Bern & PSI), A. Vögele (PSI)

INTRODUCTION

The behavior of radionuclides dissolved in liquid lead bismuth eutectic (LBE) has been studied in our laboratory for several years in context with safety studies for nuclear installations such as the spallation target MEGAPIE and the Accelerator Driven System (ADS) MYRRHA planned to be built in Mol, Belgium. Most of this work focused on the volatilization of dissolved elements from liquid LBE. To determine reliable physicochemical data for such diluted solutions via transpiration experiments, the availability of homogenous starting material is required. In a previous report [1] we found by SEM/EDX-studies that Te mixed at high temperatures with LBE to prepare I-containing LBE samples by neutron activiation of the dissolved Te tends to separate from the LBE and form precipitates. Rapid quenching of the liquid solution of Te in LBE from high temperatures to room temperature suppressed the segregation of Te. Surface enrichment of the studied element may distort the results of transpiration studies. Therefore, it needs to be avoided. In this work we study the radial distribution of various radiotracers in n-irradiated Te-doped LBE samples produced for ^{131}I-transpiration experiments, solidified using different cooling schemes, with the purpose of confirming their suitability for transpiration experiments.

EXPERIMENTAL

All manipulations during the preparation of the samples were performed in an inert gas glovebox at nominal < 1ppm of O_2 and H_2O impurities in the gas phase. Samples from different batches of LBE were studied, including samples provided by SCK•CEN (SIDECH, 5N) and samples prepared from Pb and Bi (Chempur, 6N) by co-melting in evacuated fused silica ampoules. To reduce the amount of oxygen dissolved in the LBE, the ampoule was clad with Ta-foil and the mixture was heated to 1000°C for a few days. For comparison, also non-reduced LBE samples were prepared. Mixtures of both reduced and non-reduced LBE with 2 mass % Te were prepared by mixing at 850 °C under vacuum in a sealed ampoule and rapidly quenching to room temperature in a water bath. About 0.5 to 1 g of these LBE-Te mixtures were filled into PE-irradiation capsules. Six of these capsules were placed into a second larger PE capsule, all under inert atmosphere. The samples were then irradiated for 2-3 h in a neutron flux of nominally 1×10^{13} n cm^{-2} s^{-1}. Apart from rapid quenching, two additional cooling schemes were tested to mimick the redistribution of the remaining radioactivity during the cooling of the sample after the transpiration experiments. For this purpose, the irradiated samples were initially exposed to temperatures between 285 and 485 °C under helium flow in a transpiration tube. Subsequently, they were cooled down to room temperature either 1) radiatively by just switching off the furnace of the transpiration setup (solidification time ca. 20-30 min) or 2) more quickly by blowing the inert gas of the glove box onto the transpiration tube containing the samples using a blow dryer (solidification time ca. 1-2 min). The samples obtained in this way were subjected to a step-wise dissolution procedure, where in each step the outermost part of the sample was dissolved. Thus, by measuring the activity dissolved in each step the radial distribution of the nuclides can be determined. The stepwise dissolution was achieved by submerging the samples for a defined time in 8 ml of conc. HNO_3 (65%, 14M) in a 20 ml PE LSC-vial. Afterwards, the surface of the sample was rinsed with 8 ml of water to stop the dissolution process and remove adherent acid together with the activity dissolved in it. The rinsing water was added to the HNO_3-solution. The activity contained in the solution was then measured by γ-spectrometry. The γ-measurements were performed using calibrated HPGe-detectors. Typical acquisition times ranged from 10 to 30 min depending on the activity of the samples. The samples were weighed before and after each dissolution step. Wet samples were dried on a paper towel before weighing. To obtain information on the radionuclide distribution in the near surface region, short dissolution times were applied for the first dissolution steps. Progressing to the bulk of the material, longer dissolution times were applied until the sample was completely dissolved. The samples studied in this way included the following conditions:

(1) 6N LBE, reduced, rapidly quenched (H_2O)
(2) 6N LBE, reduced, blower cooled
(3) 5N LBE, non-reduced, blower cooled
(4) 6N LBE, reduced, radiatively cooled

To determine the distribution of radionuclides in the sample from the analysis of the dissolved material, we assumed that the samples are spherical. We then calculate the radii of the samples before and after each dissolution step, from which we assess a depth profile of the activities. The real shape of the samples was not ideally spherical but rather oblate. Therefore, the values given for depth should be considered as approximate. Uncertainties of the weighing procedure were determined as standard deviation of repeated weighings of an LBE sample with interim dipping into water and drying in a manner similar to that used in the actual leaching experiments. The surface of the LBE sample had been roughened by etching in HNO_3 prior to the repeated weighing. The standard deviation determined in this way was $\pm 5 \times 10^{-4}$ g, one order of magnitude larger than the uncertainty determined without interim

water dipping. Uncertainties of activities were determined from counting statistics, the uncertainties of the activity of the calibration sources and an uncertainty accounting for variations of the sample positioning on the detector. Uncertainties are high when evaluating the activity concentrations of the nuclides contained in the samples, especially for the very first layers, where due to the short dissolution times both activity and mass can only be determined with relatively large relative uncertainties. These relative uncertainties then add up in the uncertainty of the activity concentration. Therefore, we chose to present the results in terms of activities of the individual radionuclides normalized to the activity of ^{205}Bi, one of the radiotracers for the matrix element Bi.

RESULTS AND DISCUSSION

The analysis of the γ-spectra of the irradiated samples revealed that apart from ^{131}I and ^{123m}Te and nuclides of the matrix elements (^{203}Pb, ^{205,206}Bi) also measurable amounts of ^{202}Tl were formed. Additionally, the samples that were reduced by contact with a Ta-foil contained ^{182}Ta. Results on the latter two elements will be presented elsewhere.

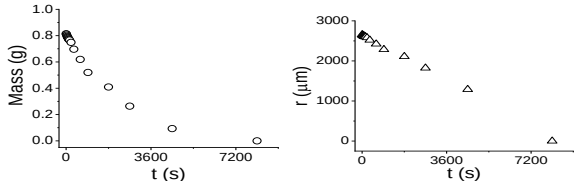

Fig. 1: Sample mass and radius as a function of dissolution time for LBE samples dissolved in 14 M HNO_3.

The plots of sample mass and radius vs. dissolution time shown in Fig. 1 indidcate that the dissolution process was smooth, with no unexpected effects occurring. The behaviour was similar for all investigated samples.

Fig. 2 shows the depth distribution of activities of several nuclides normalized to the ^{205}Bi activities in the samples, and again normalized to the weighted mean of the entire data set for the corresponding isotope in this sample. Section a) of Fig. 2 shows the results for a sample that was rapidly quenched to room temperature in a water bath. The depth profile of the normalized (^{206}Bi)/(^{205}Bi) activity ratio shows no large changes throughout the specimen. This is expected, since no isotope effects should occur that could lead to variations of this ratio. The results validate the applied evaluation method. The ratio of the activities of ^{203}Pb/^{205}Bi could in principle show fluctuations because solid LBE is composed of a lead rich and a bismuth rich phase [2]. The homogeneous depth profile detected for the raidly quenched sample depicted in Fig. 2a indicates that the grains of the two phases and the density differences between the phases are obviously too small to cause detectable inhomogeneities. This is also the case for the slower cooled samples (not shown). The depth profiles of iodine and tellurium in the rapidly quenched sample are rather homogeneous, though there seems to be a depletion of these elements in the near surface region with a depth < 30 μm. The origin of this effect remains unclear so far. For transpiration experiments, we conclude that near-surface material should be avoided when sampling the LBE to determine its initial activity. In samples that were solidified less quickly inside a transpiration setup using a blow dryer (Fig. 2 b)) a significant enrichment of iodine and tellurium is observed near the surface up to a depth of approx. 100 μm. The effect was reproducible in three samples of reduced 6N LBE and also in non-reduced 5N LBE. This finding is important because it indicates that under the cooling scheme that is currently applied in our transpiration procedure the distribution of iodine and tellurium will not be homogeneous anymore. It would be desirable to re-use samples for several experiments both for economical and radioprotection reasons. However, the re-use of samples similar to that studied in Fig. 2b) would be problematic because increased volatilization of the surface-enriched material can occur, and the reliable determination of the starting activity may be hampered by the inhomogeneity. This could be mitigated by developing an apparatus that allows more rapid quenching of the samples after the transpiration experiment.

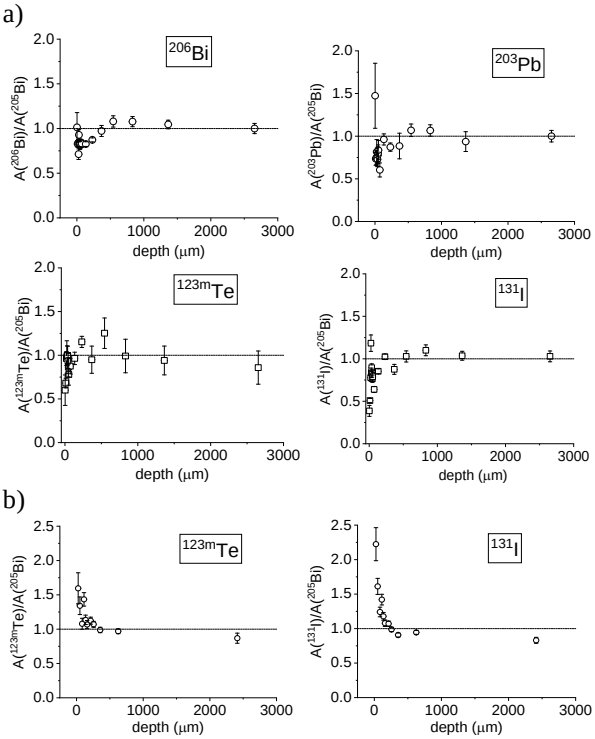

Fig. 2: Radial distribution of various radionuclides in LBE samples: a) rapidly quenched sample; b) sample cooled to solidification within 1-2 min. All plots show the activity of the indicated nuclide normalized to the ^{205}Bi activity in the same sample, and again normalized to the weighted mean of the entire data. Error bars are based on 1σ uncertainties.

This work was funded by the project MYRTE under EURATOM HORIZON2020 Grant Agreement No. 662186.).

[1] J. Neuhausen et al., Deliverable D4.3 of EURATOM H2020 Project MYRTE (2019).
[2] N. A. Gokcen, J. Phase Equil. **13**, 21 (1992).

SEARCH FOR THE FINGERPRINTS OF SHAPE ISOMERISM IN LIGHT NUCLEI: SPECTROSCOPY OF ^{64}Ni USING A ^{63}Ni RADIOACTIVE TARGET AT ILL

N. Marginean, C. Costache, R. Lica, C. Mihai, R. E. Mihai, C. R. Nita, S. Pascu, A. Turturica, S. Ujeniuc (IFIN-HH), S. Leoni, F. Crespi, S. Bottoni, A. Bracco, C. Porzio (Univ. Milano, INFN Milano), B. Fornal, N. Cieplicka-Oryńczak, L. Iskra (IFJ-PAN), M. Sferrazza (Univ. Bruxelles), C. Michelagnoli, F. Kandzia, U. Köster (ILL), G. Korschinek (TU Munich), E. A. Maugeri, D. Schumann (PSI)

The isotopic chain of the nickel isotopes offers a unique testing ground for theories predicting nuclear structure properties between the two doubly magic shell closures of ^{56}Ni and ^{78}Ni. While the doubly magicity of the highly neutron-rich ^{78}Ni has recently been proved at radioactive ion beam facilities [1], medium spin states of nickel isotopes, closer to the beta stability line, can be studied in thermal neutron induced reactions on stable (rare) or radioactive targets. Measurements using different target nuclei have been recently performed by the IFIN-HH-Milan-Cracow collaboration at the FIPPS instrument at ILL [2].

FIPPS (Fission-Product-Prompt-γ-ray-Spectrometer) is a new nuclear physics instrument of ILL consisting of a pencil-like thermal neutron beam and an array of Compton-suppressed HPGe clover detectors. The efficiency of the detector array has been recently improved by the addition of IFIN-HH HPGe clovers.

In September 2019, a 2 GBq ^{63}Ni target has been used for the first time for performing a detailed spectroscopy of ^{64}Ni via thermal neutron capture reactions. Different excited 0^+ states were populated, among which fingerprints of *shape isomerism* are searched. This phenomenon was observed for the first time in light nuclei in the ^{66}Ni nucleus populated in transfer reactions [3]. Monte Carlo Shell Model (MCSM) calculations [4] foresee the presence of deformed excited 0^+ state candidates for shape isomerism also for other nickel isotopes and in particular for ^{64}Ni.

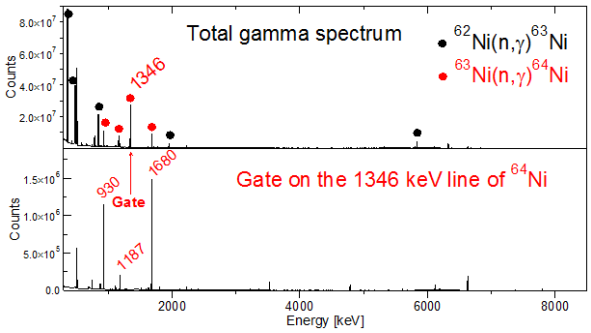

Fig. 1: Total gamma-ray spectrum detected in FIPPS after thermal neutron reactions on the radioactive ^{63}Ni target. A coincidence spectrum for ^{64}Ni is shown.

In 1990 an enriched ^{62}Ni target had been irradiated for 170 days in the in-pile position of the GAMS spectrometer at ILL, converting ^{62}Ni partly to ^{63}Ni [5]. After use as absorber for ^{63}Ni Mössbauer spectroscopy at TU Munich [6], the material was purified at PSI from the decay product ^{63}Cu and used for cross-section measurements at CERN n_TOF and LANL DANCE [7,8]. In 2019 the sample returned to PSI and a fraction (~2 GBq) was prepared for the FIPPS experiment.

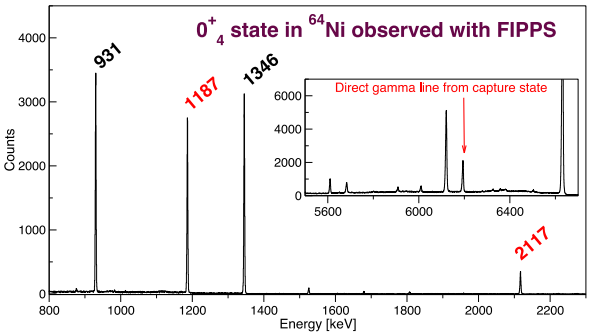

Fig. 2: Gamma-ray spectrum of ^{64}Ni obtained with a gate on the gamma ray from the capture state, directly feeding the 0^{+}_{4} state, candidate for shape isomerism.

In particular, a surface of 7×13 mm of a 12.5×25 mm Al foil was covered with a thin layer of an epoxy resin, on which 0.0121 g of NiO were homogeneously distributed. Another thin layer of epoxy resin was spread on the entire surface of the foil, which was covered with a second Al foil of the same size. The resulting sample was rinsed several times with ethanol first and distilled water after. A smear test confirmed no external contamination of ^{63}Ni on the sample surface.

The total gamma-ray spectrum detected in FIPPS is shown in Figure 1. The lines belonging to ^{64}Ni and ^{63}Ni are indicated and demonstrate the high purity of the sample. The spectrum in coincidence with the $2^{+1}\rightarrow 0^+$ decay from ^{64}Ni is also shown. Using multiple gamma-ray coincidences 8 excited 0^+ states were found. The gamma rays de-exciting 0^{+4}, candidate for shape isomerism, are shown in Figure 2. The spin and parity of the states have been determined via angular correlations.

The results are compared with MCSM calculations, which allow for a microscopic understanding of the shape coexistence phenomenon in nickel isotopes.

---

[1] R. Taniuchi et al., Nature **569**, 53 (2019).
[2] C. Michelagnoli et al., EPJ Web Conf. **193**, 04009 (2018).
[3] S. Leoni et al., Phys. Rev. Lett. **118**, 162502 (2017).
[4] T. Otsuka et al., Prog. Part. Nucl. Phys. **47**, 319 (2001).
[5] A. Harder, et al., Z.Phys. A **343**, 7 (1992).
[6] M. Trautmannsheimer et al. Phys. Lett. A **176**, 398 (1993).
[7] C. Lederer et al. Phys. Rev. Lett. **110**, 022501 (2013) & Phys. Rev. C **89**, 025810 (2014).
[8] M. Weigand et al. Phys. Rev. C **92**, 045810 (2015).

THE PRODUCTION OF THE RADIOLANTHANIDE ^{161}Tb AND ITS INTRODUCTION TO GOOD MANUFACTURING PRACTICE RADIOLABELLING

C. Favaretto (ETHZ & CRS/PSI), Z. Talip, P. V. Grundler, S. Geistlich, S. Landolt (CRS/PSI), N. Gracheva (ETHZ & CRS/PSI), J. R. Zeevaart (Necsa), U. Köster (ILL), R. Schibli (ETHZ & CRS/PSI), N. P. van der Meulen (LRC/PSI)

INTRODUCTION AND AIM

The radioisotope ^{161}Tb ($T_{1/2}$ = 6.89 d) shows similar decay characteristics and chemical behavior to ^{177}Lu, which is currently regarded as the "gold standard" of targeted radionuclide therapy. In particular it decays by β^-–particle emission ($E_{\beta\text{-av}}$ = 154 keV (100 %), $T_{1/2}$ = 6.9 d) [1]. However, on a preclinical level, ^{161}Tb was proved to be superior as a result of its co-emission of conversion and Auger electrons (~12.12 e–, ~36.1 keV per decay) [2,3]. Herein we report the results on the study to achieve the production and introduction of the novel radionuclide ^{161}Tb to the clinic. Efforts were put into development and improvement of the ^{161}Tb purification process [3] based on the production method reported previously [4]. Initial studies for the establishment of a protocol for the Good Manufacturing Practice (GMP) compliant production of ^{161}Tb-DOTATOC were performed.

METHODS

^{161}Tb production was carried out by irradiating enriched ^{160}Gd oxide targets either at the SAFARI-1 (South Africa) reactor or the high flux reactor of ILL (France), using the ^{160}Gd(n,γ)^{161}Gd→^{161}Tb nuclear reaction. ^{161}Tb was separated from ^{160}Gd target material using cation exchange chromatography and concentrated using extraction chromatography. Furthermore, the entire production process was optimized and made reproducible, and the quality of the labeling solution was assessed, in order to validate the characteristics necessary for its introduction to a clinical setting [5]. With the same product, it was then possible to carry out a promising preliminary study for the production of ^{161}Tb-DOTATOC conform to the GMP principles in a modular automated system. ^{161}Tb-DOTATOC was synthetized and subsequently, the stability of the product was evaluated. A definition of the quality control process by HPLC method was also performed in order to be able to assess the quality of the product under GMP conditions.

RESULTS

^{161}Tb production and purification process led to a production yield in the range of 8-20 GBq ^{161}Tb no-carrier-added at concentrations of 11-21 MBq/µL. As a quality control of this labeling solution, it was possible to achieve bench labelling of DOTANOC with ^{161}Tb at 180 MBq/nmol molar activity at a labelling efficiency of ≥99%. Furthermore, the chemical purity of $^{161}TbCl_3$ solution was estimated by ICP-OES and the bacterial endotoxin were found to be under the limit set by Pharmacopoeia by means of a LAL test [6]. With this quality of product, ^{161}Tb-DOTATOC was synthetized for the first time using a modular automated system in a product with characteristics and minimum quantity of activity suitable for clinical use, i.e. 1.0 GBq in 20 mL at 53 MBq/nmol molar activity. The production yield was demonstrated to be >85% and the product stable for 24 hours (Figure 1). Moreover, the HPLC method for the quality control was established and the range and linearity of UV and radio detector were assessed for the product.

CONCLUSIONS

High yields of $^{161}TbCl_3$ have been produced, using a variety of irradiation sources, in a quantity and quality suitable for potential clinical application. Thanks to the high quality of the product and the reproducibility of the process, a GMP compliant production process of ^{161}Tb-DOTATOC was preliminarily evaluated and a final validation and documentation of the whole process will be prepared for submission to the authorities.

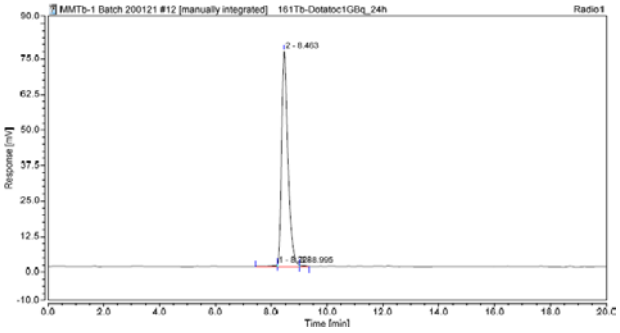

Fig. 1: HPLC chromatogram of 1 GBq ^{161}Tb-DOTATOC after 24 hours from the synthesis (2 min retention time would indicate "free" non-labeled ^{161}Tb and 8.2 min indicates ^{161}Tb-DOTATOC).

[1] "Nudat 2" https://www.nndc.bnl.gov/nudat2/.
[2] C. Müller et al., Eur. J. Nucl. Med. Mol. Imaging **41**, 476 (2014).
[3] N. Gracheva et al., EJNMMI Radiopharm. Chem. **4**, 1 (2019).
[4] S. Lehenberger et al., Nucl. Med. Biol. **38**, 917 (2011).
[5] European Directorate for the Quality of Medicines and HealthCare, "Guide for the elaboration of monographs on RADIOPHARMACEUTICAL PREPARATIONS," 2018.
[6] E. Pharmacopoeia, RADIOPHARMACEUTICAL PREPARATION Radiopharmaceutica **1**, 884 (2008).

PRODUCTION OF MASS-SEPARATED ^{169}Er TOWARDS FIRST PRECLINICAL IN VIVO INVESTIGATIONS

Z. Talip, C. Müller F. Borgna (CRS/PSI), J. Ulrich, N. P. van der Meulen (LRC/PSI), Y. Nedjadi, F. Juget, C. Bailat (IRA), C. Duchemin, T. Stora (CERN-MEDICIS), U. Köster (ILL)

The use of radioactive isotopes in the field of nuclear medicine for diagnostic and therapy has significantly increased over the last two decades. As a result, there is an urgent need to explore the effects of new radioisotopes and innovative production technologies.
^{169}Er has very promising decay properties ($T_{1/2}$ = 9.4 d, $E\beta^-_{av}$ = 100 keV [1]) for radionuclide therapy of metastasized cancer diseases. In fact, dosimetry calculations showed that ^{169}Er has high tumor-to-normal-tissue absorbed dose ratio (TND) values, in particular for small tumor sizes [2], which can be ascribed to the low β^--energy. Thus, ^{169}Er is considered as a radionuclide of interest in targeted radionuclide therapy (TRT) of disseminated disease.
To date, ^{169}Er has only been used for the treatment of chronic rheumatoid arthritis in order to treat inflammated synovium through irradiation and to improve joint function [3-5]. Low specific activities are acceptable for this purpose. However, receptor-targeted radiotherapy requires high specific activities for radiolabeling of targeting molecules such as peptides and antibodies.
The aim of this work was to produce no-carrier-added (n.c.a.) β^- emitter ^{169}Er by using mass separation and subsequent radiochemical separation to obtain ^{169}Er with high radionuclidic and chemical purity.

^{169}Er production

Enriched $^{168}Er_2O_3$ (98.0%, ISOFLEX, Russia/U.S.A. and 98.2%, Trace Sciences International, Canada) was used for the production of ^{169}Er via thermal neutron capture ^{168}Er(n,γ)^{169}Er. After irradiation for one week in the high flux position V4 of the reactor at ILL (Institut Laue-Langevin, Grenoble), the ampoules were transferred to CERN-MEDICIS for offline mass separation. ^{169}Er was implanted into a Zn-layer deposited on a gold foil. The foils were then shipped to PSI for chemical separation, quality control, and preclinical research studies.
In total, seven samples were received from CERN-MEDICIS. Figure 1 shows the images of ^{169}Er implanted Zn-coated gold foils before (a) and after (b) dissolving the Zn layer to remove the ^{169}Er activity..
Gamma spectra of the gold foils were taken before and after leaching of the Zn layer, using a high-purity germanium (HPGe) detector (Canberra, France), in combination with the Inter-Winner software package (version 7.1, Itech Instruments, France). It was observed that, except for the first foil, the ^{169}Er activities remaining on the gold foils after leaching were negligible.
The presence of traces of ^{168}Yb in the target material (Er_2O_3 enriched in ^{168}Er) led to the co-production of ^{169}Yb due to the very high thermal neutron capture cross-section of ^{168}Yb (2400 b). The mass separation method at MEDICIS is based on element selective laser ionization of erbium, but the lasers interact with the atoms in a hot tungsten tube which leads also to surface ionization of other elements. As a result, other than ^{169}Er, also ^{169}Yb ($T_{1/2}$ = 32 d) and stable ^{169}Tm (chemical impurity of stable Tm in the enriched material and decay product of ^{169}Er and ^{169}Yb respectively) was present as an isobaric contaminant in the mass-separated sample.

Chemical Separation

The ^{169}Er-containing Zn layer was dissolved in concentrated HNO_3. The solute was then passed through extraction resin, which was used to separate ^{169}Er/^{169}Yb from macro amounts of Zn. ^{169}Er and ^{169}Yb were eluted with dilute HCl. To separate ^{169}Er from the isobaric impurity ^{169}Yb, the solution was loaded onto a macroporous strongly acidic cation exchange resin and ^{169}Er eluted using dilute α-hydroxyisobutyric acid (α-HIBA) (Figure 2). The eluted ^{169}Er was finally loaded onto LN3 extraction resin to separate the complexing agent from Er and to have the final product in chloride form.

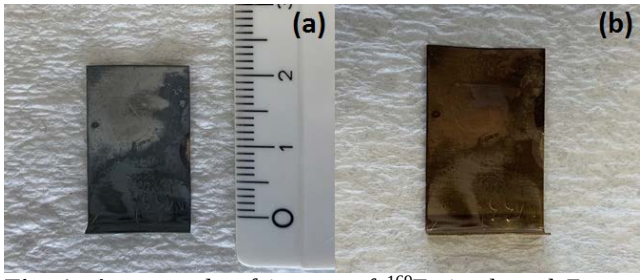

Fig. 1: An example of images of ^{169}Er implanted Zn coated gold foil before (a) and after (b) dissolving the Zn layer to remove the implanted ^{169}Er activity.

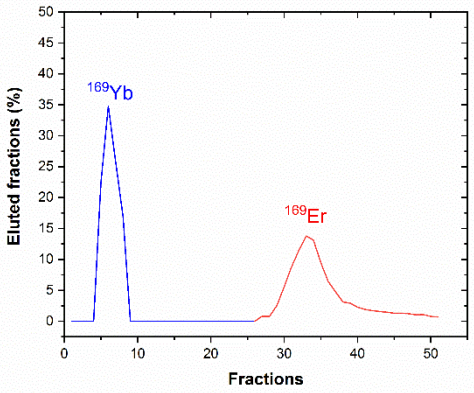

Fig. 2: Separation profile of ^{169}Yb and ^{169}Er using the Sykam cation exchange resin and α-HIBA separation system.

Activity Measurements

Activity measurements were performed on the final product using Liquid Scintillation Analyzer (Packard Tri-Carb 2250 CA). The purified ^{169}Er fraction was sent to IRA (Institut de Radiophysique, Lausanne) for standardization using the triple to double coincidence ratio technique. The activity concentration of the fraction was measured as 1798.53 ± 5.93 kBq/g (0.33%, *k*=1). Based on the activity concentration, ^{169}Er quench series were prepared and the liquid scintillation counter (LSC) was calibrated using the external standard method. The counting efficiency for typical samples was approx. 97%. Table 1 shows the measured activity of the samples received from CERN-MEDICIS.

Tab. 1: The activity of ^{169}Er samples received from CERN-MEDICIS (measured by LSC).

Sample	Activity (MBq)
M-Er169-1	52.9
M-Er169-2	23.4
M-Er169-3	8.59
M-Er169-4	4.7
M-Er169-5	73.2
M-Er169-(6-7)	93.4

Labeling Efficiency

The M-Er169-5 sample was prepared for use for preclinical research studies. The purified ^{169}Er product, in 0.1 M HCl, was used to label PSMA-617. The radiolabeling yield was determined by reverse-phase-high-performance liquid chromatography (HPLC, Merck Hitachi LaChrom) with a radioactivity detector (LB 506, Berthold, Germany) and a C18 reverse-phase column (150mm× 4.6mm; Xterra™ MS, C18; Waters). The quality of the sample was deemed insufficient for preclinical work, as the Zn amount in the final product was high (determined as 0.49 µg by ICP OES).

<u>The effect of Zn impurity on labeling efficiency</u>

It is known that the presence of Zn^{2+} in the eluate is a major obstacle for the labeling process. To investigate the effect of Zn^{2+} impurity on the labeling efficiency, different concentrations of Zn solutions were prepared from ICP standards. The addition of 2, 0.2 and 0.02 µg Zn to 0.05 M HCl solutions were used for the labeling of ^{177}Lu-DOTANOC at 100 MBq/nmol molar activity (n.c.a. ^{177}Lu was supplied from ITG, Germany) (Figure 3). The labeling was performed at pH 4.5, 95 ºC and 10 minutes incubation time. The HPLC results demonstrated that, in the presence of Zn, the formation of ^{177}Lu-DOTANOC is highly dependent on the concentration of Zn.

The samples M-Er169-6 and 7 were dissolved together and, to improve the labeling efficiency, an additional Zn separation was performed using LN3 and TK200 resin, respectively (Figure 4). As a result, the final ^{169}Er fraction was used to label PSMA-617 at a molar activity of 10 MBq/nmol (Figure 5). The quality of the final product was sufficient to perform preclinical cell studies.

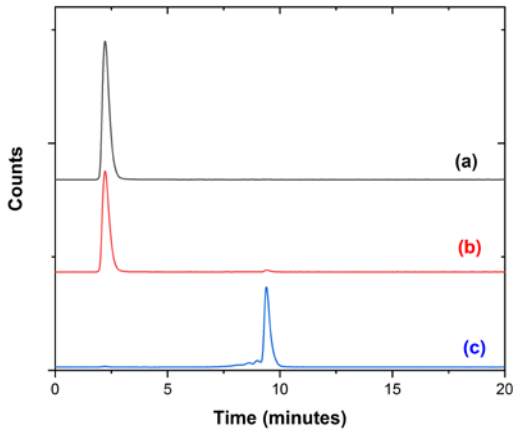

Fig. 3: Comparison of the HPLC radiochromatograms of 100 MBq/nmol ^{177}Lu-DOTANOC solutions, containing 2 µg (a), 0.2 µg (b) and 0.02 µg (c) Zn (pH: 4.5, T: 95ºC, 10 minutes incubation).

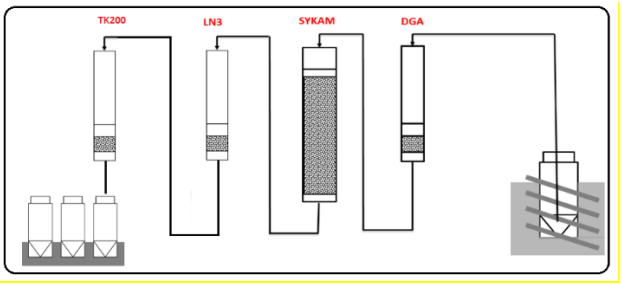

Fig. 4: Chemical separation process for the mass-separated ^{169}Er samples.

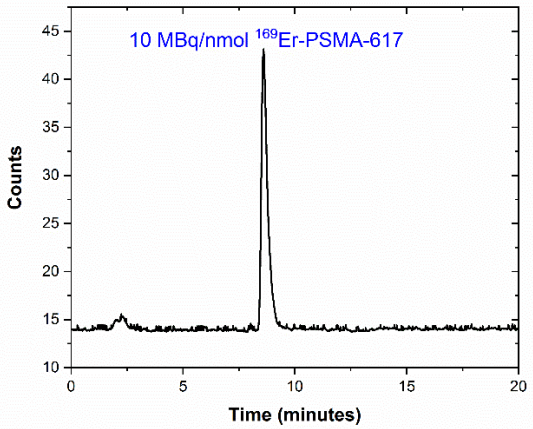

Fig. 5: HPLC radiochromatogram of 10 MBq/nmol ^{169}Er-PSMA-617 (pH: 4.5, T: 95 ºC, 20 minutes incubation).

[1] www.nndc.bnl.gov/nudat
[2] H. Uusijärvi et al., J. Nucl. Med. **14**, 807 (2006).
[3] L. Knut, World J Nucl Med. **14**,10 (2015).
[4] E. Deutsch et al., Eur. J. Nucl. Med. **20**, 1113 (1993).
[5] N. Karavida and A. Notopoulos, Hippokratia **14**, 22 (2010).

PRODUCTION OF MASS-SEPARATED ^{175}Yb FOR NUCLEAR MEDICINE APPLICATIONS

Z. Talip, C. Müller (CRS/PSI), N. P. van der Meulen (LRC/PSI), C. Duchemin, T. Stora (CERN-MEDICIS), U. Köster (ILL)

^{175}Yb is one of the potential lanthanides with suitable radionuclidic properties for radionuclide therapy. It is a moderate-energy β^--emitter ($T_{1/2}$ = 4.2 days, $E_{\beta av}$: 113 keV) and it also emits γ-photons of 114 keV (3.9%), 283 keV (6.1 %) and 396 keV (13.2 %) [1], which are suitable for Single Photon Emission Computed Tomography (SPECT). Moreover, dosimetry calculations showed that ^{175}Yb shows very high tumor-to-normal-tissue absorbed dose ratio (TND) [2].

The specific activity of ^{175}Yb produced via the ^{174}Yb(n,γ)^{175}Yb production route is sufficient for therapeutic applications such as bone pain palliation [3] and small joint synovectomy, however, high specific activities are required for receptor-targeted radionuclide therapy.

The use of mass separators to produce carrier-free radionuclides for nuclear medicine is becoming more and more attractive. For first generation demo experiments the ISOLDE facility at CERN was used where radionuclides are produced via high-energy proton induced reactions combined with an online mass separator, known as Isotope Separation On-Line (ISOL). At CERN-MEDICIS similar techniques are used, but with off-line mass separation of batch irradiations. Moreover, targets which are activated by proton or neutron-irradiation at other facilities can be used for offline mass separation, thus providing a larger choice and higher activities of novel radionuclides which are less populated in high-energy proton induced reactions. At MEDICIS the mass separation is often combined with resonant laser ionization to enhance element selectively the ionization of the element of interest. Still, other elements with moderate ionization potential may be surface ionized in the hot metal cavity where the laser beams interact with the atoms effusing from the heated target. This could cause contamination with surface ionized isobars in the collected ion beam. The mass-separated radionuclide beam is implanted into a solid catcher. As a result, radiochemical separation processes must be developed to separate the mass-separated radionuclides from soluble residues of the catcher matrix and from possible isobaric contaminants and make the wanted isotope available in purified form for nuclear medicine applications.

^{175}Yb production

^{175}Yb was produced by thermal neutron capture ^{174}Yb(n,γ)^{175}Yb on isotopically enriched ^{174}Yb (98%; ISOFLEX, Russia and U.S.A.). The production yield of ^{175}Yb is relatively high due to the neutron capture cross-section of this process (63 b) [4]. Five $^{174}Yb_2O_3$-containing ampoules were prepared at PSI and the irradiations were performed in the high flux position V4 at the reactor of ILL (Institut Laue-Langevin, France).

Activity measurements

After irradiation, the first ampoule was sent directly to PSI for the activity measurement to determine the production yield. Activity measurements were performed using a high-purity germanium (HPGe) detector (Canberra, France). Efficiency calibration of the detector system was performed with a certified ^{152}Eu standard source from PTB (Physikalisch-Technische Bundesanstalt, Germany). The activity of the sample was measured as 11 GBq. The ampoule was then crushed in a designated hot cell and the target (Yb_2O_3) dissolved in 7.0 M HNO_3. A fraction was taken to perform gamma spectrometry measurements to determine radionuclidic purity and for the calibration of SPECT device, used for preclinical imaging. Figure 1 shows the gamma spectrum of the sample, where only ^{169}Yb ($T_{1/2}$ = 32 d) was determined as a radionuclidic impurity.

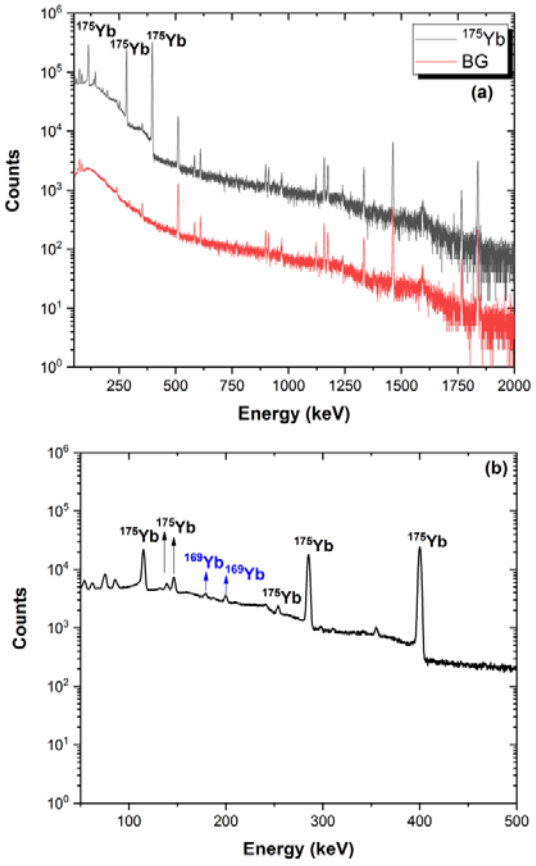

Fig. 1: Comparison of the gamma spectra of the carrier added (ca) ^{175}Yb (black line) and background measurements (red line) (measurements were performed for 86400 s, sample detector distance (SDD): 50 cm) (a), the pronounced ^{169}Yb gamma lines (b).

The other four ampoules were shipped to CERN-MEDICIS for the offline mass separation process. Mass-separated ^{175}Yb was implanted in solid catcher foils (Zn-coated gold foils). The samples were then transferred to PSI for chemical separation, quality control, and preclinical research studies.

Before chemical separation, the activities of the four samples were measured using gamma spectrometry (Table 1). The first two samples were used for the optimization of the chemical separation method, while the last two, benefitting from the radiochemical separation, were used for preclinical studies.

Tab. 1: The ^{175}Yb activities of the collection foils (post-mass separation) (activities measured using gamma ray spectrometry).

Sample	Activity (MBq)
M-Yb175- 1	136
M-Yb175-2	15
M-Yb175-3	72
M-Yb175-4	71

Chemical Separation

The Zn layer containing ^{175}Yb was dissolved in concentrated HNO_3 and the resultant solution passed through extraction resin to separate ^{175}Yb from Zn. ^{175}Yb and ^{175}Lu (a decay product of ^{175}Lu and isobaric impurity) was eluted with dilute HCl. To perform the lanthanide separation, the eluent was loaded onto a macroporous strongly acidic cation exchange resin and the Yb eluted using dilute α-hydroxyisobutyric acid (α-HIBA). The Yb eluent was, finally, introduced to LN3 and TK200 extraction resins to separate the complexing agent and to decrease the amount of Zn in the final fraction, respectively.

Labeling Efficiency

The final ^{175}Yb fractions were used to label PSMA-617 at a molar activity of 10 MBq/nmol. The radiolabeling yield was determined by reverse-phase-high-performance liquid chromatography (HPLC, Merck Hitachi LaChrom) with a radioactivity detector (LB 506, Berthold, Germany) and a C18 reverse-phase column (150mm× 4.6mm; Xterra™ MS, C18; Waters).

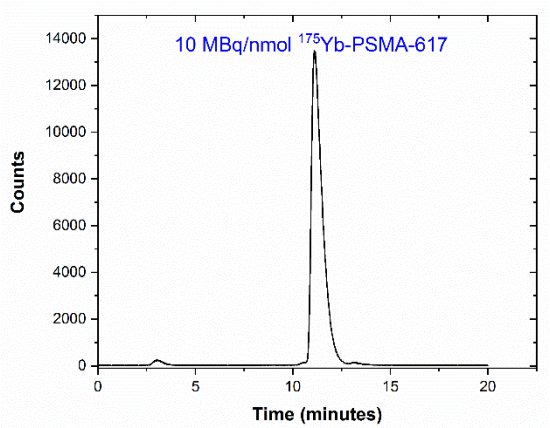

Fig. 2: HPLC radiochromatogram of 10 MBq/nmol ^{175}Yb-PSMA-617 (98.7 % labelled) (pH: 4.5, T: 95°C, 20 minutes incubation).

The quality of the final products was sufficient to perform preclinical cell studies. The first animal SPECT with ^{175}Yb-PSMA-617 was obtained.

[1] www.nndc.bnl.gov/nudat
[2] H. Uusijärvi et al., J. Nucl. Med. **14**, 807 (2006).
[3] N. Salek et al., Australas. Phys. Eng. S. **41,** 69 (2018).
[4] Atlas of Neutron Resonances (6th Edition) **2**, 111 (2018).

LIST OF PUBLICATIONS

N.M. Chiera, T.K. Sato, T. Tomitsuka, M. Asai, Y. Ito, K. Shirai, H. Suzuki, K. Tokoi, A. Toyoshima, K. Tsukada, Y. Nagame
Optimization of an isothermal gas-chromatographic setup for the chemical exploration of dubnium (Db, Z= 105) oxychlorides
J. Radioanal. Nucl. Chem. **320**, 633 (2019), DOI: 10.1007/s10967-019-06505-w

R. Eichler
The periodic table – an experimenter's guide to transactinide chemistry
Radiochim. Acta **107**, 9 (2019), DOI: 10.1515/ract-2018-3080

R. Eichler
The periodic table of elements: superheavy in chemistry
Nucl. Phys. News. **29**, 1 (2019). DOI:10.1080/10619127.2019.1571803

H.W. Gäggeler, I. Usoltsev, R. Eichler
Reactions of fission products from a ^{252}Cf source with NO and mixtures of NO and CO in an inert gas
Radiochim. Acta **107**, 7 (2019). DOI: DOI: 10.1515/ract-2018-3076

M. Lin, I. Kajan, D. Schumann, A. Türler
The concept for disposal of highly acidic spent nuclear fuel solutions at PSI
J. Radioanal. Nucl. Chem. **322**, 1857 (2019). doi.org/10.1007/s10967-019-06847-5

M.A.J. Mertens, A. Aerts, I. Infante, J. Neuhausen, S. Cottenier
Po-containing molecules in fusion and fission reactors
J. Phys. Chem. Lett. **10**, 2879 (2019). https://doi.org/10.1021/acs.jpclett.9b00824

T. Carzaniga, N.P. van der Meulen, R. Hasler, C. Kottler, P. Peier, A. Türler, C. Vermeulen, C. Vockenhuber, S. Braccini
Measurement of the ^{43}Sc production cross-section with a deuteron beam
Appl. Radiat. Isot. **145**, 205 (2019). DOI: 10.1016/j.apradiso.2018.12.031

N.P. van der Meulen, R. Hasler, A. Blanc, R. Farkas, M. Benešová, Z. Talip, C. Müller, R. Schibli
Implementation of a new separation method to produce qualitatively improved ^{64}Cu
J. Label Compound **62**, 460 (2019). DOI:10.1002/jlcr.3730

R. Mikolajczak, N.P. van der Meulen, S.E. Lapi
Radiometals for imaging and theranostics, current production and future perspectives
J. Label Compound **62**, 615 (2019). DOI: 10.1002/jlcr.3770

M. Pretze, N.P. van der Meulen, C. Wängler, R. Schibli, B. Wängler
Targeted ^{64}Cu-labeled gold nanoparticles for dual imaging with positron emission tomography and optical imaging
J. Label Compound **62**, 471 (2019). DOI: 10.1002/jlcr.3736

C. Mueller, C.A. Umbricht, N. Gracheva, V.J. Tschan, G. Pellegrini, P. Bernhardt, J.R. Zeevaart, U. Köster, R. Schibli, N.P. van der Meulen
Terbium-161 for PSMA-targeted radionuclide therapy of prostate cancer
Eur. J. Nucl. Med. Mol. I. **46**, 1919 (2019). DOI: 10.1007/s00259-019-04345-0

F. Cicone, S. Gnesin, T. Denoël, T. Stora, N.P. van der Meulen, C. Müller, C. Vermeulen, M. Benešová, U. Köster, K. Johnston, E. Amato, L. Auditore, G. Coukos, M. Stabin, N. Schaefer, D. Viertl, J. O Prior
Internal radiation dosimetry of a ^{152}Tb-labelled antibody in tumour-bearing mice
EJNMMI Res. **9**, 53 (2019). DOI: 10.1186/s13550-019-0524-7

N. Gracheva, C. Müller, Z. Talip, S. Heinitz, U. Köster, J.R. Zeevaart, A. Vögele, R. Schibli, N.P. van der Meulen
Production and characterization of no-carrier-added ^{161}Tb as an alternative to the clinically-applied ^{177}Lu for radionuclide therapy
EJNMMI radiopharm. chem. **4**, 12 (2019). DOI: 10.1186/s41181-019-0063-6

A. Lopez-Martens, A.V. Yeremin, M.S. Tezekbayeva, Z. Asfari, P. Brionnet, O. Dorvaux, B. Gall, K. Hauschild, D. Ackermann, L. Caceres, M.L. Chelnokov, V.I. Chepigin, M.V. Gustova, A.V. Isaev, A.V. Karpov, A.A. Kuznetsova, J. Piot, O.N. Malyshev, A.G. Popeko, Yu. A. Popov, K. Rezynkina, H. Savajols, A.I. Svirikhin, E.A. Sokol, P. Steinegger
Measurement of proton-evaporation rates in fusion reactions leading to transfermium nuclei
Phys. Lett. B **795**, 271 (2019). DOI: 10.1016/j.physletb.2019.06.010

J. Zhang, A. Singh, H.R. Kulkarni, C. Schuchardt, H.-J. Wester, T. Maina, F. Rösch, N.P. van der Meulen, C. Müller, H. Mäcke, R.P. Baum
From bench to bedside - the Bad Berka experience with first in human studies
Sem. Nucl. Med. **49**, 422 (2019). DOI: 10.1053/j.semnuclmed.2019.06.002

C. Müller, A. Singh, C.A. Umbricht, H.R. Kulkarni, K. Johnston, M. Benešová, S. Senftleben, D. Müller, C. Vermeulen, R. Schibli, U. Koester, N.P. van der Meulen, R.P. Baum
Preclinical investigations and first-in-human application of ^{152}Tb-PSMA-617 for PET/CT imaging of prostate cancer
EJNMMI Res. **9**, 68 (2019). DOI: 10.1186/s13550-019-0538-1

K. Siwowska, P. Guzik, K. Domnanich, J. Monné Rodríguez, G. Pellegrini, P. Bernhardt, B. Ponsard, U. Köster, R. Hasler, F. Borgna, R. Schibli, N.P. van der Meulen, C. Müller
Therapeutic Potential of ^{47}Sc in Comparison to ^{177}Lu and ^{90}Y: Preclinical Investigations
Pharmaceutics **11**, 424 (2019). DOI:10.3390/pharmaceutics11080424

C.A. Umbricht, U. Köster, P. Bernhardt, N. Gracheva, K. Johnston, R. Schibli, N.P. van der Meulen, C. Müller
Alpha-PET for Prostate Cancer: Preclinical investigation of ^{149}Tb-PSMA-617
Sci. Rep. **9**, 17800 (2019). DOI: 10.1038/s41598-019-54150-w

C. Mueller, M. De Prado Leal, M.D. Dominietto, C.A. Umbricht, S. Safai, R.L. Perrin, M. Egloff, P. Bernhardt, N.P. van der Meulen, D.C. Weber, R. Schibli, A.J. Lomax
Combination of proton therapy and radionuclide therapy in mice: Proof-of-concept study at the Paul Scherrer Institute
Pharmaceutics **11**, 450 (2019). DOI: 10.3390/pharmaceutics11090450

H. Zhang, R. Eichler, J. Grillenberger, W. Hirzel, S. Joray, D.C. Kiselev, N.P. van der Meulen, J.M. Schippers, J. Snuverink, R. Sobbia, A. Sommerhalder, Z. Talip, L.J. Nevay
BDSIM simulation for the complete radionuclide production beam line on PSI cyclotron facility from beam splitter to target station
In *Proc. Cyclotrons2019*, Cape Town South Africa, September 2019, JACoW Publishing, Geneva. ISBN: 978-3-95450-205-9. DOI:10.18429/JACoW-Cyclotrons2019-WEB04. (https://cyclotrons2019.vrws.de/papers/web04.pdf)

N.P. van der Meulen, R. Eichler, P.V. Grundler, R. Hasler, W. Hirzel, S. Joray, D.C. Kiselev, R. Sobbia, A. Sommerhalder, Z. Talip, H. Zhang, S. Braccini
The use of PSI's IP2 beam line towards exotic radionuclide development and its application towards proof-of-principle preclinical and clinical studies
In *Proc. Cyclotrons2019*, Cape Town South Africa, September 2019, JACoW Publishing, Geneva. ISBN: 978-3-95450-205-9. DOI:10.18429/JACoW-Cyclotrons2019-TUA03. (https://cyclotrons2019.vrws.de/papers/tua03.pdf)

Y. Wang, S. Cao, J. Zhang, F. Fan, J. Yang, H. Haba; Y. Komori T. Yokokita, K. Morimoto, D. Kaji, Y. Wittwer, R. Eichler, A. Türler, Z. Qin
The study of rhenium pentacarbonyl complexes using single-atom chemistry in the gas phase
Phys. Chem. Chem. Phys. **21**, 13 (2019), DOI: 10.1039/c8cp07844k

INTERNAL REPORTS AND TECHNICAL NOTES

N. Gracheva
Center of Radiopharmaceutical Sciences-ETH Seminar Day
Production and characterization of the novel therapeutic radiolanthanides Terbium-161 and Erbium-165
PSI Education Centre, 22 March, 2019

J. Neuhausen, E.-O. Karlsson, I. I. Danilov, E. A. Maugeri, A. Colldeweih, R. Eichler, R. Dressler, J. Ulrich, Chr. Schneider, E. Müller, D. Hermann, D. Piguet, A. Vögele, B. Gonzalez-Prieto, A. Aerts
Report on volatilization and deposition studies
Deliverable D4.3 of EURATOM Horizon 2020 Framework Programme project MYRTE,
Grant Agreement number: 662186, NFRP-09-2015: Transmutation of minor actinides (Towards industrial application)

CONTRIBUTIONS TO CONFERENCES, WORKSHOPS AND SEMINARS

N.M. Chiera
Establishment of the volatility trend in Group-5 Elements via gas-chromatographic experiments with Nb-, Ta-, and Db-oxychlorides
6th International Conference on the Chemistry and Physics of the Transactinide Elements (TAN19), Wilhelmshaven, Germany. 25-30 August, 2019

I.I. Danilov
Determination of thermochemical data of iodine, caesium and polonium in dilute liquid lead bismuth solutions
Seminar of the Laboratory of Radiochemistry, Paul Scherrer Institute, Villigen, Switzerland, 11 October, 2019

R. Dressler
Measurement of the ^{53}Mn (n, γ) cross-section at stellar energies
Heavy Ion Accelerator Symposia on Fundamental and Applied Science 2019 (HIAS 2019), Canberra, Australia, 09-13 September, 2019

R. Eichler
Prospects of Gas Phase Chemistry with Short-lived Transactinides "microsecond chemistry?"
International symposium "The present and the future of the Periodic Table of Chemical Elements", Dubna, Russian Federation, 30-31 May, 2019

R. Eichler
The Periodic Table a Driver for Transactinide Chemistry
XXI Mendeleev Congress General and Applied Chemistry, Sankt Petersburg, Russian Federation, 09-13 September, 2019

R. Eichler
Current and Future Chemistry Experiments with Transactinides
4th International Symposium on Superheavy Elements (SHE2019), Hakone, Japan, 01-05 December, 2019

P. Ionescu
Superheavy Element Cn (Z = 112) & Fl (Z = 114) – Selenium Interaction Using COLD Setup
NES-PhD-Day, Paul Scherrer Institut, Villigen, Switzerland, 23 May, 2019

P. Ionescu
Superheavy Element Cn & Fl - Chalcogen Interactions Using Gas Chromatography
6th International Conference on the Chemistry and Physics of the Transactinide Elements (TAN19), Wilhelmshaven, Germany. 25-30 August, 2019

P. Ionescu
The Chemistry of Copernicium - Past Results Guiding the Future
Seminar of the Laboratory of Radiochemistry, Paul Scherrer Institut, Villigen, Switzerland, 11 October, 2019

I. Kajan, S. Heinitz, M. Florianova, R. Dressler, A. Fankhauser, P. Sprung
Towards the first experimental determination of the 93Mo half-life
14th International Conference on Nuclear Data for Science and Technology (ND2019), Beijing, China, 19-24 May, 2019

E. Karlsson
Polonium deposition behavior in the event of a beam guide window puncture in an accelerator driven system
Seminar of the Laboratory of Radiochemistry, Paul Scherrer Institute, Villigen, Switzerland, 02 March, 2019

E. Karlsson
Polonium transport behavior in the event of a beam guide window puncture in an accelerator driven system (ADS)
NES-PhD-Day, Paul Scherrer Institute, Villigen, Switzerland, 23 May, 2019

E. Karlsson
Fission product chemistry in an LBE-cooled reactor
Seminar of the Laboratory of Radiochemistry, Paul Scherrer Institute, Villigen, Switzerland, 25 October, 2019

B. Kraus
Optimization of Vacuum Adsorption Chromatography for Superheavy Element Chemistry
NES-PhD-Day, Paul Scherrer Institut, Villigen, Switzerland, 23 May, 2019

B. Kraus
Vacuum Chromatography on the Long Hard Road to the Accelerator
6th International Conference on the Chemistry and Physics of the Transactinide Elements (TAN19), Wilhelmshaven, Germany, 25-30 August, 2019

M. Lin
The concept for disposal of highly acidic spent nuclear fuel solutions at PSI
2nd International Conference on Radioanalytical and Nuclear Chemistry (RANC 2019), Budapest, Hungary, 10 May, 2019

M. Lin
Selective removal of Cs from highly acidic spent nuclear fuel solutions
NES-PhD-Day, Paul Scherrer Institute, Villigen, Switzerland, 23 May, 2019

M. Lin
Selective removal of Cs from highly acidic spent nuclear fuel solutions.
Seminar of the Laboratory of Radiochemistry, Paul Scherrer Institute, Villigen, Switzerland, 14 June, 2019

E.A. Maugeri
Targetry of Exotic Radionuclides at PSI
NUSPRASEN SHE-Workshop, GSI, Darmstadt, Germany 25-27 February, 2019

E.A. Maugeri
Targetry of rare isotopes at PSI
14th International Conference on Nuclear Data for Science and Technology (ND2019), Beijing, China, 19-24 May, 2019

E.A. Maugeri
Production of exotic radionuclides targets for nuclear astrophysics experiments
7th Heavy Ion Accelerator Symposium on Fundamental and Applied Science, Canberra, Australia, 09-13 September, 2019

I. Mihalcea
Implementing new isotopes for environmental research: Redetermination of the ^{32}Si half-life
Bi-annual Meeting (SINCHRON Project), Physikalisch-Technische Bundesanstalt (PTB), Brunswick, Germany, 19 November, 2019

J. Neuhausen
Chemistry of volatile radionuclides: Introduction to MYRTE WP4 and results of I, Cs and Po evaporation and deposition experiments at PSI
MYRTE Final International Workshop, Von Karman Institute for Fluid Dynamics, Sint-Genesius-Rode, Belgium, 06 February, 2019

J. Neuhausen
Chemistry of volatile radionuclides
Final MYRTE TEC-Meeting, SCK·CEN Headquarters, Brussels, Belgium, 24 September, 2019

J. Neuhausen
Release and deposition of volatile radionuclides in LBE-cooled ADS: Selected Results of the MYRTE H2020 Project
4th International Workshop on Technology and Components for Accelerator Driven Systems (TCADS-4), Antwerp, Belgium, 14-17 October, 2019

D. Schumann
How accurate are the half-lives of long-lived isotopes?
14th International Conference on Nuclear Data for Science and Technology (ND2019), Beijing, China, 19-24 May, 2019

D. Schumann
Harvesting Exotic Radionuclides at PSI
Seminar at Research School of Earth Sciences ANU Canberra, Australia, 13 September, 2019

D. Schumann
How to separate Pb from Tl?
LOREX Meeting, GSI, Germany, 11-12 December, 2019

P. Steinegger
Online Studies with Thallium and the Prospects for a future Chemistry Experiment with Nihonium
6th International Conference on the Chemistry and Physics of the Transactinide Elements (TAN19), Wilhelmshaven, Germany, 25-30 August, 2019

P. Steinegger
Fast Gas-Phase Chemistry Experiments with Heaviest Group 13 Elements
Mendeleev Congress 2019, St. Petersburg, Russian Federation, 09-13 September, 2019

P. Steinegger
Gas-phase chemistry experiments with thallium for future investigations of nihonium (Z = 113)
4th International Symposium on Superheavy Elements (SHE2019), Hakone, Japan, 01-05 December, 2019

Z. Talip
Radionuclide development at PSI for nuclear medicine applications
WSIC-PSI Seminar day, Schwarzwald, Germany, 06 February, 2019

Z. Talip
CERN-MEDICIS 4rd Board Meeting
Project proposals to the MEDICIS collaboration board
CERN, Geneva, Switzerland, 30 March, 2019

Z. Talip
Radionuclide development at PSI for nuclear medicine applications
MEDICIS PRISMAS MAP, Kick-off event Erice, Sicily, Italy, 30 April, 2019

Z. Talip
Use of a new cation exchange resin for the separation of ^{64}Cu from proton irradiated ^{64}Ni
2nd International Conference on Radioanalytical and Nuclear Chemistry (RANC2019), Budapest, Hungary, 10 May, 2019

Z. Talip
Production cross-section of long-lived radionuclides in proton irradiated Pb, Ta, and W
14th International Conference on Nuclear Data for Science and Technology (ND2019), Beijing, China, 19-24 May, 2019

Z. Talip
Non-conventional isotopes collected by mass separation for new medical applications
CERN EN-departmental/KT seminar, CERN, Geneva, Switzerland, 14 November, 2019

Z. Talip
CERN-MEDICIS 5th Board Meeting,
Status of MEDICIS Projects
CERN, Geneva, Switzerland, 18 September, 2019

Z. Talip
PRISMAS-MAP Proposal Meeting,
PSI Transnational Activity" and "PSI Joint Research Activity
CERN, Geneva, Switzerland, 19 September, 2019

J. Ulrich
Measurement of astrophysical relevant properties of ^{53}Mn
NES-PhD-Day, Paul Scherrer Institut, Villigen, Switzerland, 23 May, 2019

J. Ulrich
Determination of astrophysical relevant properties of Mn-53
Seminar of the Laboratory of Radiochemistry, Paul Scherrer Institut, Villigen, Switzerland, 08 November, 2019

M. Veicht
Implementing new isotopes for environmental research: Redetermination of the ^{32}Si half-life
NES-PhD-Day, Paul Scherrer Institute, Villigen, Switzerland, 23 May, 2019

M. Veicht
Implementing new isotopes for environmental research: Redetermination of the ^{32}Si half-life
Seminar of the Laboratory of Radiochemistry, Paul Scherrer Institute, Villigen, Switzerland, 14 June, 2019

M. Veicht
Implementing new isotopes for environmental research: Redetermination of the ^{32}Si half-life
Candidacy Exam, École Polytechnique Fédérale de Lausanne, Lausanne, Switzerland, 16 July, 2019

M. Veicht
Implementing new isotopes for environmental research: Redetermination of the ^{32}Si half-life
Bi-annual Meeting (SINCHRON Project), Physikalisch-Technische Bundesanstalt (PTB), Brunswick, Germany, 19 November, 2019

M. Veicht
SINCHRONized: Status (6/16)
Seminar of the Laboratory of Radiochemistry, Paul Scherrer Institute, Villigen, Switzerland, 29 November, 2019

Y. Wittwer
On the formation and stability of metal carbonyl complexes from superheavy elements and their homologues
NES-PhD-Day, Paul Scherrer Institut, Villigen PSI, Switzerland, 23 May, 2019

Y. Wittwer
Optimization of Transactinide Carbonyl Complex Formation and Transport using Fission Products from Cf-252
6th International Conference on the Chemistry and Physics of the Transactinide Elements (TAN19), Wilhelmshaven, Germany, 25-30 August, 2019

N. van der Meulen
Horizon scanning – overview of emerging technologies
EC workshop on "Medical Radioisotopes in the Future: European Perspective" (SAMIRA), Brussels, Belgiun, 07 February, 2019

N. van der Meulen
The use of ^{149}Tb and ^{152}Tb in preclinical and clinical investigations: its mass separation and subsequent application for imaging and therapy
MEDICIS Radiochemistry Day CERN, Geneva, Switzerland, 19 March, 2019

N. van der Meulen
Tb radionuclides for imaging and therapy: how far have we progressed?
2nd International Conference on Radioanalytical and Nuclear Chemistry (RANC2019), Budapest, Hungary, 10 May, 2019

N. van der Meulen
Investigations on Sc radioisotopes for medical applications
Accelerated based Materials Science at ETH Workshop Zurich, Switzerland, 27 June, 2019

N. van der Meulen
Radionuclides for nuclear medicine: the triumphs and challenges
University of Pisa Summer School 2019, Rewriting Nuclear Physics textbooks, one more step forward, Pisa, Italy, 23 June, 2019

N. van der Meulen
The Use of PSI's IP2 Beam Line Towards Exotic Radionuclide Development and its Application Towards Proof-Of-Principle Preclinical and Clinical Studies",
CYC2019, Cape Town, South Africa, 24 September, 2019

N. van der Meulen
The development of ^{161}Tb production and its characterization towards clinical application
EANM'19, Barcelona, Spain, 13 October, 2019

N. van der Meulen
Sc radionuclides towards imaging and therapy: how far have we progressed?
IAEA Consultation Meeting, Vienna, Austria, 26 November, 2019

POSTER PRESENTATIONS

I.I. Danilov
Volatilisation of ^{134}Cs, $^{131, 126}$I and ^{210}Po from lead bismuth liquid metal solutions studied by the transpiration method
NES-PhD-Day, Paul Scherrer Institute, Villigen, Switzerland, 23 May, 2019

I.I. Danilov
Volatilisation of ^{134}Cs, $^{131, 126}$I and ^{210}Po from lead bismuth liquid metal solutions studied by the transpiration method
NES-ENE Poster Event, Paul Scherrer Institute, Villigen, Switzerland, 11 December, 2019

Gideon F. Steyn, Tjaart N. van der Walt, Charisse Perang, Ferenc Szelecsényi, Zoltan Kovács, Christiaan Vermeulen, Nicholas P. van der Meulen
Optimization of the cyclotron production of ^{88}Zr/^{88}Y generators with a 70 MeV proton beam
2nd International Conference on Radioanalytical and Nuclear Chemistry (RANC2019), Budapest, Hungary, 07 May, 2019

P. V. Grundler, N. Gracheva, Z. Talip, J. R. Zeevaart, U. Köster, C. Bailat, Y. Nedjadi, T. Duran, R. Schibli, C. Müller, N. P. van der Meulen
Developing the production of radiolanthanide ^{161}Tb and its characterization towards clinical application
Swiss Chemical Society Autumn Meeting, Zurich, 6 September, 2019

P. V. Grundler, Z. Talip, C. Favaretto, R. Schibli, C. Müller, N. P. van der Meulen
Developing the production of radiolanthanide ^{161}Tb and its characterization towards clinical application
NES-ENE Poster Event, Paul Scherrer Institute, Villigen, Switzerland, 11 December, 2019

E. Karlsson
Polonium transport behavior in the event of a beam guide window puncture in an accelerator driven system (ADS)
NES-ENE Poster Event, Paul Scherrer Institute, Villigen, Switzerland, 11 December, 2019

M. Veicht
Implementing new isotopes for environmental research: Redetermination of the ^{32}Si half-life
NES-PhD-Day, Paul Scherrer Institute, Villigen, Switzerland, 23 May, 2019

M. Veicht
Implementing new isotopes for environmental research: Redetermination of the ^{32}Si half-life
NES-ENE Poster Event, Paul Scherrer Institute, Villigen, Switzerland, 11 December, 2019

MEMBERS OF SCIENTIFIC COMMITTEES
EXTERNAL ACTIVITIES

Dr. Robert Eichler

- Associate Editor of the International Journal of Modern Physics E (IJMPE)World Scientific Publishing

Dr. Dorothea Schumann

- Nuklearforum Schweiz, member
- Schweizerische Gesellschaft der Kernfachleute, member

Dr. Nicholas van der Meulen

- United States Department of Energy (DOE Isotope R&D FOA), Panel Reviewer
- Accelerator for Research in Radiochemistry and Oncology at Nantes Atlanti (ARRONAX) International Scientific Committee, member
- PSI internal research commission (FoKo), member
- PSI NFO Deko Group member
- international Advisory Committee for the Workshop on Targetry and Target Chemistry
- Academic Editor for Public Library Of Science (PLOS)

PUBLIC RELATIONS AND OUTREACH ACTIVITIES

M. Veicht
Sonntagsdienst psiFORUM – PSI's outreach to the public exhibition

Chemical & Engineering News (c&en)
Exploring the superheavies
27 May, 2019

LECTURES AND COURSES

R. Eichler
Lecture Nuclear and Radiochemistry: Heavy Elements
University of Bern, Fall Semester 2019

I.I. Danilov
Practical lab course: "Physical Chemistry", AKTIV, VOLTAM
University of Bern, PC-I, Spring Semester 2019

P. Ionescu
Supervision: "Allgemeine Chemie"
University of Bern, Autumn Semester 2019

E. Karlsson
Supervision : "Physical Chemistry I"
University of Bern, Spring Semester 2019

B. Kraus
Supervision of "Fachpraktikum Chemie für Studierende der Medizin"
University of Bern, Spring Semester 2019

M. Lin
Practical lab course: "VISKOS 1", "VISKOS 2", "BELZHAS", "METHO"
University of Bern, PC-I, Spring Semester 2019

J. Ulrich
Supervision: "Praktikum Allgemeine Chemie"
University of Bern, Spring Semester 2019

M. Veicht
Practical lab course: "Introduction to Chemical Engineering"
École polytechnique fédérale de Lausanne (EPFL), ChE-203, Spring Semester 2019

M. Veicht
Practical lab course: "General and Analytical Chemistry I (for BIO+PHARM)",
University de Lausanne (UNIL), UNIL-101, Autumn Semester 2019

M. Veicht
Supervision and Exam corrections: "Mathematics 1A (for MAN)"
École polytechnique fédérale de Lausanne (EPFL), PREPA-031(a), Spring Semester 2019

M. Veicht
Supervision: "Chemistry Analytic Laboratory I (for BIO)"
University de Lausanne (UNIL), UNIL-103, Autumn Semester 2019

SEMESTER WORK

Shaohuang Chen

Determination of Excitation Function for the Production of ^{44}Ti in Proton-Irradiated Vanadium Samples

Dr. Dorothea Schumann (PSI)
Prof. Dr. Horst-Michael Prasser (ETHZ)
April 2019

MASTER THESIS

Shaohuang Chen

Development of a Wet Chemical Separation Process for ^{26}Al, ^{41}Ca and ^{32}Si from Proton-Irradiated Vanadium Samples

Dr. Dorothea Schumann (PSI)
Prof. Dr. Horst-Michael Prasser (ETHZ)
October 2019

DOCTORAL THESIS

Nadezda Gracheva

Development of Terbium and Erbium Radiolanthanides for Radiopharmaceutical Application

Dr. Nicholas van der Meulen (PSI)
Prof. Dr. Roger Schibli (ETHZ)
October 2019

AWARDS

Mario Veicht

Implementing new isotopes for environmental research: Redetermination of the ^{32}Si half-life

Best presentation AWARD (1st year PhD)
NES PhD Day, Villigen, Switzerland
May 2019

PAUL SCHERRER INSTITUT

LABORATORY OF RADIOCHEMISTRY of the PAUL SCHERRER INSTITUTE
as of December 31, 2019

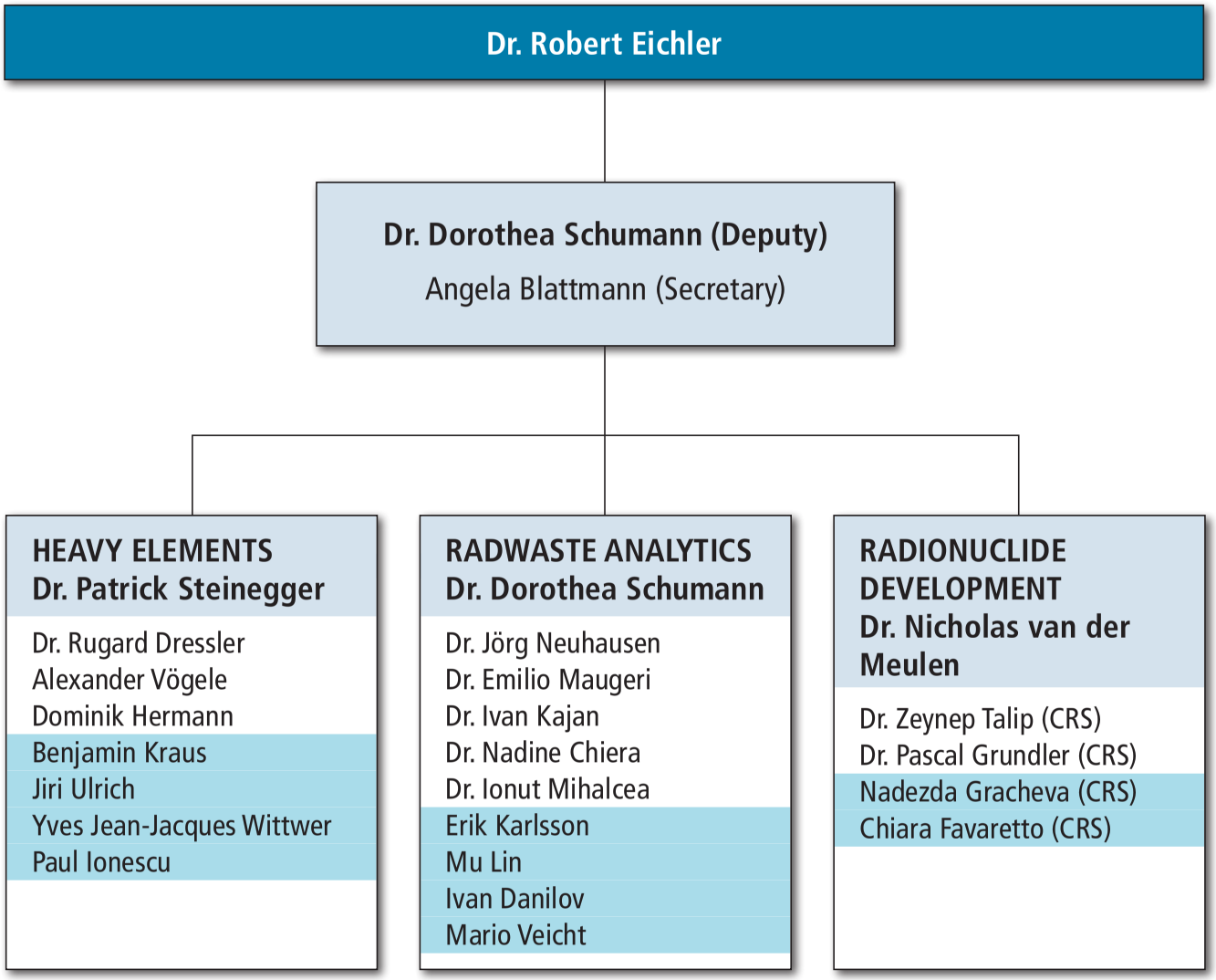

Graduate student

AUTHOR INDEX

AFFILIATION INDEX

AHL	Hot Laboratory Division of the Nuclear Energy and Safety Department (NES), Paul Scherrer Institut, 5232 Villigen, Switzerland
CERN	European Organization for Nuclear Research, CERN, 1211, Genève 23, Switzerland
CERN-MEDICIS	European Organization for Nuclear Research Esplanade des Particules 1, 1217 Meyrin, Switzerland
CIVIDEC	Instrumentation GmbH, Schottengasse 3A/1/41, AT-1010 Wien, Austria
CNR-Bari	Consiglio Nazionale Delle Ricerche Area Della Ricerca Di Bari, Via Giovanni Amendola, 118, 70126 Bari, Italy
CRS	Center for Radiopharmaceutical Sciences, Paul Scherrer Institut, 5232 Villigen, Switzerland
CVUT	Czech Technical University in Prague, Břehová 7, 115 19 Praha 1, Czech Republic)
ENEA-Bologna	Agenzia nazionale per le nuove tecnologie, l'energia e lo sviluppo economico sostenibile, Via Martiri di Monte Sole, 4, 40129 Bologna, Italy
EPFL	École polytechnique fédérale de Lausanne, Route Cantonale, 1015 Lausanne, Switzerland
ETHZ	Eidgen. Technische Hochschule Zürich, 8092 Zürich, Switzerland
EU	European Union
FLNR	Flerov Laboratory of Nuclear Reactions, Joliot-Curie, 6, Dubna, Moscow region 141980, Russia
IFIC / CSIC	Instituto de Física Corpuscular, Parc Científic de la Universitat de València, C/ Catedrático José Beltrán, 2 46980 Paterna, Spain
IFJ-PAN	Institute of Nuclear Physics, Polish Academy of Sciences, Waleregо Eljasza Radzikowskiego 152, 31-342 Kraków, Poland
IFIN-HH	Horia Hulubei National Institute for R&D in Physics and Nuclear Engineering, Str. Reactorului no.30, P.O.BOX MG-6, Bucharest - Magurele, Romania
ILL	Institut Laue-Langevin, 71 avenue des Martyrs 38000 Grenoble, France
INFN Bari	Istituto Nazionale di Fisica Nucleare Sezione di Bari, Via E. Orabona 4, 70125 Bari, Italy
INFN Bologna	Istituto Nazionale di Fisica Nucleare Sezione di Bologna, Viale Carlo Berti Pichat, 6/2 Portineria, 40127 Bologna, Italy
INFN-LNS Catania	Istituto Nazionale Di Fisica Nucleare-Laboratori Nazionali del Sud, Via S. Sofia 62, 95123 Catania, Italy
INFN Milano	Istituto Nazionale di Fisica Nucleare Sezione di Milano, Via F.lli Cervi, 201, 20090 Segrate (Milano), Italy
INFN Napoli	Istituto Nazionale di Fisica Nucleare Sezione di Napoli, Complesso universitario di Monte S. Angelo ed. 6, via Cintia, 80126, Napoli, Italy
INFN Perugia	Istituto Nazionale di Fisica Nucleare Sezione di Perugia, via A. Pascoli, 6123 Perugia, Italy
IRA	Institut de Radiophysique, Rue du Grand-Pré 1, 1007 Lausanne, Switzerlan
JAEA	Japan Atomic Energy Agency, Tokai, Ibaraki 319-1195, Japan
JINR	International Intergovernmental Organization, Joint Institute for Nuclear Research Joliot-Curie, 6, Dubna, Moscow region 141980, Russia
KIT	Karlsruhe Institute of Technology, 76021 Karlsruhe, Germany
Leibniz Univ.	Gottfried Wilhelm Leibniz Universität Hannover, Welfengarten 1, 30167 Hannover, Germany

LRC	Laboratory of Radiochemistry, Paul Scherrer Institut, 5232 Villigen, Switzerland
LOG	Fachbereich Logistik (LOG), Paul Scherrer Institut, 5232 Villigen, Switzerland
n_TOF	n_TOF Collaboration, European Organization for Nuclear Research (CERN), Genève 23, Switzerland
NCSR Demokritos	National Center for Scientific Research, Neapoleos 10, Ag. Paraskevi 153 10, Greece
Necsa	South African Nuclear Energy Corporation, Brits 0242, South Africa
Niigata Univ.	8050 Ikarashi 2-no-cho, Nishi-ku, Niigata, 950-2181, Japan
PSI	Paul Scherrer Institut, 5232 Villigen, Switzerland
SCK-CEN	Studiecentrum voor Kernenergie- Centre d'Étude de l'énergie Nucléaire, 2400 Mol, Belgium
STMicroelectronics	STMicroelectronics Catania, Str. Primosole 50, 95121 Catania CT, Italy
TU Bergakademie	Technische Universität Bergakademie Freiberg, Akademiestraße 6, 09599 Freiberg, Germany
TU Munich	Technical University of Munich, Arcisstraße 21, 80333 München, Germany
Univ. Bruxelles	Université Libre de Bruxelles, Avenue Franklin Roosevelt 50, 1050 Bruxelles, Belgium
Univ. Bern	Departement für Chemie und Biochemie, Universität Bern, Freiestr. 3, 3012 Bern, Switzerland
Univ. Bologna	University of Bologna Via Zamboni, 33, 40126 Bologna BO, Italy
Univ. de Strasbourg	Université de Strasbourg, 4 rue Blaise Pascal, CS 90032, 67081 Strasbourg Cedex, France
Univ. Goethe	Goethe-Universität Frankfurt am Main, 60323 Frankfurt am Main, Germany
Univ. Granada	University of Granada, Calle Periodista Daniel Saucedo Aranda, sn, 18071 Granada, Spain
Univ. Mainz	Johannes Gutenberg-Universität Mainz, Saarstr. 21, 55122 Mainz, Germany
Univ. Manchester	University of Manchester, Oxford Rd, Manchester M13 9PL, United Kingdom
Univ. Milano	University of Milan, Via Festa del Perdono, 7, 20122 Milano, Italy
Univ. of Cologne	Universität zu Köln, Albertus-Magnus-Platz, 50923 Köln, Germany
Univ. Valencia	University of Valencia, Av. de Blasco Ibáñez, 13, 46010 València, Valencia, Spain
Univ. York	University of York, York YO10 5DD, United Kingdom

Paul Scherrer Institut :: 5232 Villigen PSI :: Switzerland :: Tel. +41 56 310 21 11 :: Fax +41 56 310 21 99 :: www.psi.ch